University of Alaska Fairbanks

Quarterly Research Performance Progress Report

Federal Agency and Organization Element to Which Report is Submitted	U.S. Department of Energy Office of Fossil Energy
FOA Name	Advanced Technology Solutions for Unconventional Oil & Gas Development
FOA Number	DE-FOA-0001722
Nature of the Report	Research Performance Progress Report (RPPR)
Award Number	DE-FE0031606
Award Type	Cooperative Agreement
Name, Title, Email Address, and Phone Number for the Prime Recipient	**Technical Contact (Principal Investigator):** Abhijit Dandekar, Professor, adandekar@alaska.edu 907-474-6427 **Business Contact:** Rosemary Madnick Executive Director UAF Office of Grants and Contracts Administration rmadnick@alaska.edu, 907-474-6446
Name of Submitting Official, Title, Email Address, and Phone Number	Same as PI
Prime Recipient Name and Address	University of Alaska Fairbanks Grants and Contracts Administration PO Box 757880, Fairbanks AK 99775
Prime Recipient Type	Not for profit organization
Project Title	**FIRST EVER FIELD PILOT ON ALASKA'S NORTH SLOPE TO VALIDATE THE USE OF POLYMER FLOODS FOR HEAVY OIL EOR a.k.a ALASKA NORTH SLOPE FIELD LABORATORY (ANSFL)**

Principal Investigator(s)	**PI:** Abhijit Dandekar, *University of Alaska Fairbanks* **Co-PIs:** Yin Zhang, *University of Alaska Fairbanks* John Barnes and Samson Ning, Hilcorp Alaska LLC Randy Seright, *New Mexico Institute of Mining & Technology* Baojun Bai, *Missouri University of Science and Technology* Dongmei Wang, *University of North Dakota*
Prime Recipient's DUNS number	615245164
Date of the Report	June 30, 2020
Period Covered by the Report	March 1, 2020 – May 31, 2020
Reporting Frequency	Quarterly
Signature of Principal Investigator:	Abhijit Dandekar

Disclaimer

TABLE OF CONTENTS

LIST OF FIGURES

LIST OF TABLES

NOMENCLATURE

ANS   Alaska North Slope
bpd   Barrel Per Day
BHP   Bottomhole Pressure
BP   Budget Period
BS   Backscattering
BS&W   Basic Sediment and Water
CMG   Computer Modeling Group

cp or cP	Centipoise
DMP	Data Management Plan
DSD	Drop Size Distribution
DSL	Dynamic Scale Loop
EB	Emulsion Breaker
EOR	Enhanced Oil Recovery
EOS	Equations of State
ESP	Electrical Submersible Pump
FPV	Fracture Pore Volume
FR	Filter Ratio
Fr	Resistance Factor
Frr	Residual Resistance Factor
f_w	Fractional Flow of Water
G'	Elastic Modulus
G"	Viscous Modulus
HPAM	Hydrolyzed Polyacrylamide
HM	History Matching
HSPF	High Salinity Polymerflood
HSWF	High Salinity Waterflood
IAPV	Inaccessible Pore Volume
ICD	Inflow Control Device
IMEX	Implicit Pressure Explicit Saturation Simulator
IOR	Incremental Oil Recovery
IPROF	Injection Profile Log
KI	Potassium Iodide
k or K	Permeability (generally absolute)
Kc	Channel Permeability
Kh	Horizontal Permeability (intrinsic)
Km	Matrix Permeability
Kro	Relative Permeability to Oil
Krw	Relative Permeability to Water
Kv	Vertical Permeability (intrinsic)
LSWF	Low Salinity Waterflood
LSPF	Low salinity Polymerflood
md or mD	MilliDarcy
mg	Milligram
nm	Nanometer
No	Corey Exponent for Oil
Nvf	Viscous Fingering Number
Nw	Corey Exponent for Water
OIW	Oil in Water
OOIP	Original Oil in Place
PF	Polymerflood
PFO	Pressure Falloff

PMP	Project Management Plan
PPB	Parts Per Billion
PPG	Preformed Particle Gel
PPM	Parts Per Million
PRV	Pressure Release Valve
PSU	Polymer Skid Unit
PV	Pore Volume
QC	Quality Control
RF	Recovery Factor or Resistance Factor
RPM	Rotation Per Minute
RRF	Residual Resistance Factor
SC	Standard Conditions
SCTR	Abbreviation of Sector as used in CMG
SEM	Scanning Electron Microscopy
SHR	Keyword in CMG for shear rate dependent polymer viscosity
SHV	Keyword in CMG for Darcy velocity dependent polymer viscosity
S_{or}	Residual Oil Saturation
S_{orw}	Residual Oil Saturation due to Water
S_{orp}	Residual Oil Saturation due to Polymer
SPE	Society of Petroleum Engineers
STB	Stock Tank Barrel
STOOIP	Stock Tank Original Oil in Place
S_{wc} or S_{wi}	Connate/Irreducible Water Saturation
TDS	Total Dissolved Solids
T_o	Oil Content in the Water Sample
TPV	Total Pore Volume
μ	Viscosity
μg	Microgram
ULSPF	Ultra Low Salinity Polymerflood
URTeC	Unconventional Resources Technology
USBM	United State Bureau of Mines
UV	Ultraviolet
VE	Viscoelasticity
VRR	Voidage Replacement Ratio
VRV	Vacuum Release Valve
WC	Water Cut
WF	Waterflood
WOR	Water Oil Ratio
XRD	X-ray Diffraction
XRF	X-ray Fluorescence

1. ACCOMPLISHMENTS

a. Project Goals

The overall objective of this project is to perform a research field experiment to validate the use of polymer floods for heavy oil Enhanced Oil Recovery (EOR) on the Alaska North Slope (ANS).

The main scientific/technical objectives of the proposed project are:
1. Determine the synergy effect of the integrated EOR technology of polymer, low salinity water, horizontal wells, and conformance treatments (e.g., gels), and its potential to economically enhance heavy oil recovery.
2. Assess polymer injectivity into the Schrader Bluff formations for various polymers at various concentrations.
3. Assess and improve injection conformance along horizontal wellbore and reservoir sweep between horizontal injectors and producers.
4. Evaluate the water salinity effect on the performance of polymer flooding and gel treatments.
5. Optimize pump schedule of low-salinity water and polymer.
6. Establish timing of polymer breakthrough in Schrader Bluff N-sands.
7. Screen an optimized method to control the conformance of polymer flooding at the various stages of the polymer flooding project.
8. Estimate polymer retention from field data and compare with laboratory and simulation results.
9. Assess incremental oil recovery vs. polymer injected.
10. Assess effect of polymer production on surface facilities and remediation methods.

The technical tasks proposed in these studies focus on the following: (1) optimization of injected polymer viscosity/concentration and quantification of polymer retention via laboratory scale experiments; (2) optimization of injection water salinity and identification of contingencies for premature polymer breakthrough via laboratory scale experiments and numerical analyses; (3) reservoir simulation studies for optimization of polymer injection strategy; (4) design and implementation of a field pilot test at Milne Point on the ANS; (5) identification of effective ways to treat produced water that contains polymer (including polymer fouling of heater tubes), and finally (6) the feasibility of commercial application of the piloted method in ANS heavy oil reservoirs. The project milestones, and current milestone status are shown toward the end in **Table A**.

b. Accomplishments

The primary focus of the research program, since the start of the polymer injection in August 2018, has been monitoring the performance of the pilot in the injection wells J-23A and J-24A, and production wells J-27 and J-28 respectively. In order to complement the field pilot, focus of other supporting tasks has been advancing reservoir simulation, tackling flow assurance challenges and laboratory corefloods. The accomplishments to date are summarized in the following bullet points:

- First and foremost, despite the adverse conditions manifested by Covid-19 (lab access limitation), the project progress has remained on track, by careful planning and management of various tasks.
- Publications resulting from the project continues to be a success. In the reporting quarter two manuscripts (one on emulsion and one on fouling), following rigorous peer review, have been accepted in the SPE Production and Operations Journal. It is expected that both will be available online soon and the final versions documented in EDX. Abstract submitted for presentation at the 2020 SPE ATCE also has been accepted (see products). Finally, another paper is scheduled for presentation at the 2020 URTeC conference (see products).
- Streamlined polymer solution quality control procedure.
- No polymer production or breakthrough has been observed more than 20 months after start of polymer injection, which has been monitored with both the clay flocculation and water composition analyses. Although clay flocculation test shows positive results, water composition analysis still could not detect presence of polymer.
- The project team continues to be cautiously optimistic from the standpoint of incremental oil, which is estimated to be ~700 bopd (over waterflood) from polymer injection.
- Estimated polymer utilization to date is approximately 2.4 pounds per barrel of incremental oil, which is much lower than the reported "utility factor" of 3.9 pounds per barrel of incremental oil for a polymer pilot in Argentina (Juri et al., 2020) that uses the same polymer.

Since the official project start date of June 1, 2018, the entire project team has continued the practice of working meetings every other Friday for three hours to discuss the various tasks and the project as a whole. A summary of these bi-weekly meetings is provided to the project manager. Additionally, separate meetings, as needed, between the sub-groups also take place. In the bi-weekly meeting of February 28 the team extensively discussed the possibility of gradually lowering the polymer concentration from the current 1700 ppm down to 1400 ppm to lower the viscosity to ~30 cP (at 7.3 S^{-1}) and potentially improve the injectivity. Accordingly, in this reporting period the polymer concentration has been between 1500 ppm to 1700 ppm to achieve a viscosity of 40 cP (at 7.3 S^{-1}).

The following summarizes the team's progress to date in relation to the various tasks and sub-tasks outlined in the Project Management Plan (PMP):

- Task 1.0 - Project Management and Planning

Revised PMP and DMP are on file with DOE, which were submitted on April 30th 2019.

- Task 2.0 - Laboratory Experiments for Optimization of Injected Polymer Viscosity/Concentration and Quantification of Polymer Retention

Floods to Investigate "Tailing" of Polymer Retention. During this quarter, four additional polymer retention experiments were performed using Milne Point OA sand packs to investigate the shape of the polymer breakout curve as a function of polymer concentration and molecular weight. All four floods

used 15.24-cm long native-state Milne OA sand packs with 500 psi confining pressure applied. Entries 15-18 in **Table 2.1** summarize the results and allow a comparison with previous retention results. For 600-1750-ppm Flopaam 3630S HPAM (in Milne injection brine), **Figure 2.1** shows that initial polymer breakout (red, green and black curves) occurred near the same time as the water tracer (blue curve) and tracked the tracer curve up until 70%-80% of the injected concentration values. However, thereafter, the tracer rapidly rose to 100% of the injected value, but the three polymer curves "tailed" up to the injected concentrations over the course of the next nine pore volumes. Polymer retention is calculated by the difference in areas between a given polymer curve and the blue tracer curve. Polymer retention would be near zero, except for this tailing effect. With the tailing effect included, retention values rose from 66 to 205 μg/g as the 3630 concentration rose from 600 to 1750 ppm. Even so, **Figure 2.1** reveals that the tailing effect occurred to about the same extent with all three concentrations of 3630 HPAM. **Figure 2.2** shows that the same tailing effect occurred for 2000-ppm Flopaam 3430S—a solution providing about the same polymer viscosity as 1750-ppm 3630, but using a lower-molecular-weight HPAM (11 million g/mol versus 18 million g/mol). Polymer retention was about the same for the two cases (i.e., 236 μg/g for 2000-ppm 3430 versus 205 μg/g for 1750-ppm 3630). Investigations will continue to understand the reason for the "tailing" effect and its significance to the Milne Point polymer flood.

Table 2.1: Summary of polymer retention results.

Pack	Sand	Polymer	ppm	k_{abs}, mD	k_w at S_{or}, mD	Pack length, cm	Sand cleaned?	Confining pressure, psi	Polymer retention, μg/g
1	NB#1	3630	1750	11250	11250	60.1	no	0	290
2	NB#1	3630	1750	6330	--	60.1	yes	0	153
3	NB#1	3630	1750	9240	--	60.1	yes	0	170
4	NB#1	3630	1750	10900	7000	60.1	Greatly	0	28
5	NB#1	3630	1750	548	50	15.24	yes	1000	240
6	NB#1	3630	1750	625	73	15.24	yes	1700	533
7	NB#1	3430	1750	673	116	15.24	yes	1700	236
8	NB#3	3630	1750	4100	4100	30.48	no	200	30
9	NB#3	3630	1750	1778	1778	30.48	no	1000	32
10	OA	3630	1750	233	19	15.24	yes	800	126
11*	OA	3630	1750	470	20	30.48	yes	1000	65
12	OA	3630	1750	158	--	15.24	yes	500	87
13	OA	3630	1750	680	--	30.48	yes	500	56
14	OA	3430	1750	328	--	15.24	yes	1000	0
15	OA	3630	1750	544	544	15.24	no	500	205
16	OA	3630	1200	113	113	15.24	no	500	71
17	OA	3630	600	100	100	15.24	no	500	66
18	OA	3430	2000	232	232	15.24	no	500	236

* Pack 11 was aged for 6 days at 60°C at high oil saturation.
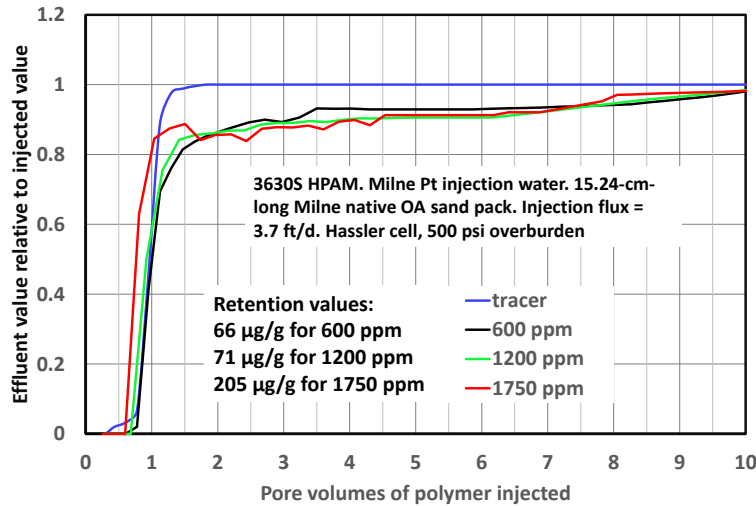
Figure 2.1: "Tailing" effect for 600-1750-ppm Flopaam 3630S HPAM during retention studies.
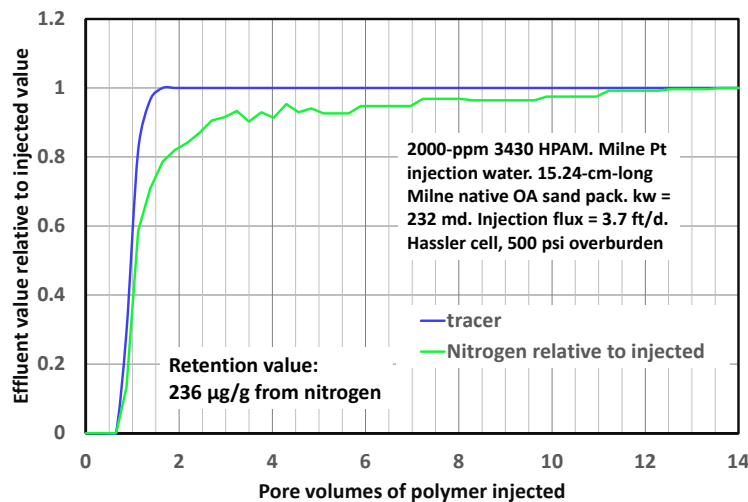
Figure 2.2: "Tailing" effect for 2000-ppm Flopaam 3430S HPAM during retention studies.

Polymer Viscosity/Resistance Factor versus Shear Rate/Velocity in Porous Media. For the original design of the Milne Point polymer flood, the chosen polymer solution viscosity was based on a shear rate of 7.3 s^{-1}. This shear rate has been a standard throughout the industry for many years—and was developed based on expected velocities in a five-spot pattern. At the Milne Point polymer flood, a viscosity of 45 cp was chosen for the injected polymer solution to give the presumed optimum displacement of the reservoir's viscous oil. Achieving this viscosity (measured at 7.3 s^{-1}) requires 1750-ppm 3630 HPAM. Recently, injectivity at the field project has declined enough to question whether a lower polymer concentration could be used. Upon examining the original basis for selecting the polymer concentration, we realized that the effective velocity or shear rate in the field was closer to 1 s^{-1}, instead of 7.3 s^{-1}. At Milne Point, parallel horizontal injection and production wells are used—which provide lower average

11

velocities in the reservoir than those associated with vertical wells. We found that the viscosity measured at 1 s^{-1} is about twice that at 7.3^{-1}—implying that the target reservoir viscosity of 45 cp could be achieved with a much lower polymer concentration than the original design (specifically 1200 ppm instead of 1750 ppm, see **Figure 2.3**).
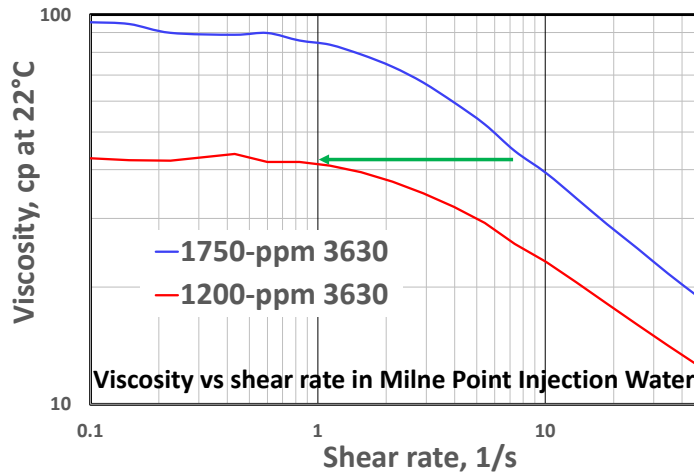
Figure 2.3: Viscosity versus shear rate in Milne Point injection brine.

In the laboratory, we measured viscosity versus shear rate in a viscometer and also resistance factor (apparent viscosity in porous media) versus darcy velocity in Milne Point cores (see **Figure 2.4**). We found that in 2183-md Milne Point cores at low velocities, the viscosity-vs.-shear-rate data could be made to match the resistance-factor data by shifting the curves horizontally. More specifically, the equivalent darcy velocity (in ft/d) in a 2183-md core is equal to 1/20 of the shear rate (in s^{-1}). In other words, in 2183-md rock, 0.05 ft/d is equivalent to a shear rate of 1 s^{-1}. Assuming that the flow is evenly distributed along a given Milne Point horizontal well, the average darcy velocity in the Milne Point reservoir is 0.05 ft/d—or the equivalent of 1 s^{-1} shear rate. This information will be of value for use during the Milne Point reservoir simulation effort and in the decision to potentially reduce the injected polymer (3630S) concentration from 1750 ppm down to 1200 ppm. (Incidentally the mismatch of the blue and red curves in **Figure 2.4** is due to a well-known viscoelastic or shear thickening behavior for HPAM in porous media. This mismatch only occurs at velocities that are too high to be encountered at Milne Point, and so is not relevant to the key decision on the correct polymer concentration.)
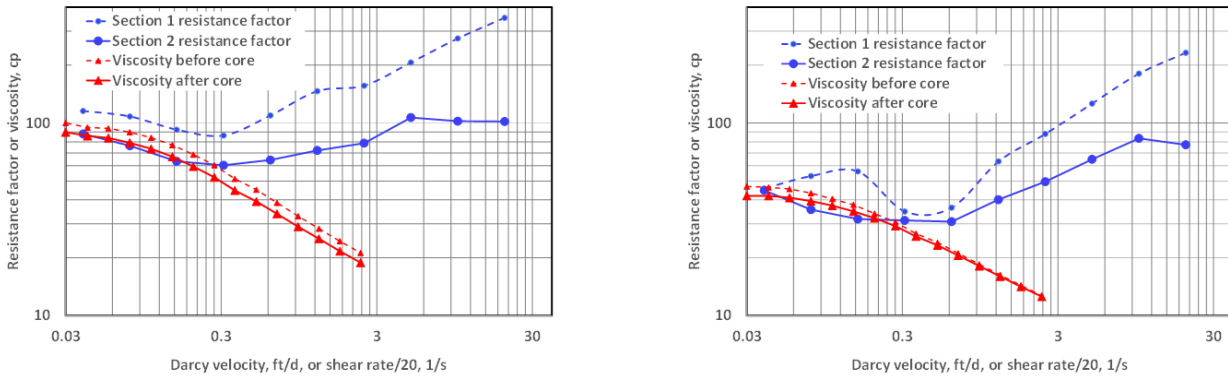
Figure 2.4: Viscosity vs. shear rate and resistance factor vs. velocity in 2183 md NB#3 Milne Point sand. 1750 ppm polymer (left) and 1200 ppm polymer (right).

A similar set of experiments was performed in 1094-md native NB#3 sand to examine the effect of permeability on the shear-rate-velocity shift. In 2183 mD native NB#3 sand (Liviano well), experimentally, we find that shear rate in a viscometer must be divided by 20 to get the right darcy velocity in ft/d. So, 0.05 ft/d is 1 s^{-1}. In other permeabilities, one should use $[(1-\varphi)/\varphi]\ [k/\varphi]^{0.5}$ to shift to the correct permeability (Seright et al., 2011). More specifically, the theory suggests that to obtain shear rate in other permeabilities, multiply darcy velocity by: shift factor = $20*[(1-\varphi)*(k\varphi)^{0.5}]/[(1-0.28)*(0.28*2183)^{0.5}]$. For a permeability of 1094 md, a shift factor of 14.2 is predicted. This factor fits the new results for 1750-ppm 3630 in 1094-md sand (see **Figure 2.5**), but the data scatter would also be consistent other formulations of shift factor.
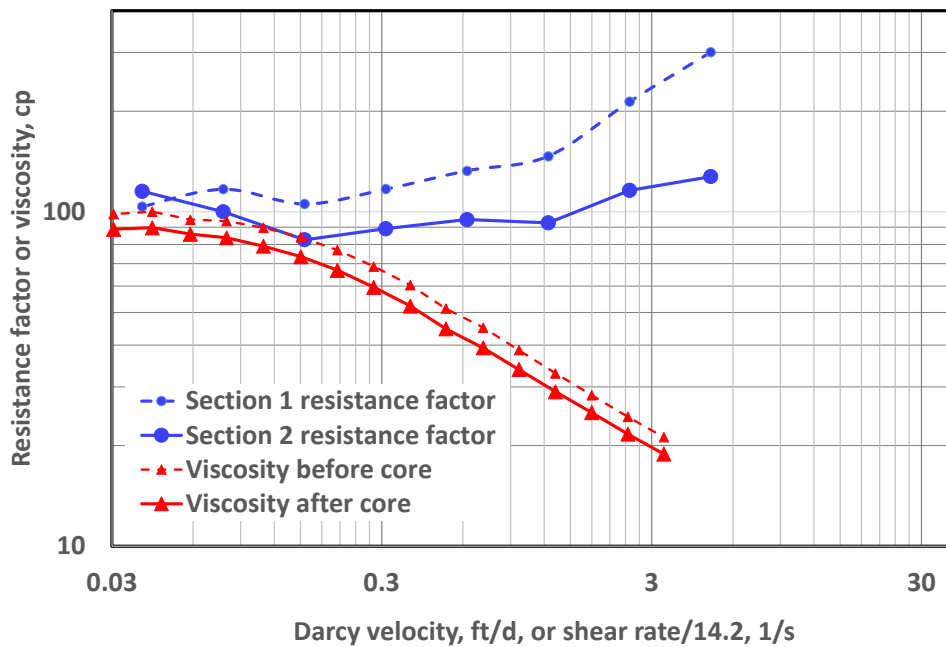
Figure 2.5: 1750-ppm 3630 in Milne Injection brine, 22°C, 1094-md NB#3 sand.

Activity is ongoing.

● Task 3.0 - Laboratory Experiments for Optimization of Injection Water Salinity and Identification of Contingencies in Premature Polymer Breakthrough in the Field

The main progress achieved during this quarter includes:
(1) Performed two more experiments to investigate the impact of heterogeneities on polymer flooding performance and the effectiveness of gel treatment;
(2) Summarized the endpoint relative permeability of water of high salinity and low salinity based on the coreflooding results using NB sandpacks. The coreflooding experiments were performed previously and had been reported in previous quarter reports.
(3) Performed experiments to investigate the impact of salinity on rheology behavior of polymer solutions transporting through porous media;
(4) A conference paper was prepared and submitted to the URTeC 2020.
(5) Numerical simulation study conducted on the performance of polymer flooding and influencing factors. The sensitivity test of flow rate, reservoir condition and polymer rheology were investigated.
(6) Optimization of the type and concentration of the polymer based on the heterogeneity conditions and injection operations.

Gel Treatment Experiments.
During this quarter, two more experiments were carried out to investigate the impact of heterogeneities on polymer flooding performance and the effectiveness of gel treatment. The key parameters of the models are summarized in **Table 3.1**. The highlighted were the experiments performed during this quarter. The preparation procedure of the models and the coreflooding processes were similar as before, which had been described in the last two quarter reports. The model of Channeled #4 was prepared by packing the fracture with 60/80 mesh NB sand. The fracture of the open-frac model was left empty without packing sand. The matrix was Berea cores with a permeability of about 500 md. The thickness of the channel/fracture was 0.3 cm. The Channeled #4 had the lowest permeability and thus this model has the smallest heterogeneity. The open-frac model, on the other hand, had the largest heterogeneity.

Table 3.1: The key parameters of the models.

Exp #	L×d, cm	Channel thickness, cm	Channel width, cm	Sand size, mesh	Heterogeneity
Homog. model	30×3.8	/	/	/	Low ↓ ↓ High
Channeled #4	14.5×5	0.3	4.1	60-80	
Channeled #3	14.5×5	0.3	4.1	30-60	
Channeled #2	14.5×5	0.3	4.1	20-30	

| Channeled #1 | 14.5×5 | 0.3 | 4.1 | 10-20 | |
| Open-frac | 14.5×5 | 0.3 | 4.1 | Open fracture | |

Prior to gel treatment, waterflooding was performed by injecting synthetic Milne Point injection brine. The flooding was switched to polymer flooding after the water cut climbed to 80%. The polymer flooding was continued until no oil was produced and the injection pressure became stable. The breakthrough behavior, oil recovery performance from the initial waterflooding and polymer flooding are summarized in **Table 3.2** and **Figure 3.1** – **3.2**. The results of the four channeled models indicate that as the size of the filled sand increases (i.e. the severity of the heterogeneity becomes greater), the water broke through to the outlet (producer) earlier. The oil recovery from the initial waterflooding at the water cut of about 80% decreased. The oil recovery was 29.3% for the model of Channeled #4, while for the open-frac model, the oil recovery was much lower. The value was slightly higher compared with Channeled #1. This was because the fracture volume accounted for a larger portion of the total pore volume of the model compared with the channeled models. Remarkable incremental oil was recovered in the following polymer flooding in Channeled #4, and the water cut was reduced to as low as 50%. The oil recovery was increased to 67.7%, which was comparable to the homogeneous model. The incremental recovery was much lower for the open-frac model and the overall recovery was only 24.0% after extensive polymer flooding. Note that most of the oil was from the open fracture and most of the oil present in the matrix was left behind. The polymer solution alone is insufficient to correct the heterogeneity problem and establish a satisfactory displacement. On the other hand, for the channeled models, it seems the polymer solution was effective to overcome the heterogeneity issue and achieve satisfactory oil recovery performance.

Table 3.2: Oil recovery performance before gel treatment.

Exp #	Heterogeneity	Water breakthrough	WF, % fw=80%)	PF, %	WF+PF
Homog. model		0.24PV	49.0	22.7	72.9
Channeled #4		0.20PV	29.3	36.7	67.7
Channeled #3	Low ↓ ↓ High	0.11PV	19.0	32.1	58.4
Channeled #2		0.10PV	16.7	32.1	48.9
Channeled #1		0.09PV	10.8	22.7	34.7
Open-frac		0.11PV (0.43FPV)	12.7	11.3	24.0
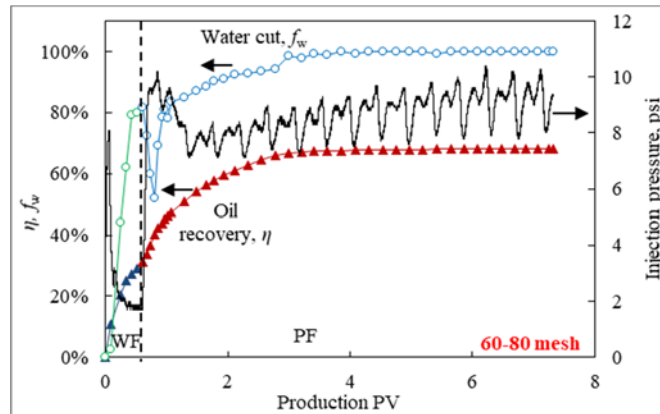
Figure 3.1: Before gel treatment (sand size=60-80 mesh).
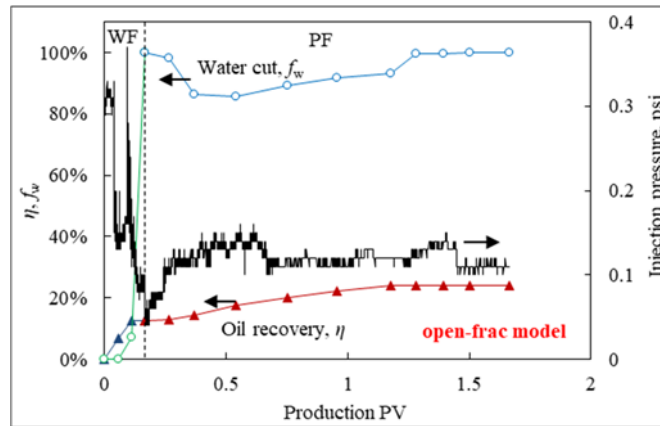
Figure 3.2: Before gel treatment (open-fracture model).

Microgel was tried to shut off the super-k channels/fractures and improve the conformance. The size of the dry microgel was 170-230 mesh. The volumetric swelling ratio of the microgel in the Milne Point injection brine was 40. Microgel dispersion with a concentration of 1 wt% was injected until the gel was observed at the outlet and the injection pressure became stable (if possible). After the gel treatment, post polymer flooding and waterflooding were followed sequentially. The residual resistance factor established by the microgel treatment was evaluated.

The gel injection pressure for Channel #4 is shown in **Figure 3.3**. The injection pressure first showed a steady increase at the early stage and then showed fluctuation in a wide range. At the initial stage, leak-off would occur at the matrix surface. In this process, the water of the gel dispersion was forced into the matrix while the microgel was left at the surface. As more gel accumulated at the surface, a gel cake would be formed. The gel cake prevented further leak-off of the gel dispersion into the matrix. The injection pressure continued to increase to over 700 psi then it became relatively flat with fluctuations. No gel was produced out. The treatment was stopped as the injection pressure climbed to the preset limit.

16

About 13 fracture pore volumes (FPV) of gel dispersion was injected. The high injection pressure indicates the microgel is hard to penetrate into the channel because the pore size is much smaller than the other three channeled models. A check of the gel placement in the channel reveals that the injected microgel only accumulated at the near inlet section and could not transport deep into the channel.

For the open-frac model, however, no significant pressure buildup was observed when injecting the microgel dispersion, indicating the microgel was insufficient to shut off the open fracture. Milli-sized preformed particle gels (PPG) were attempted. The milli-sized PPG had the same properties as the microgel, but the size was 0.45-0.90 mm. After fully swelled in the Milne Point injection brine, free water was removed. The swollen gel was pumped into the open-frac model. The injection pressure is shown in **Figure 3.5**. The placement of the gel in the fracture is also shown in the figure. Stable injection pressure was established after about 7 pore volumes of gel was injected. The injection pressure indicated the fracture was effectively blocked by the PPG.
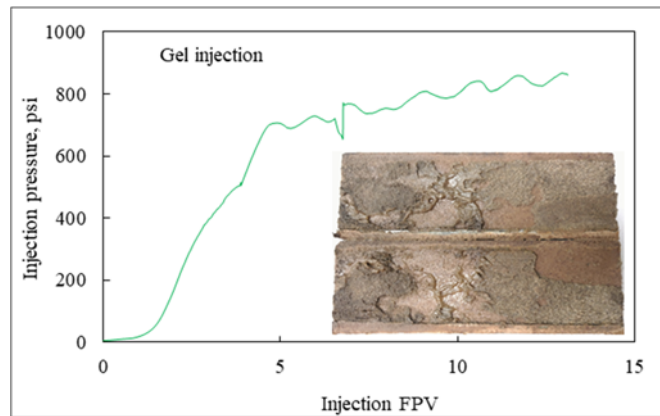
Figure 3.3: Injection pressure during gel treatment (sand size=60-80 mesh).
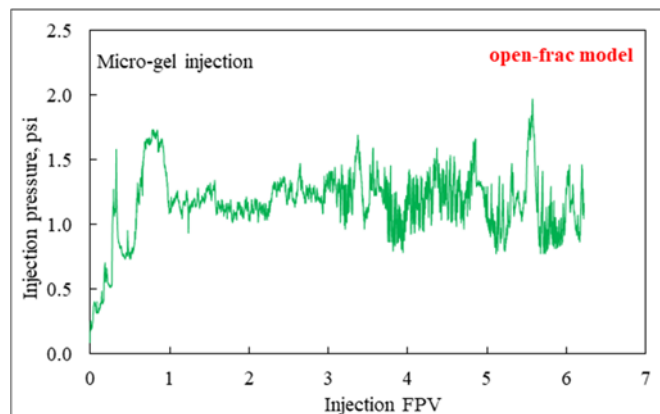
Figure 3.4: Injection pressure during microgel injection (open-frac model).

17
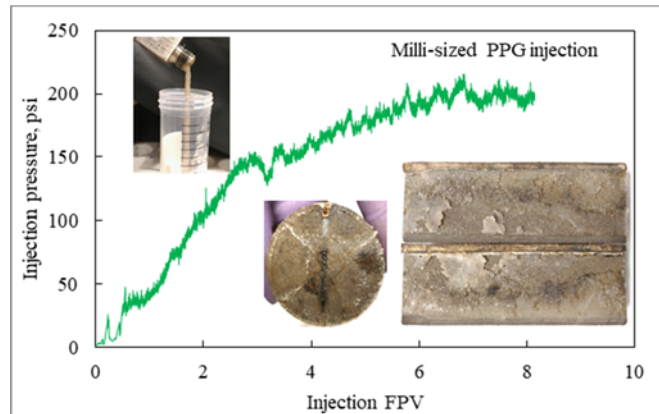
Figure 3.5: Injection pressure during milli-sized PPG injection (open-frac model).

Polymer flooding and waterflooding were performed after the gel treatment. Polymer flooding was performed until no oil was produced. Afterwards, water was injected at the same flow rate until the pressure became stable. The oil recovery performance after gel treatment is shown in **Figure 3.6**. For Channeled #4, incremental oil recovery after gel treatment was 15.9% OOIP. The oil recovery was increased to 83.8%. For the open-frac model, though the microgel could not effectively block the high-permeability fracture, remarkable incremental oil was recovered when injecting the dispersion of microgel. The oil recovery improvement after treatment with milli-sized gel was limited. The final oil recovery was increased to 55%.
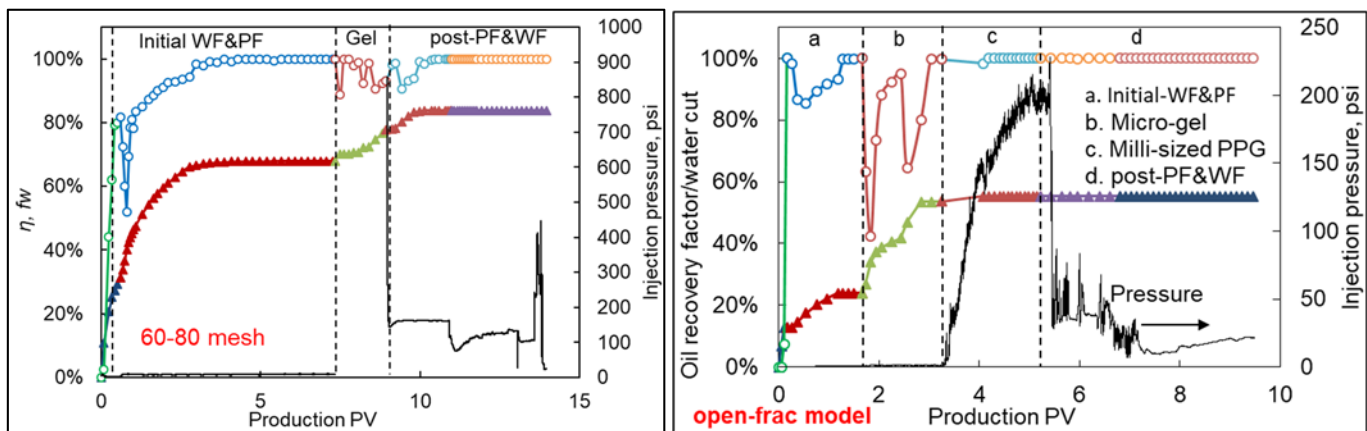
(a) sand size=60-80 mesh   **(b) open-fracture model**
Figure 3.6: Oil recovery performance after gel treatment.

Endpoint relative permeability
The experimental results of coreflooding using NB sandpack performed previously was analyzed. The end point relative permeability of water is summarized in **Table 3.3**. The endpoint relative permeabilities of both the LSW and HSW were pretty low, generally below 0.2. The endpoint relative permeability of LSW was lower than that of HSW. The ratio of the Krw (LSW) to Krw (HSW) ranged from 0.5 to 1.

More experiments will be performed with confining pressure to validate the observations from the sandpack coreflooding experiments. In new experiments, confining pressure will be applied to avoid possible water channeling along the tubing wall when no confining pressure is applied. The results would provide direct support for lab scale and field scale history matching and simulation in determining/adjusting the relative permeability inputs.

Table 3.3: Summary of endpoint relative permeability of low salinity water (Milne Point injection brine) and high salinity water (Milne Point formation brine).

#	Kabs(w) mD	Sand	Flood sequence	Krw (HSW)	Krw (LSW)	Krw$_{(LS)}$/Krw$_{(HS)}$
#1A	16,000	Native NB	HSW->LSW	0.113	0.105	0.93
#1B	16,000	Native NB	LSW->HSW	0.141	0.105	0.74
#2	1770	Native NB	HSW->LSW	0.036	0.034	0.94
#3	1470	Cleaned NB	HSW->LSW	0.249	0.128	0.51
#4	478	Cleaned NB	HSW->LSW	0.035	0.023	0.66
NB3-7	91	Cleaned NB plug	LSW->0.1LSW	0.061	0.059	0.96

Impact of Salinity on Rheology Behavior of Polymer in Porous Media

Four tests were performed to investigate the impact of salinity on rheology behavior of polymer in porous media. Boise Buff sandstone cores were used (5.07×14-15 cm). These cores have a high permeability of 3000-5000 md, which allows a wide range of flow rate (flux/shear rate) without causing a super high injection pressure at high flux. The porosity was about 30%. The cores were first 100% saturated with Milne Point formation brine and the permeability was measured following the standard procedure. Test #1 was to investigate the rheology behavior of LSP (prepared with LSW, 3630, 1400 ppm) at no oil condition. Test #2 was to investigate the rheology behavior of HSP (prepared with HSW, 3630, 2280 ppm) at no oil condition. Tests #3 and #4 were to study the rheology behavior of LSP and HSP at residual oil saturation condition, respectively. The residual oil saturation was established with the corresponding polymer solution at normal flux (0.5 ml/min, i.e. 1.2 ft/d). The viscosity of the LSP and HSP at 7.3 s^{-1} was close as 45 cp. More detailed description of the tests is summarized below.

Test #1: LSP rheology with no oil
- 5.07x14 cm; Kabs=3.4 darcy, porosity=0.30, PV=84.8 cm^3,
- Inject LSW, and measure injection pressure (P$_{brine1}$) at different flow rates (10-0.1 ml/min)
- Polymer rheology test (flow rate from 10 to 0.1 ml/min)
- Calculate resistance factor: P$_{polymer}$/P$_{brine1}$ at the same injection rate

Test #2: HSP rheology with no oil
- 5.07x14 cm; Kabs=3.4 darcy, porosity=0.31, PV=87.1 cm^3,
- Inject HSW, and measure brine injection pressure (P$_{brine1}$) at different flow rates (10-0.1 ml/min)

- Polymer rheology test (flow rate from 10 to 0.1 ml/min)
- Calculate resistance factor: $P_{polymer}/P_{brine}$ at the same injection rate

Test #3: LSP rheology with residual oil

- 5.07x14 cm; Kabs=3.4 darcy, porosity=0.30, PV=85.5 cm^3,
- Inject LSW, waterflood to fw=80%, q=0.5 ml/min (1.2 ft/D), recovery=39%, P_{brine1}=1.06 psi (not stabilized)
- Inject LSP, polymer flood to no oil production, q=0.5 ml/min (1.2 ft/D), recovery=66% (Sor=0.29)
- Polymer rheology test (flow rate from 10 to 0.1 ml/min; oil produced at high rate and the Sor reduced to 0.11)
- Inject LSW until pressure stabilized, measure $P_{brine\ 2}$ at different flow rates;
- Calculate resistance factor: $P_{polymer}/P_{brine\ 1}$, $P_{polymer}/P_{brine\ 2}$ at the same injection rate

Test #4: HSP rheology with residual oil

- Use the same core as Test #3, flush with HSW at 30 ml/min until pressure stabilized
- Inject HSW, measure brine injection pressure (P_{brine}) at different flow rates (10-0.1 ml/min)
- Polymer rheology test (flow rate from 10 to 0.1 ml/min)
- Calculate resistance factor: Ppolymer/Pbrine at the same injection rate

The results are shown in **Figure 3.7 – 3.8**. At no oil condition, the LSP shows higher resistance factor compared with the HSP. Both the LSP and HSP show shear-thickening behavior at high flux. However, the onset of shear thickening of the LSP was observed at a significantly lower critical velocity (shear rate) compared with the HSP. This is consistent with the viscoelastic property of the polymer solutions, as the relaxation time of the LSP solution is about eight times of the HSP. When dividing the shear rate with a factor of 30, the viscosity curve of the LSP converges with the resistance factor curve at around 0.4 ft/d, which is close to the velocity in the field. However, for the HSP, the viscosity and resistance factor curves cross over at about 2 ft/d. When residual oil was present in the porous media, we also observed a higher resistance factor of the LSP compared with the HSP, and the shear thickening behavior occurred at lower flux.
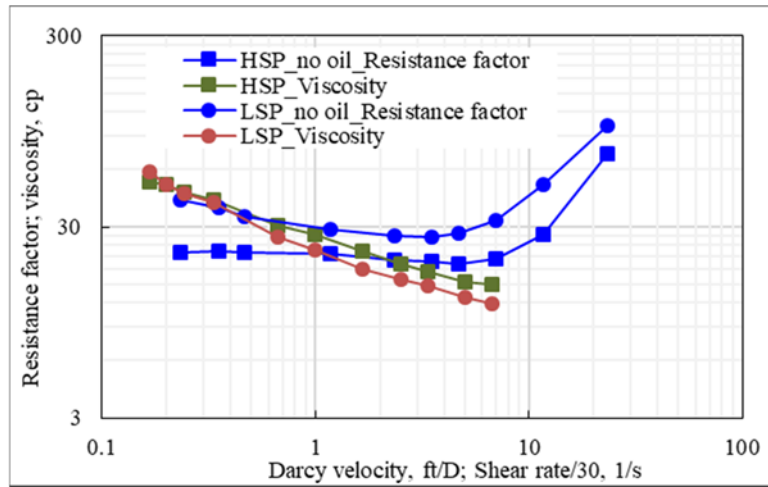
Figure 3.7: Rheology of LSP and HSP with no oil (Test #1 and Test #2).
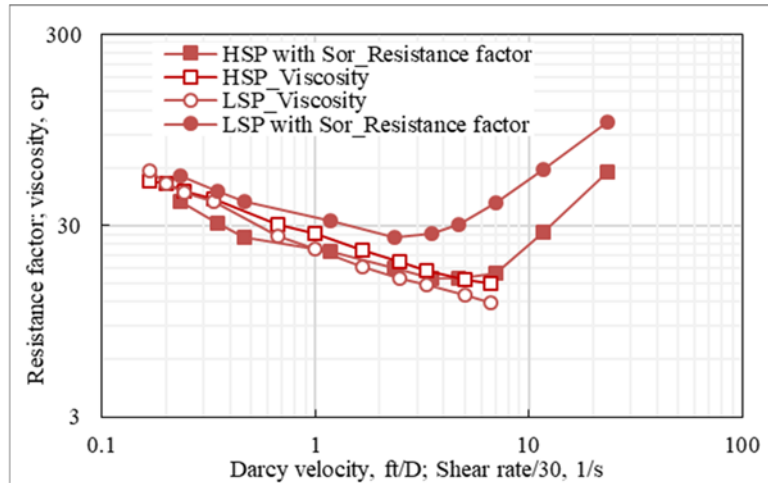
Figure 3.8: Rheology of LSP and HSP with residual oil (Test #3 and Test #4).

Simulation Studies of Polymer Flooding

The major target of simulation work in this quarter is the optimization of polymer flooding based on the polymer rheology and reservoir heterogeneity. The influence factors investigated include the flow rate, permeability ratio (Kc:Km), grids density, channel width, and polymer concentration.

Model Description

To simplify the computational complexity and to better analyze the mechanisms behind the enhanced oil recovery, we implemented a 2D conceptual model (shown in **Figure 3.9**) with similar size to the actual interested field. The model descriptions are listed in **Table 3.4**.
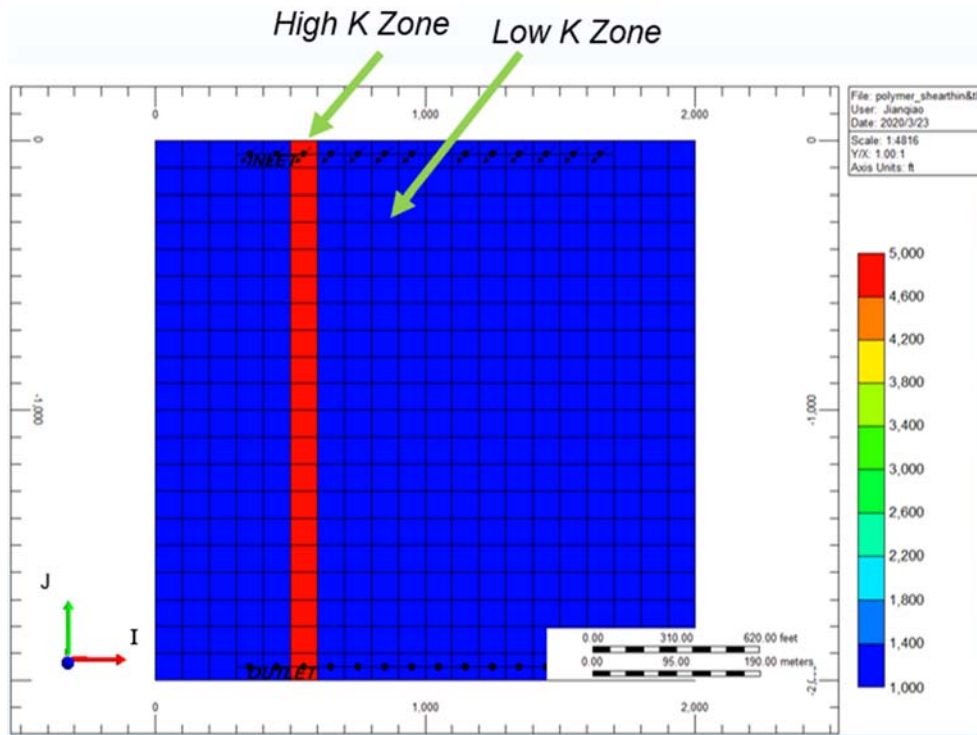
Figure 3.9: Illustration of 2D conceptual model.

Table 3.4: Base model setup.

Model Size, ft3	Model Top Depth, ft	Grids Design	K Ratio
2000*2000*10	3930	20*20*1	5:1
Channel Location	Channel Width, ft	Injector Type	Producer Type
Perf 3	100	Horizontal	Horizontal

The data of the polymer rheology is based on the literature (Seright et al., 2011). The rheology data is shown in **Figure 3.10a** (Lab Result) and **Figure 3.10b** (Fitting Result).
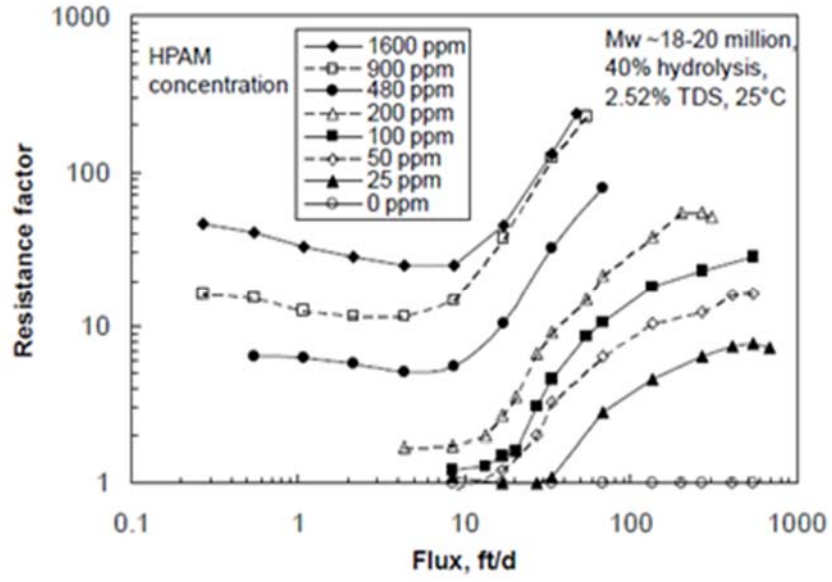
(a) Lab data
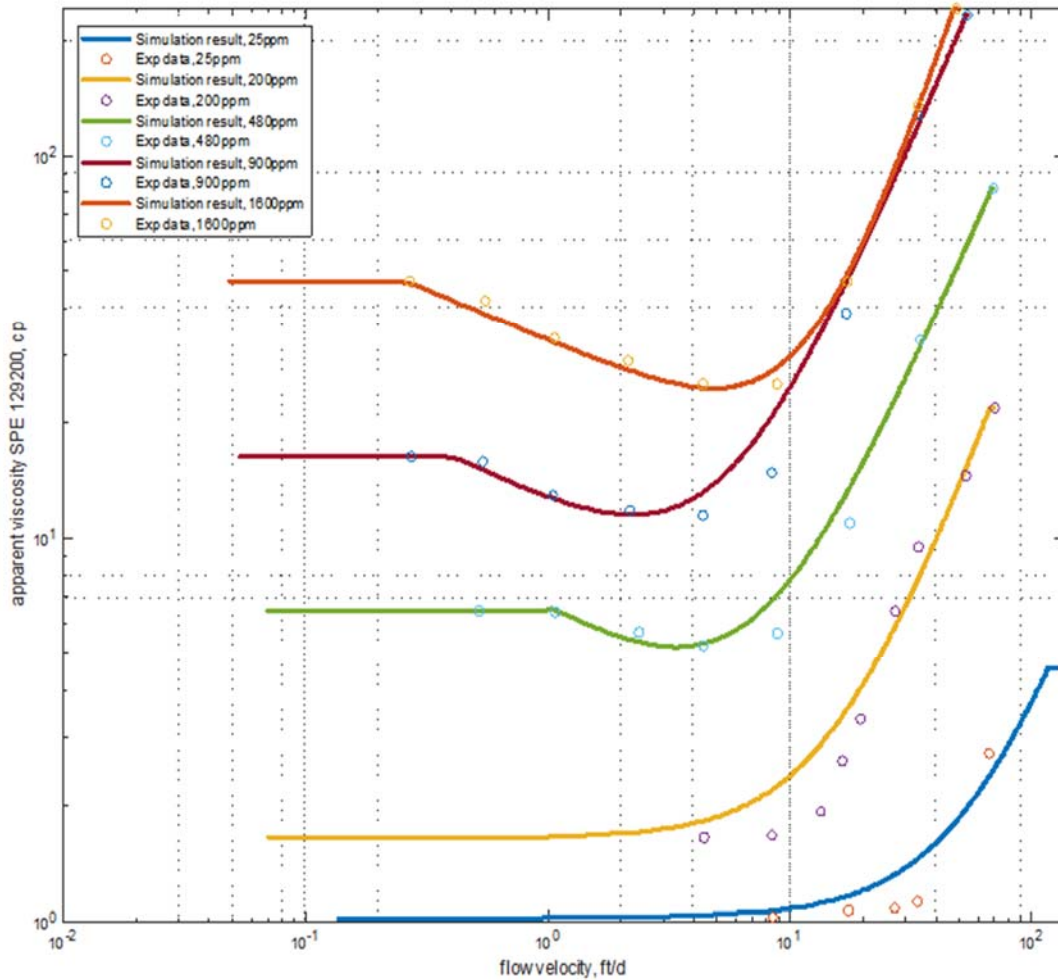
(b) Fitting data
Figure 3.10: Rheology data and fitting result.

Operations

The base case flow rate is 1500 bbls/d and the initial water flooding stops when water cut reaches 80%. Then, polymer flooding is initiated. The concerned results of polymer flooding are observed after 0.07 PV of polymer injected.

Simulation Result 1

The first sets of simulation target at the sensitivity of channel-matrix permeability ratio on oil recovery and water cut. As a result, the rheologies are assumed using the theoretical curves including three cases: no shear considered, shear thinning and both shear thinning and shear thickening. The water cut and Oil recovery factor results for three cases including K ratio = 5, 10, and 50 are shown in **Figure 3.11 – 3.13**.
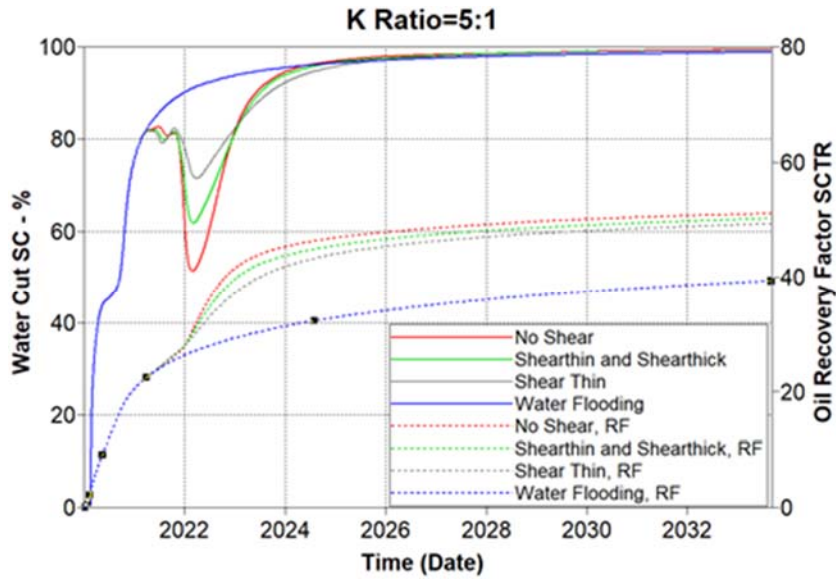
Figure 3.11: Simulation result of K ratio = 5:1.
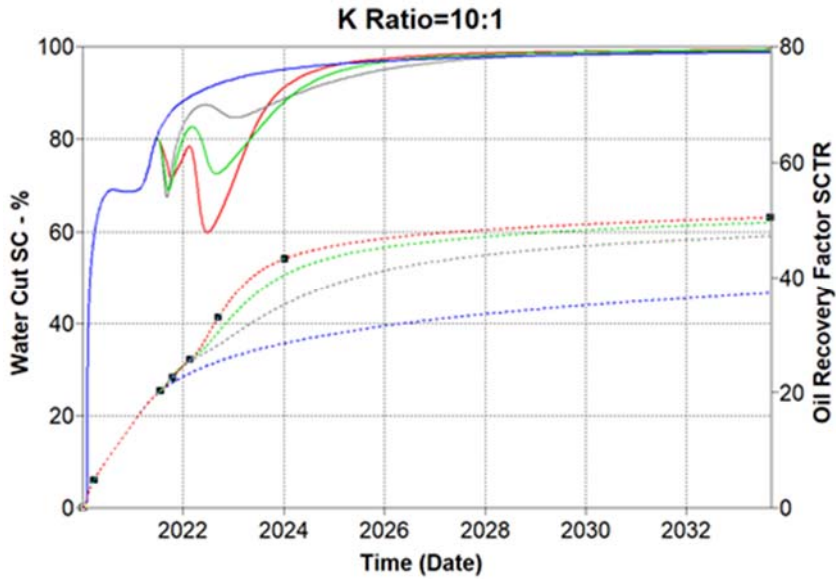
Figure 3.12: Simulation result of K ratio = 10:1.
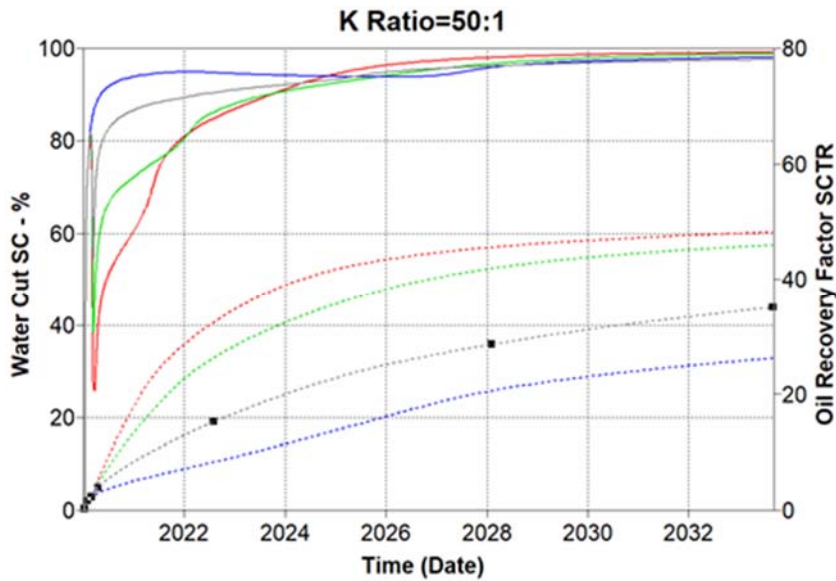
Figure 3.13: Simulation result of K ratio = 50:1.
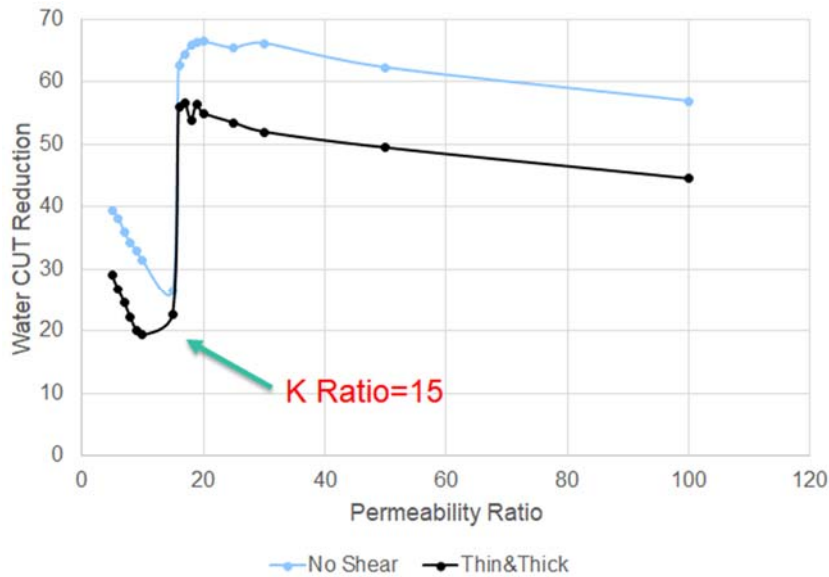
Figure 3.14: Permeability ratio effect on water cut reduction.

Discussion 1

For the first sets of simulation, the result of no shear case provides the optimal oil recovery and highest water cut reduction, followed by the case considering both shear thinning and shear thickening. This is because the velocity ratio of channel to matrix does not fall at the preferred zone for shear thinning and thickening cases. Thus, the rheology decreases the performance of polymer flooding. The other point that can be observed in the results are that the water cut reduction favors the K ratio = 50 case followed by K ratio = 5 then K ratio = 10, which are not coincident as expected. To figure out the reason, we conducted

more simulation cases that range from K ratio = 5 to K ratio = 100. The results are listed in **Figure 3.14**. Obviously, there is a sharp change when K ratio increase from 15 to 16. After further analysis, we found that the sharp change results from the polymer flooding initiation time compared with matrix water breakthrough. For cases with K ratio from 16 to 100, the polymer flooding initiates before matrix water breakthrough, which indicates much higher water cut reduction, and for cases with K ratio from 5 to 15, the polymer flooding initiates after matrix water breakthrough, which conducted much lower water cut reduction. Moreover, increased permeability ratio will decrease the effect of polymer flooding in terms of water cut reduction if we only consider cases before or after matrix water breakthrough, separately.

Simulation Result 2

For second sets of simulation, we target at the influence of different concentration of polymer on the injection profile improvement. Also, three types of K ratios are investigated. The oil recovery and water oil ratios are shown in **Figure 3.15 – 3.17**.
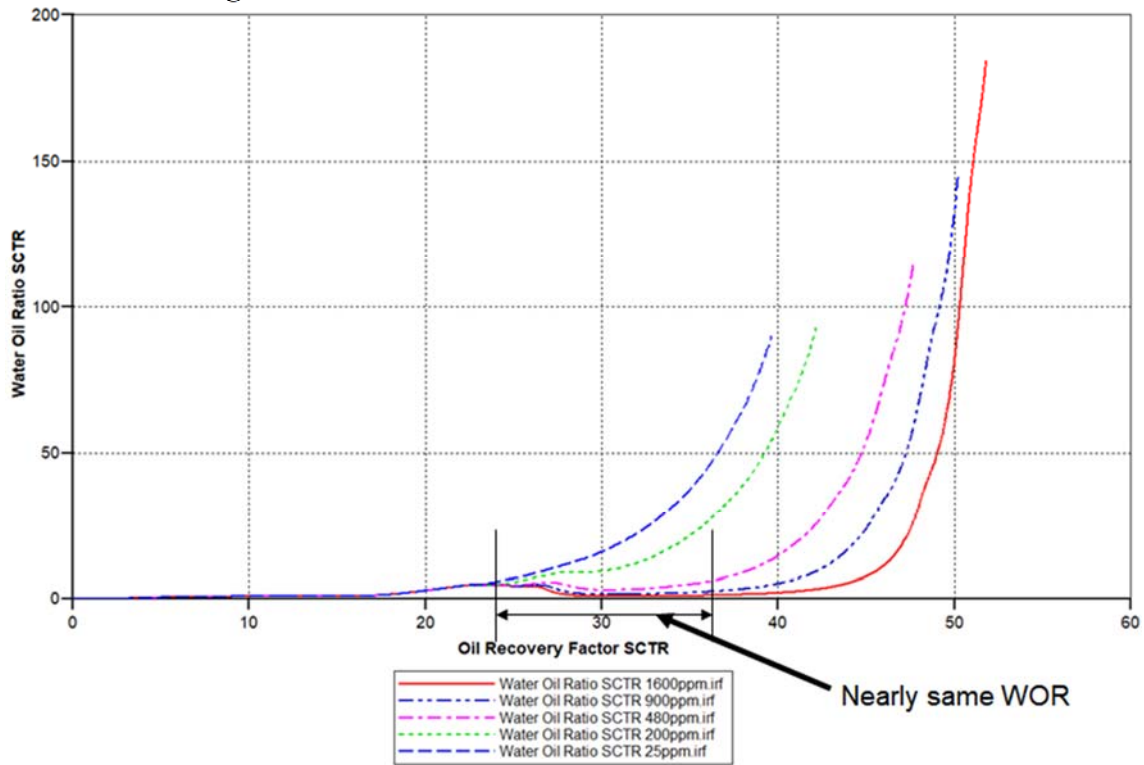
Figure 3.15. K Ratio = 5 oil recovery factor and WOR.

27
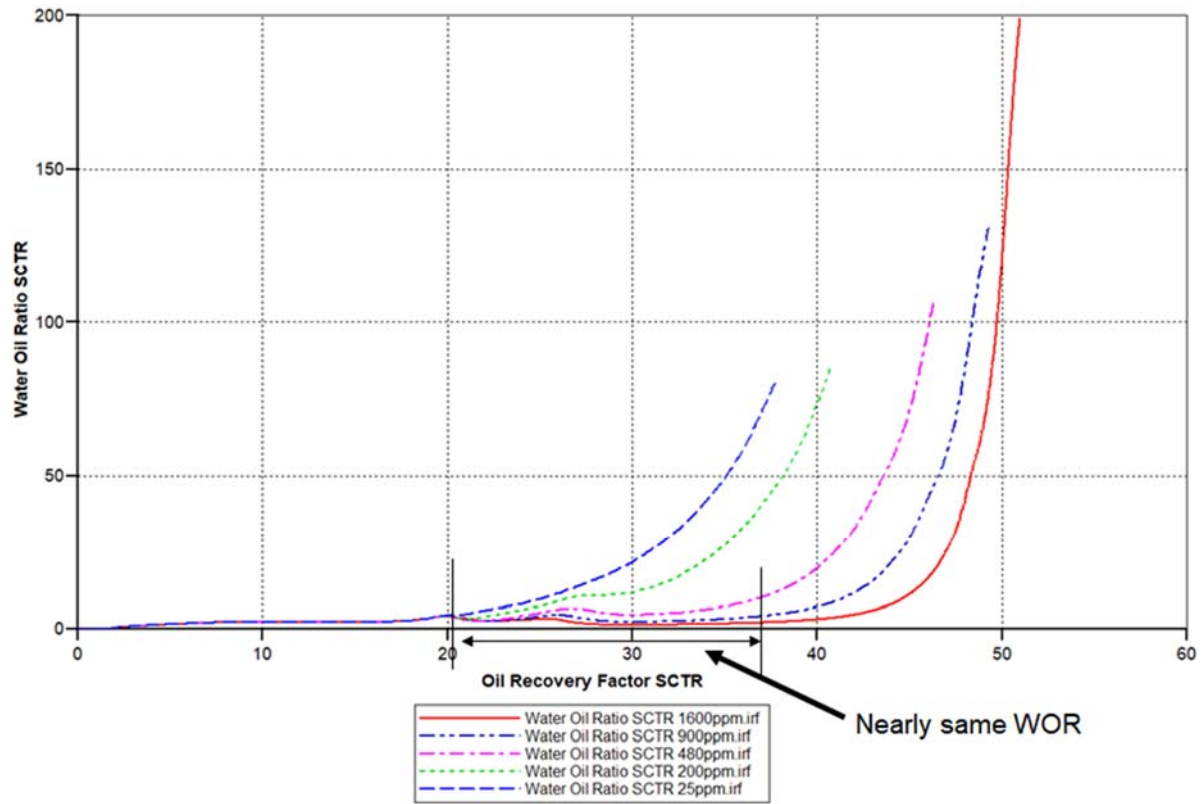
Figure 3.16. K Ratio = 10 oil recovery factor and WOR.
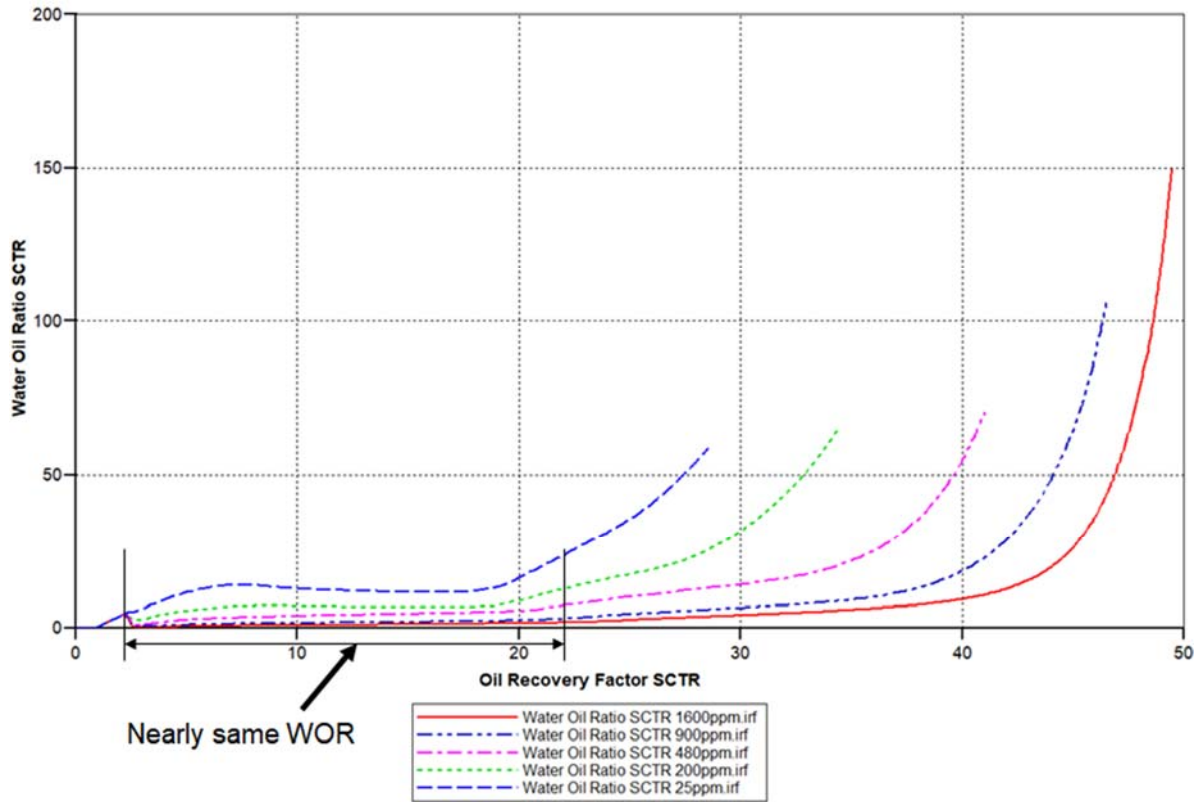
Figure 3.17. K Ratio = 50 oil recovery factor and WOR.
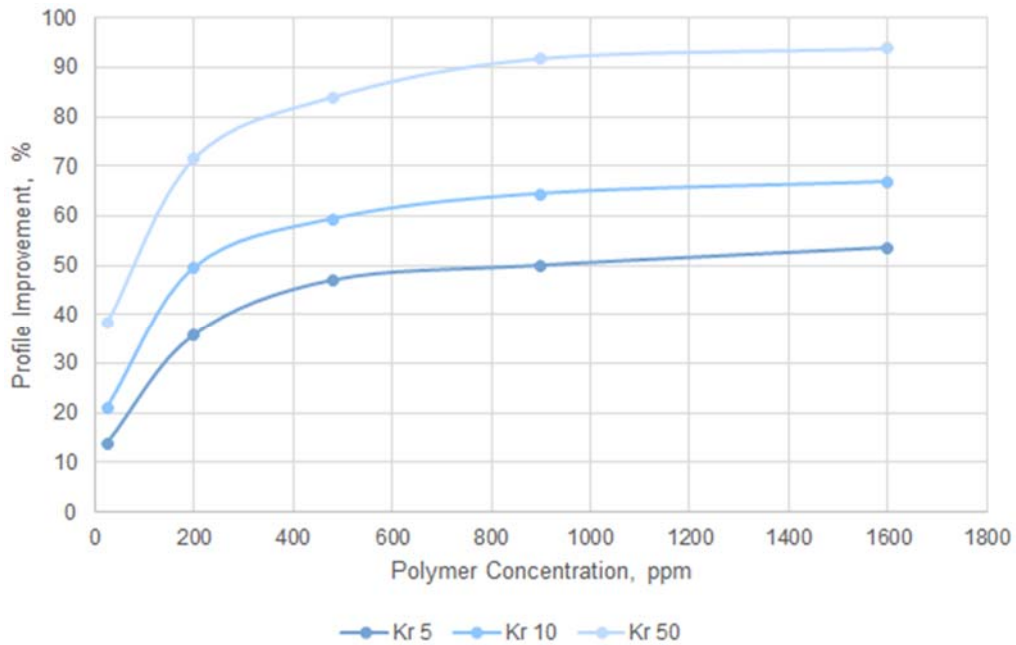
Figure 3.18. Injection profile improvement for five types of polymers.

29

Discussion 2

From the results of oil recovery and WOR, we can conclude the following:

1. Higher concentration polymer can provide higher oil recovery.
2. Higher concentration polymer has the higher final WOR.
3. After polymer flooding initiated, for a long period, the WOR can be very similar for cases with 480ppm, 900ppm and 1600ppm.
4. The similar WOR period increases with higher K ratio.

To further analyze the effect of concentration and rheology on polymer performance, we concluded the injection profile improvement shown in **Figure 3.18**. We can observe that the higher the concentration, the better is the improvement in the injection profile. However, when polymer concentration is higher than 900 ppm, there is limited benefit in terms of profile improvement. As a result, it is quite possible that higher concentration of polymer over 900 ppm may not provide much better improvement for both oil recovery, WOR and profile improvement than the concentration around 900 ppm.

   Activity is ongoing.

● Task 4.0 - Reservoir Simulation Studies for Coreflooding Experiments and Optimization of Field Pilot Test Injection Strategy

Activities and progress during March 2020 through May 2020, completed by UND include:
  • Coreflooding phase behavior simulation to investigate the relationship of pore volume injection of brine and residual resistance factor using lab-scale model.
  • Shear rate vs viscosity behavior history match for the NB # 3 with 2183 md permeability.
  • Incorporated an average viscous fingering number to the field-scale model history match using Milne Point field data.
  • Studies of vertical permeability effect on water-cut change.
  • Incorporated random permeability function from Petrel (geological model) to the field-scale model to observe water-cut history match.

4.1 Core Flooding Behavior Investigation Using Lab-Scale Models

4.1.1 Numerical simulation to investigate the relationship of pore volume injection of brine and residual resistance factor

Two sand packs were simulated to investigate the residual resistance factor (RRF) changes as brine injection volume increases. The parameters and polymer retention are listed in **Table 4.1** for the sand pack OA #2, and NB #3. Eq. 4.1 was used for the RRF estimation based on the pressure changes, assuming the flow rates and all other injection conditions are identical. During simulation, polymer injection was before brine injection.

Table 4.1: Sand pack parameters for lab-scale simulation.

Sand	Polymer	k_{abs}, mD	k_w at S_{or}	Pack length, cm	Injected PV of polymer	Polymer retention, µg/g

OA#2	3630	470	20	30.48	6.4	65
NB#3	3630	4100	4100	30.48	5.4	30

$$RRF_{(n)} = RRF_{(n-1)} \bullet \left(\Delta P_{(n)} / \Delta P_{(n-1)} \right)$$

(4.1)

Where, $RRF_{(n)}$ and $\Delta P_{(n)}$ are the residual resistance factor and pressure drops in the current time step, respectively; $RRF_{(n-1)}$ and $\Delta P_{(n-1)}$ are the residual resistance factor and pressure drops in the previous time step, respectively.

Figures 4.1 and **4.2** show the simulation results on the relationships of injected pore volume vs polymer resistance factor. As illustrated in the two figures, the residual resistance factors were approximate to 2.3 and 1.0 for OA#2 and NB#3 sands with low polymer retentions (65 and 30 µg/g), respectively. The history matches by lab-scale simulations and laboratory experimental results show good agreement. As seen in **Figures 4.1** and **4.2**, the dotted red spots (**Figure 4.1**) and blue triangles (**Figure 4.2**) were the results from laboratory experiments, the other various curves were the results of numerical simulation. The dashed lines in the two figures were extrapolations due to the challenges of opening very large size files of simulation results associated with large injected pore volumes (over 20 PV).

Since the numerical simulation agreed with the laboratory research, these two values of residual resistance factors are suggested to be applied to the field-scale models.
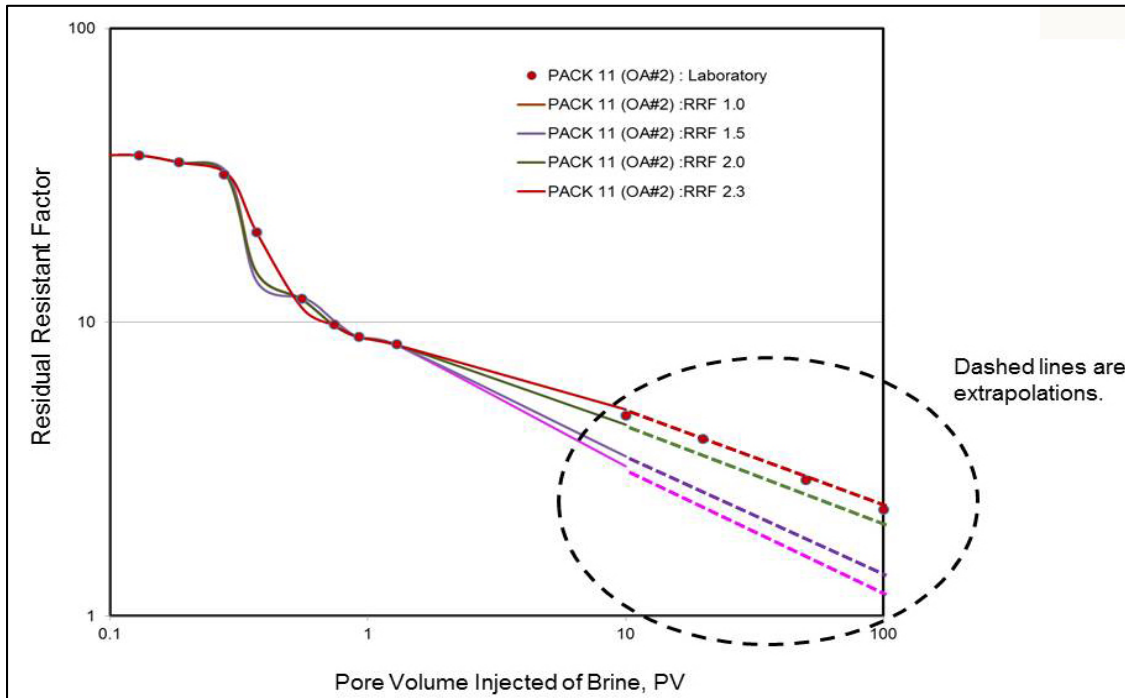
Figure 4.1: Residual resistance factor vs. brine injection in pore volume of OA #2.
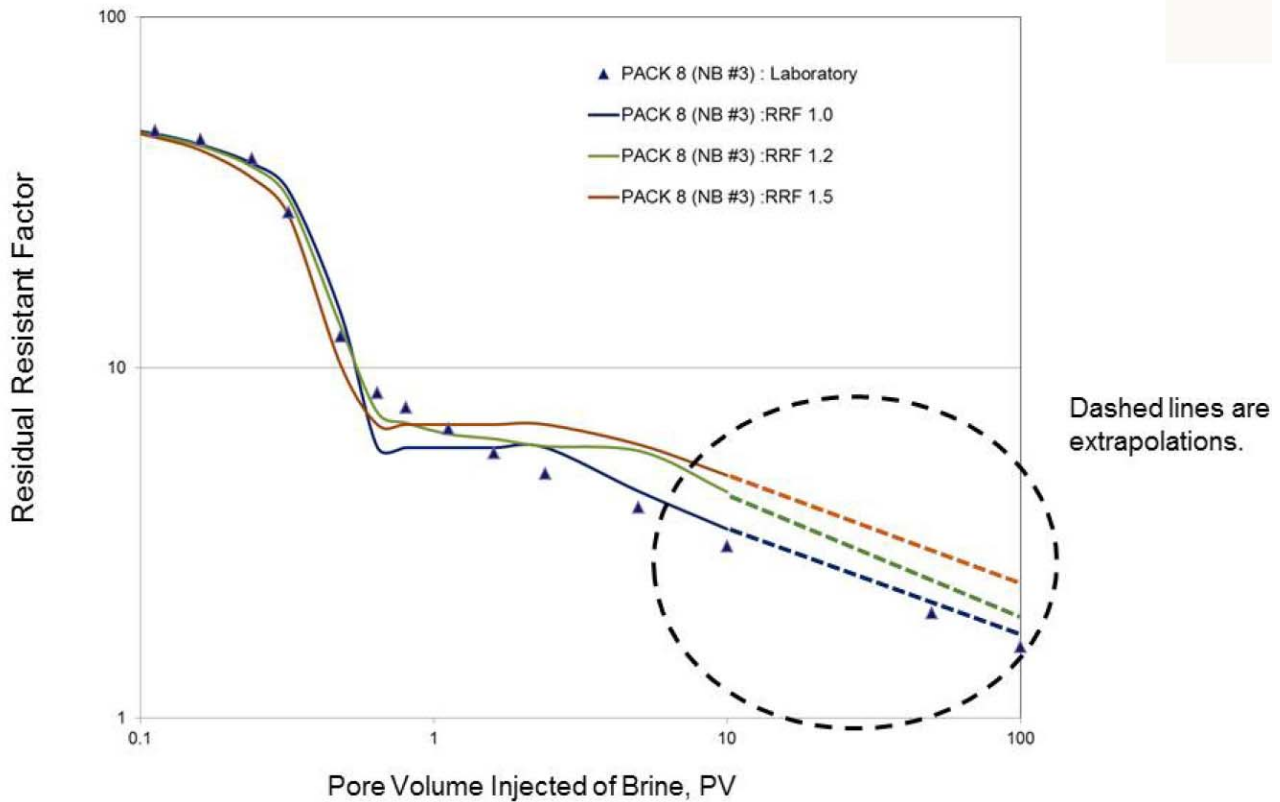
Figure 4.2: Residual resistance factor vs. brine injection in pore volume of NB #3.

4.1.2 Shear rate vs. polymer viscosity change behavior simulation

One sandpack NB #3 was used for simulating the shear rate behavior vs polymer viscosity change. All other conditions of the sandpack were same as the NB #3 in **Table 4.1** except the permeability of the sandpack was 2183 md. In order to simulate the viscosity change, two shear effect rheology were used during simulation: SHR and SHV. SHR represents the polymer viscosity depends on the shear rate change, and SHV represents the polymer viscosity depends on the Darcy's velocity.

Figures 4.3 and **4.4** illustrate the polymer viscosity change as functions of SHR and SHV at various polymer concentrations from 600 ppm to 1750 ppm. The three sets of green triangles, blue dots, and purple diamonds were the laboratory experimental data sourced from NMT, and three solid curves with green, blue, and purple curves were the simulation results for the model of viscosity as a function of shear rate rheology. The corresponding dashed curves were the simulation results using the function of SHV – viscosity as a function of Darcy's velocity. As observed from the figures, with a 2183 mD native NB#3 sand, Darcy velocity was about 1/20 (expressed in ft/day) of shear rate in a viscometer (expressed in s^{-1}).

Based on the simulation, we believe the numerical simulation using the lab-scale models agreed with the observation from the laboratory studies for the sandpack NB#3 with 2183 md permeability. More work on simulation with different permeability will be reported in the next quarter.

On the other hand, as **Figure 4.4** suggests, for a 1750 ppm polymer (3630S), viscosity at 1 s^{-1} was about twice that at 7.3 s^{-1} as experimental results from laboratory. In other words, the standard utilization in industry of using 7.3 s^{-1} shear rates to anticipate the viscosity change in the reservoir, might be not be appropriate for the Milne Point reservoir.
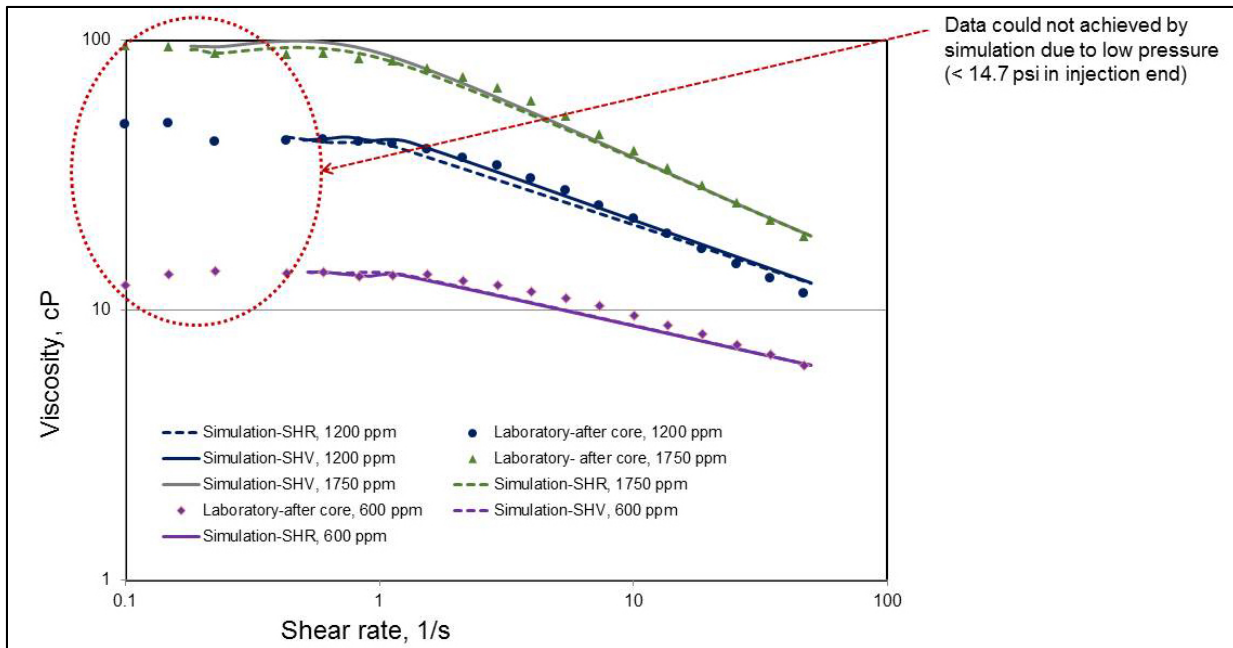
Figure 4.3: Polymer viscosity vs. shear rate of NB #3 (2183 md).
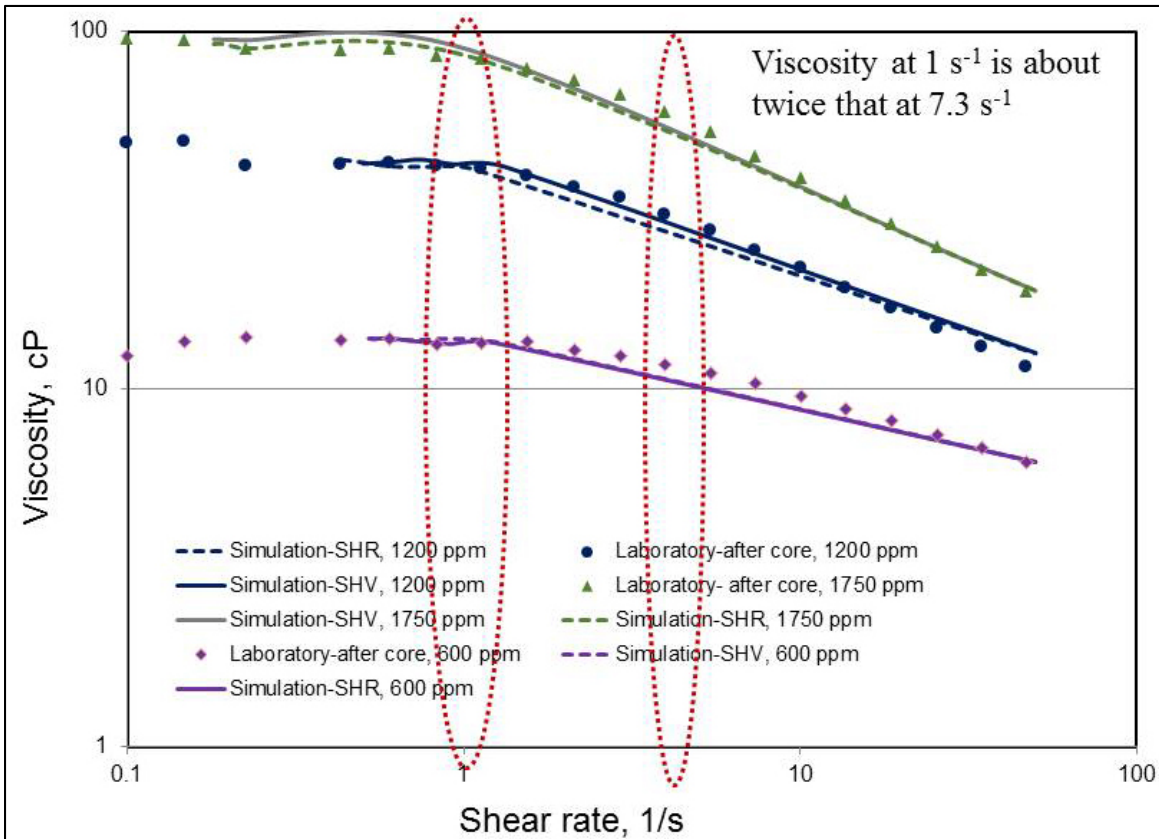
Figure 4.4: Polymer viscosity at 1 s^{-1} of shear rate is about twice at 7.3 s^{-1} of shear rate for NB #3.

4.2 Field-Scale Models for Production History Match

In order to obtain more accurate low water-cut (15% to 30% from 70%) in history matching for the ultimate purpose of polymer performance prediction, three approaches were explored using field-scale models at UND: *a.* modified the proportion of vertical permeability and horizontal permeability; *b.* incorporation of viscous fingering number to each grid block in the simulation model, and *c.* a random permeability function from geological modeling in PETREL was integrated with CMOST. Results from the approach "*c*" will be presented in next report.

4.2.1 Permeability differential (between vertical and horizontal directions) effects on water-cut history match

From a geological view, for the different types of accumulation of sediment of sandstone, the relation between vertical permeability (K_v) and horizontal permeability (K_h) varies with the sediment types (quartzose type, greywacke type, and arkose type). Among them, the greywacke type of sediment accumulation is characterized with a low oil recovery during primary production but exhibits excellent production during secondary or tertiary recovery. Since the exceptional low water-cut stage has been stable and lasted for nearly 10 months in the Milne Point polymer project with good production, we believe the target reservoir of polymer flooding belongs to this sediment accumulation. In this type of accumulation, the permeabilities vary considerably over short distances, and the K_v is usually much lower

34

than K_h. Therefore, reduced permeability proportions between K_v and K_h were used for history matching in the field-scale model and its effect on water-cut change were studied.

Figures 4.5 and **4.6** present the simulation results using various permeability differentials (between K_v and K_h) from 0.1 to 0.7. As illustrated, the most favorable agreements in water-cut history of Well #J27 and #J28 in the low water-cut stage (middle of 2019 to May 2020) was K_v: K_h = 0.25 (red curves).
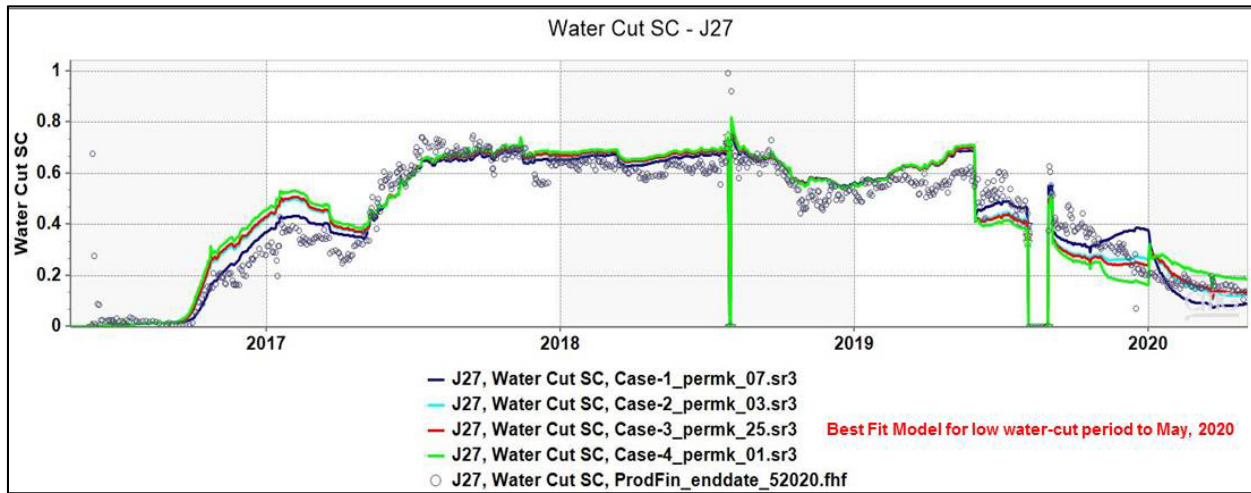
Figure 4.5: J-27 water-cut history matches at varied permeability differential (K_v to K_h).
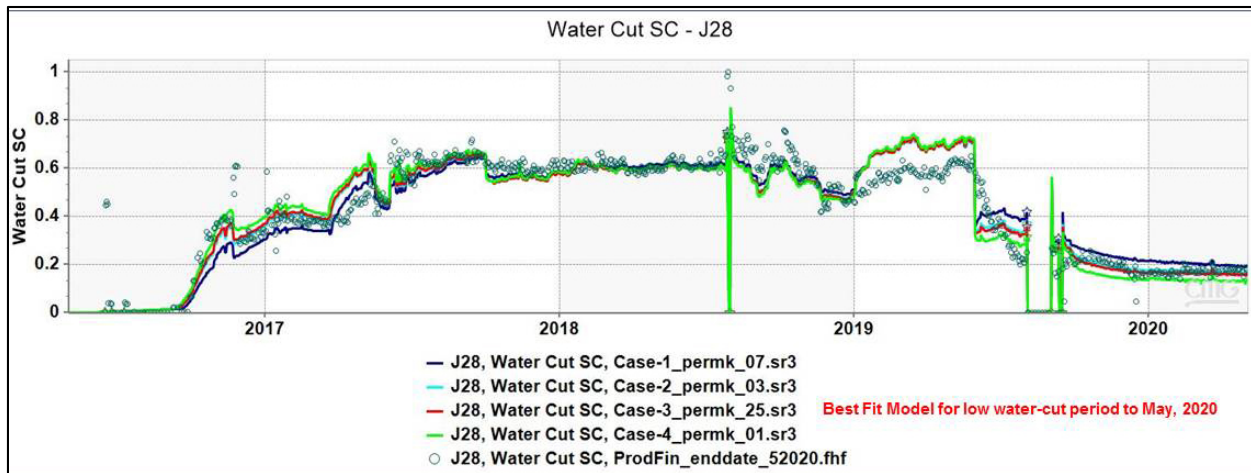
Figure 4.6: J-28 water-cut history matches at varied permeability differential (K_v to K_h).

4.2.2 Viscous fingering number incorporation

Considering a possibility of viscous fingering issue, a viscous fingering number which was referred to in Luo's research (Luo, *et al* 2017) was calculated using Milne Point reservoir condition and production data (**Table 4.2**), and applied to the field-scale model for history matching. Eqs. 4.2 to 4.8 were employed for A_c (characterized cross-section number) estimation, as well as the parameter correlations (α_e, β_1 and

β_2) for the relative permeability curves in our studied field-scale model.

$$N_{vf} = \mu_r^2 N_c A_c k^{-1} \tag{4.2}$$

$$N_c = \frac{\mu_w \mu_t}{\sigma} \tag{4.3}$$

$$\lambda_e = \alpha_e \overline{S}_w^{\beta_1} \tag{4.4}$$

$$\lambda_b = (1 - \alpha_e) \overline{S}_w^{\beta_2} \tag{4.5}$$

$$\lambda_o = 1 - (\lambda_e + \lambda_o) \tag{4.6}$$

$$k_{rw,e} = \lambda_e k_{rw}^0 (\overline{S}_w)^{n_w} \tag{4.7}$$

$$k_{ro,e} = \lambda_e k_{ro}^0 (1 - \overline{S}_w)^{n_o} + \lambda_o k_{ro}^0 \tag{4.8}$$

Where, N_{vf} is the viscous-fingering number, μ_r is the viscosity ratio, μ_t is the total velocity of water and oil phase (m.s^{-1}), N_c is a capillary number, A_c is the square of diameter of the core (m^2), k is the permability (m^{-2}), σ is the water-oil interfacial tention (N.m^{-1}), λ_e, λ_b, λ_o are the fraction of the cross section occupied by the effective finger, the bypassed oil region, and the oil signle-phase region, respectively; α_e, β_1 and β_2 are the maximum cross section of the effective finger, the growth rate exponent of λ_e, the growth rate exponent of λ_b, respectively.

Table 4.2: Parameters used for viscous finger number incorporation.

Water viscosity, μ_w	1.1	cP
Velocity of total water and oil, u_t	vary in each grid and each time step	ft/day
Characterized Cross-section number, A_c	10E-8	ft^2
IFT, σ	25	dyne/cm
Oil-water viscosity ratio, μ_r	200	
k (Permeability)	(vary in each grid block)	md
N_{vf} (Viscous Fingering number)	(vary in each grid block)	

An example of Well # J28 of water-cut simulation after viscous fingering incorporation is shown in **Figure 4.7**. In **Figure 4.7**, since the characterized cross section number A_c is an important factor for Luo's viscous fingering model, A_c =10E-8 was found to provide a basic match of the production data after experiments through CMOST, but not a very good agreement in the later stage of water cuts compared to the results without viscous fingering model incorporation. On the other hand, even though the flow velocities varied vs time step and grid cells during simulation, permeability varied at each grid. The A_c

we used was a constant during simulation because the CMG simulator has no provision for a dynamic A_c input with dynamic relative permeability curves during simulation. Therefore, we divided the permeability and velocity domains into different regions and ran CMG manually. Consequencely, we could not obtain an idealized history match of water-cuts in the later stage of 2019, and we decided to abandon this approach (viscous fingering number incorporation).
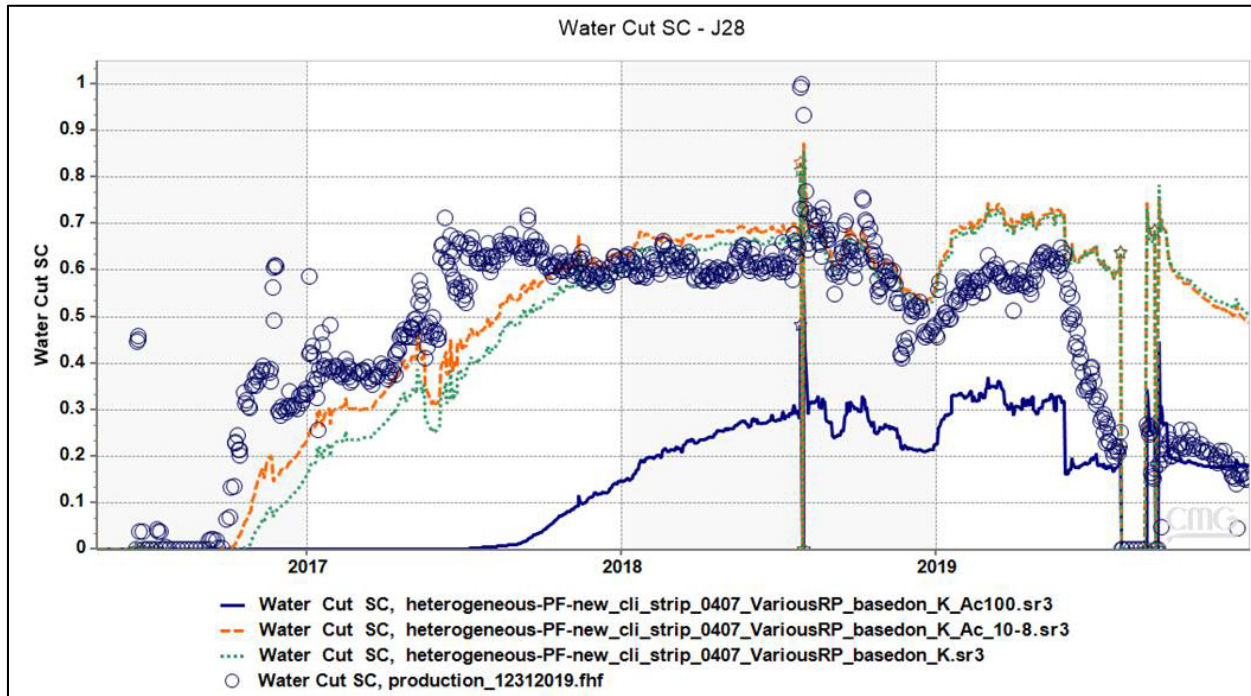
Figure 4.7: History match with viscous fingering model incorporation for well #J28.

In this quarter, UAF's work focuses on introducing high permeable channels into the heterogeneous model and layercake model to history matching the water cut of polymer flooding, which is reported below.

Heterogeneous model with high permeable channels

To improve history matching results, two high permeable channels are set between the adjacent injection and production wells in the heterogeneous model, resulting in six channels in total, as shown in **Figure 4.8**. The injection wells are constrained to the water injection rates, while the production wells are constrained to the oil production rates in the reservoir simulation model. The transmissibility multipliers and widths of the high permeable channels are manually tuned with time to history matching the water cut curves. The production history used to tune the reservoir simulation model is extended to December 31, 2019 by collecting new production data.

(a) Channel in the layer #1   (b) Channel in the layer #3

(c) Channel in the layer #4   (d) Channel in the layer #6

(e) Channel in the layer #8
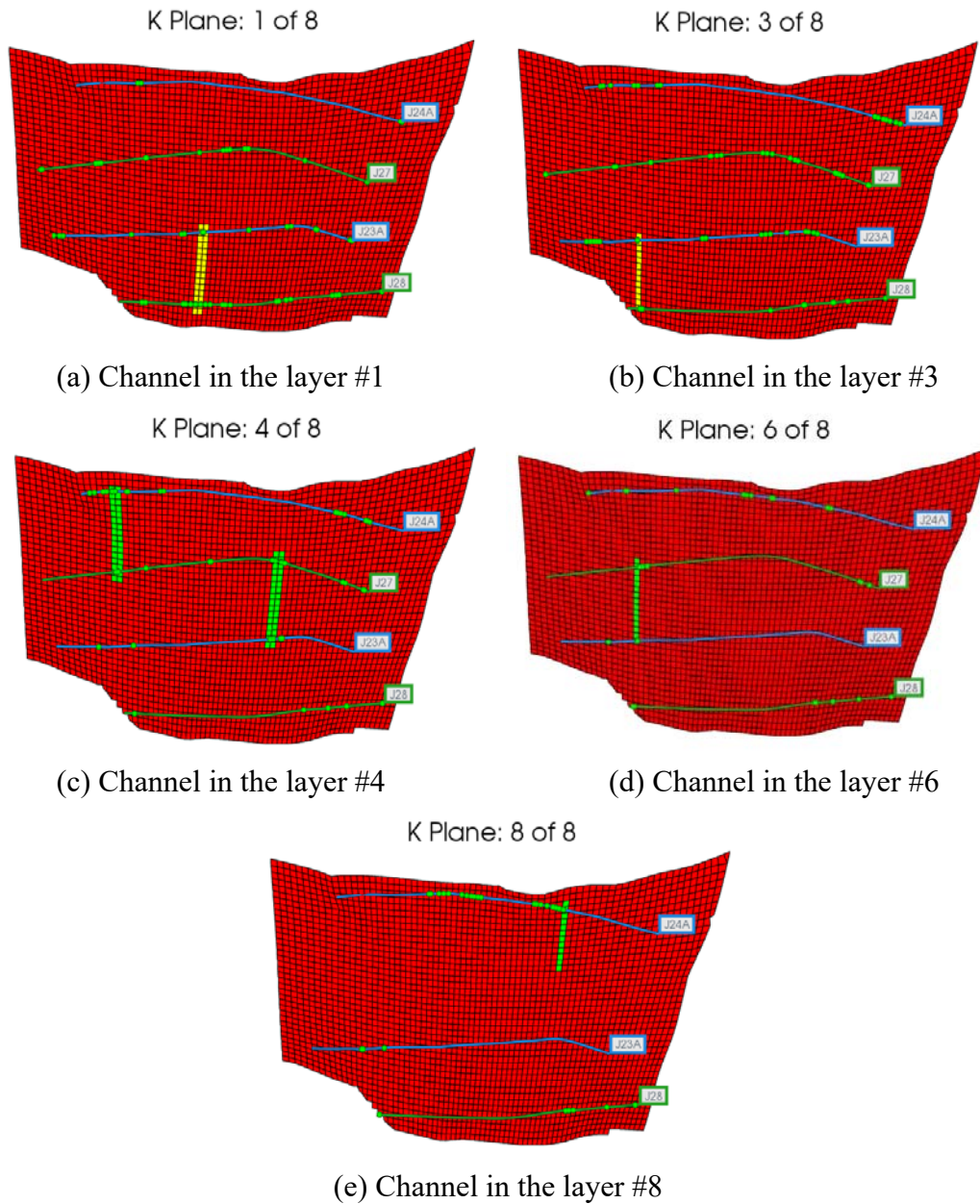
Figure 4.8: Location of high permeable channels in the reservoir model.

History matching results

The optimal history matching results of water cut for two production wells are presented in **Figure 4.9**. As can be seen, the simulated water cut curves of two production wells are consistent with the observations during the waterflooding period. During the polymer flooding period, the transmissibility multipliers of six high permeable channels are set to the default value 1, which indicates that the high permeable channels have been plugged, to reduce the water cut. However, the water cut curves of two

production wells are still larger than the actual production data from February to December 2019. To decrease the water cut in polymer flooding stage, a new set of relative permeability curves with lower water relative permeability is used in the reservoir simulation model.
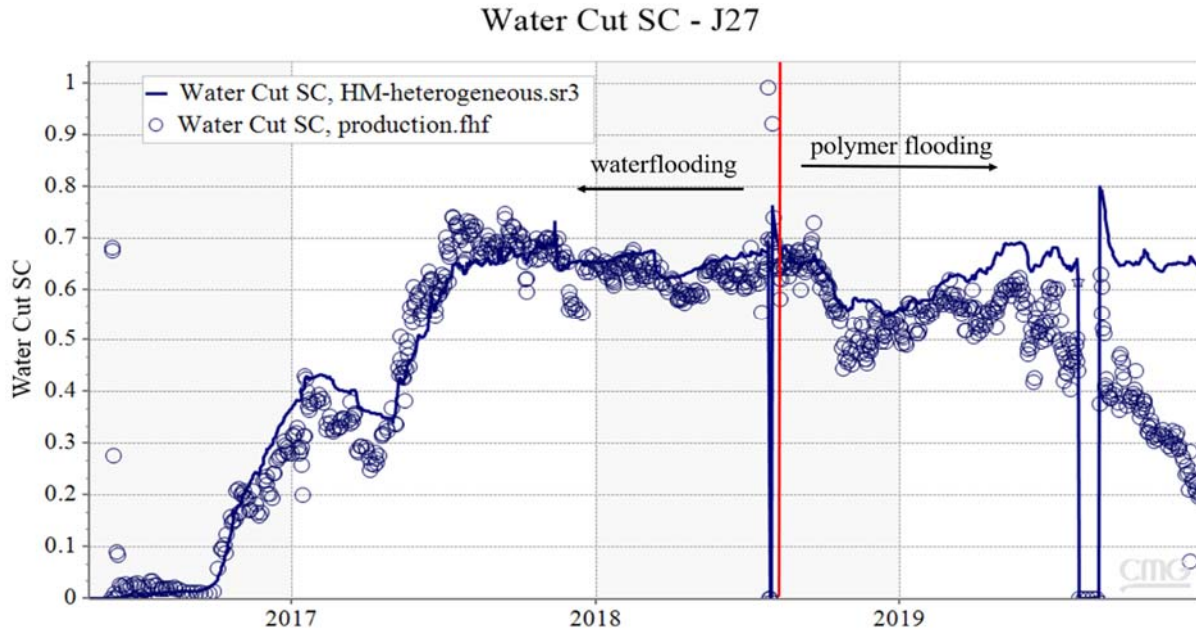
(a) Water cut of producer J27
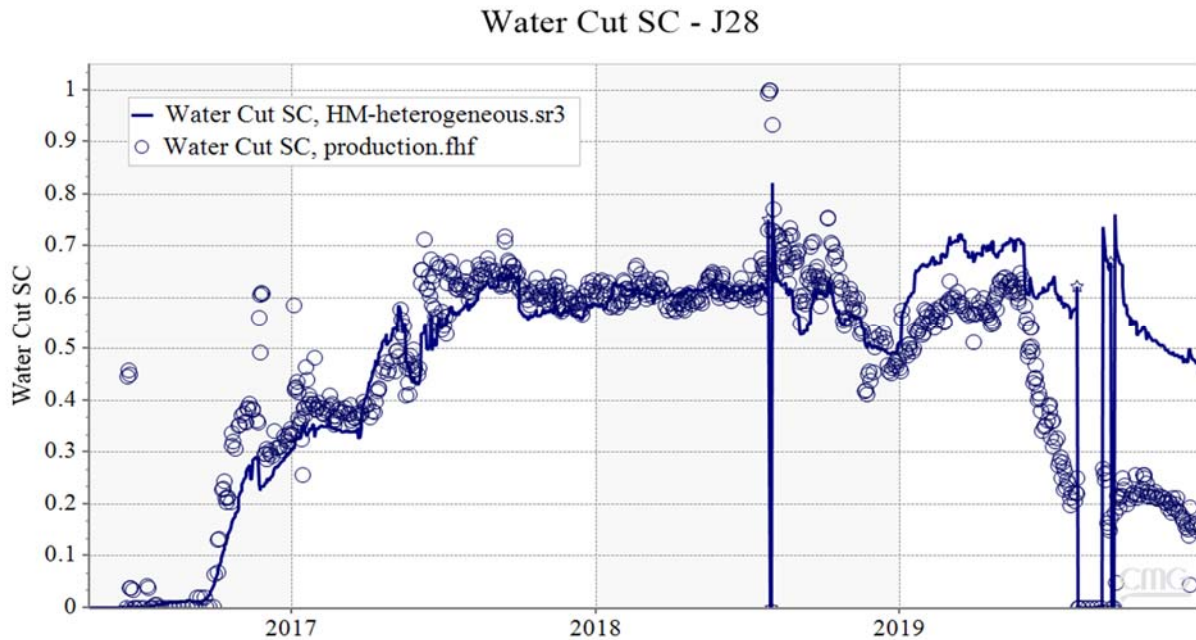
(b) Water cut of producer J28

Figure 4.9: History matching results of water cut for two producers.

New relative permeabilities. The new set of relative permeability curves, as shown in **Figure 4.10**, is generated using the power law model. Compared with the original oil/water relative permeability curves, the endpoint of water relative permeability decreases from 0.181 to 0.05. The transmissibility multipliers of six high permeable channels are manually retuned with time to history matching the water cut curves using the new reservoir simulation model. And the updated transmissibility multipliers of six high permeable channels are listed in **Table 4.3**.
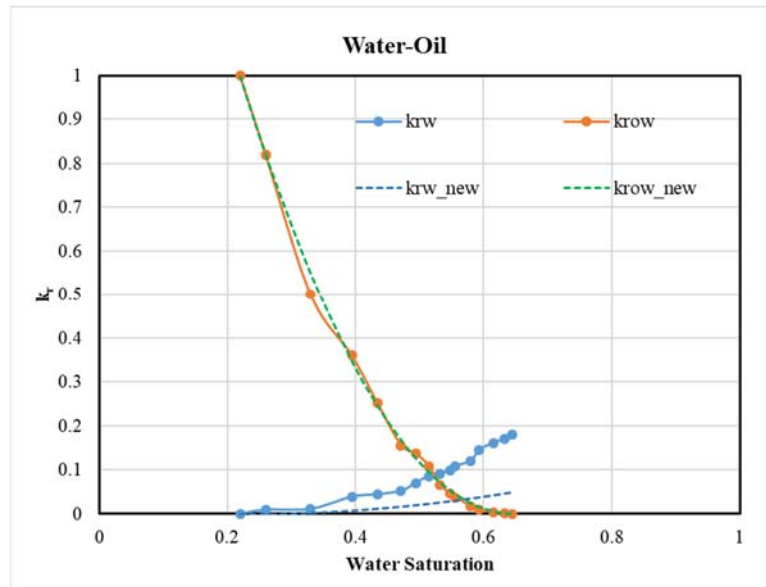
Figure 4.10: Oil/water relative permeability curves.

Table 4.3: Updated transmissibility multipliers of six high permeable channels.

	Sep 1, 2016	Jan 1, 2017	May 1, 2017
Channels between J23A and J28	8	12	20
Channels between J23A and J27	20	30	40
Channels between J24A and J27	20	30	40

The optimal history matching results of water cut for two production wells are presented in **Figure 4.11**. The blue line represents the history matching result using the original relative permeabilities, and the green line represents the history matching result using the new relative permeabilities. It can be seen that, during the waterflooding period, the history matching results agree with the actual production data by tuning the transmissibility multipliers of the high permeable channels whether the water relative permeability is large or small. During the polymer flooding period, the water cut with lower water relative permeability decreases considerably from September 2018 to July 2019. However, the water cut is still larger than the observations from September 2019 to December 2019. The history matching results of water cut cannot reproduce the actual water production profiles by employing the heterogeneous reservoir model with high permeable channels.
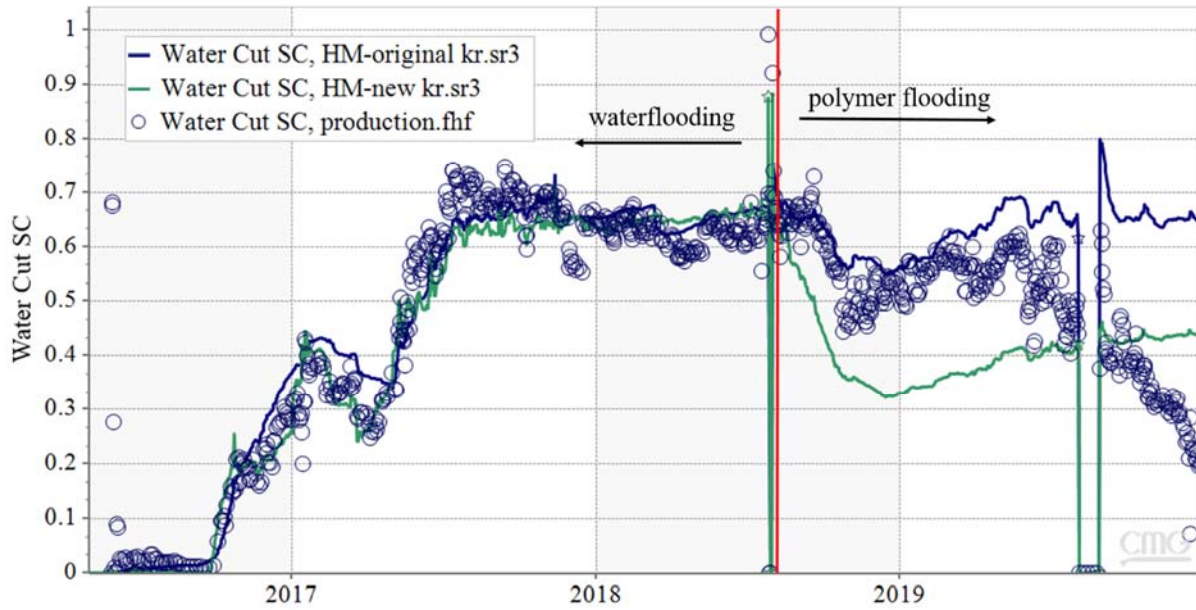
(a) Water cut of producer J27
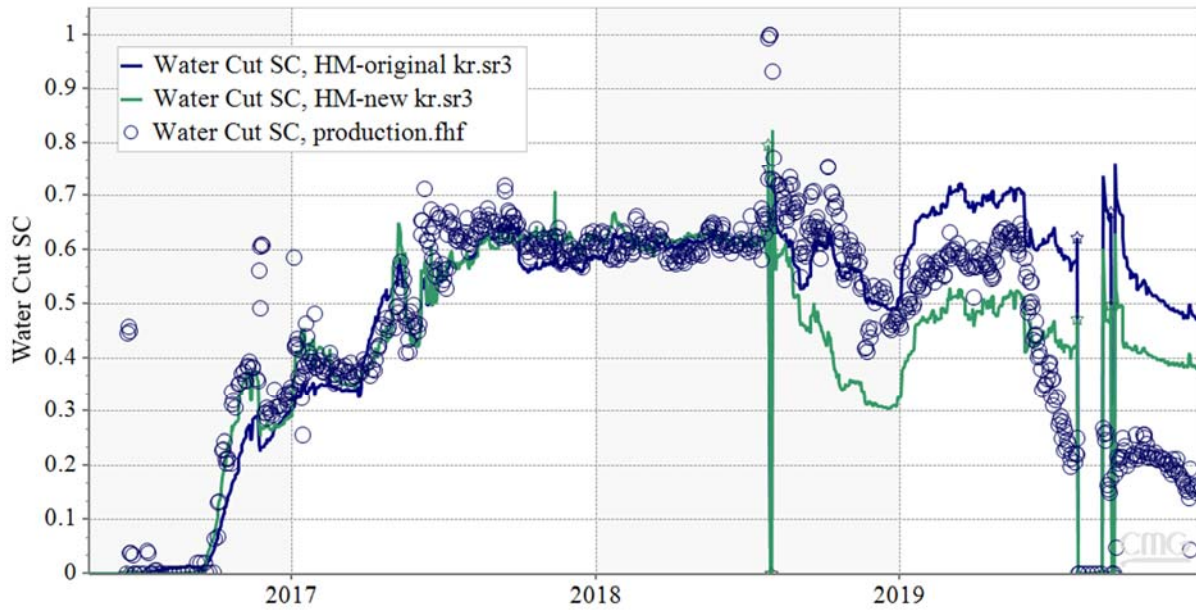
(b) Water cut of producer J28

Figure 4.11: History matching results of water cut for two producers.

Layercake model with high permeable channels

To obtain better history matching results, layercake model is employed to conduct the history matching process. The porosity and permeability of each layer in the layercake model are listed in **Table 4.4**. The region between injection wells and production wells is divided into six stripes in each layer, as shown in **Figure 4.12**, resulting in 48 stripes in the whole reservoir simulation model. The injection wells are constrained to the water injection rates, while the production wells are constrained to the oil production rates during the reservoir simulation process. The transmissibility multipliers of all stripes are tuned with time to history matching the water cut and liquid production rate using CMOST. In the history matching process, the historical production data is divided into five parts. The transmissibility multipliers are tuned at the beginning of each part and the production data of five parts is history matched sequentially.

Table 4.4: Porosity and permeability of layercake model.

	Layer #1	Layer #2	Layer #3	Layer #4	Layer #5	Layer #6	Layer #7	Layer #8
Porosity	0.3464	0.3474	0.3495	0.3491	0.3527	0.3470	0.3472	0.3423
Permeability (mD)	1791	1958	2000	1826	1935	1668	1572	1510
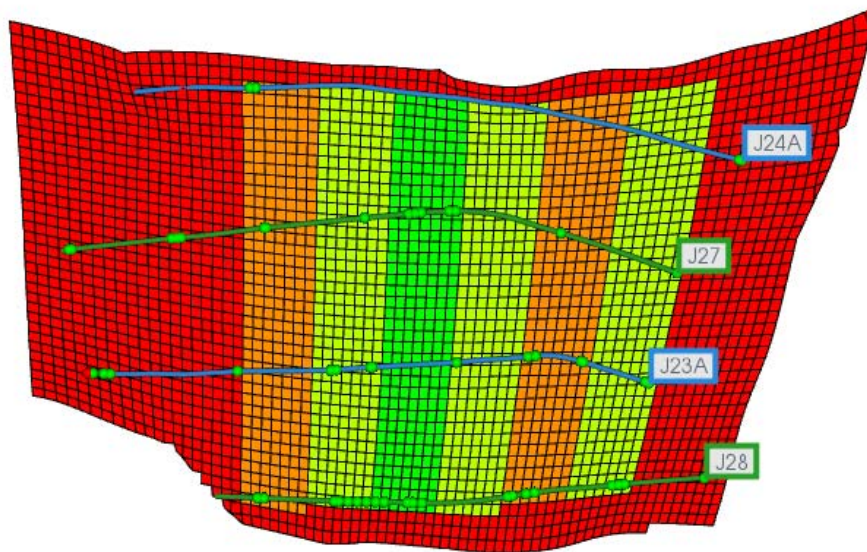


Figure 4.12: Location of six stripes in each layer.

History matching results

The optimal history matching results of water cut for two production wells are presented in **Figure 4.13**. It can be found that the history matching results have been improved compared with the results obtained from the heterogeneous model. The water cut curves of two production wells obtained from the layercake model with updated transmissibility multipliers agree with the actual production data during the waterflooding period. The simulated water cut of production well J27 is consistent with the observations

42

during the polymer flooding period. However, the water cut of production well J28 cannot reproduce the decreasing trend from May to December 2019.
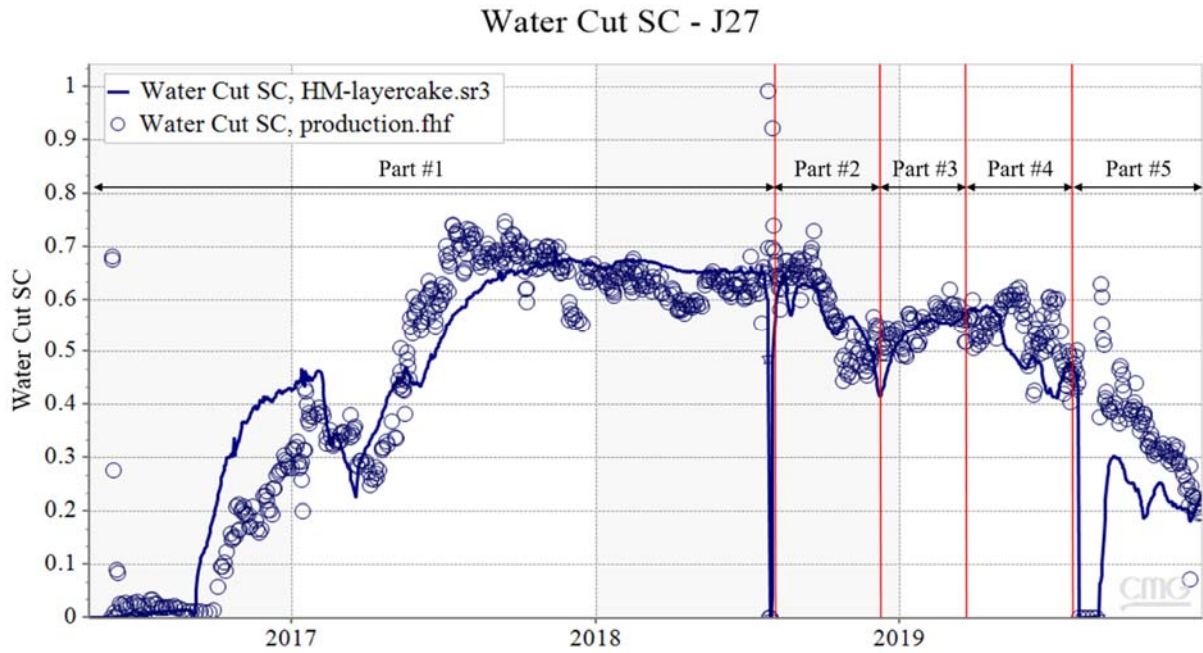
(a) Water cut of producer J27
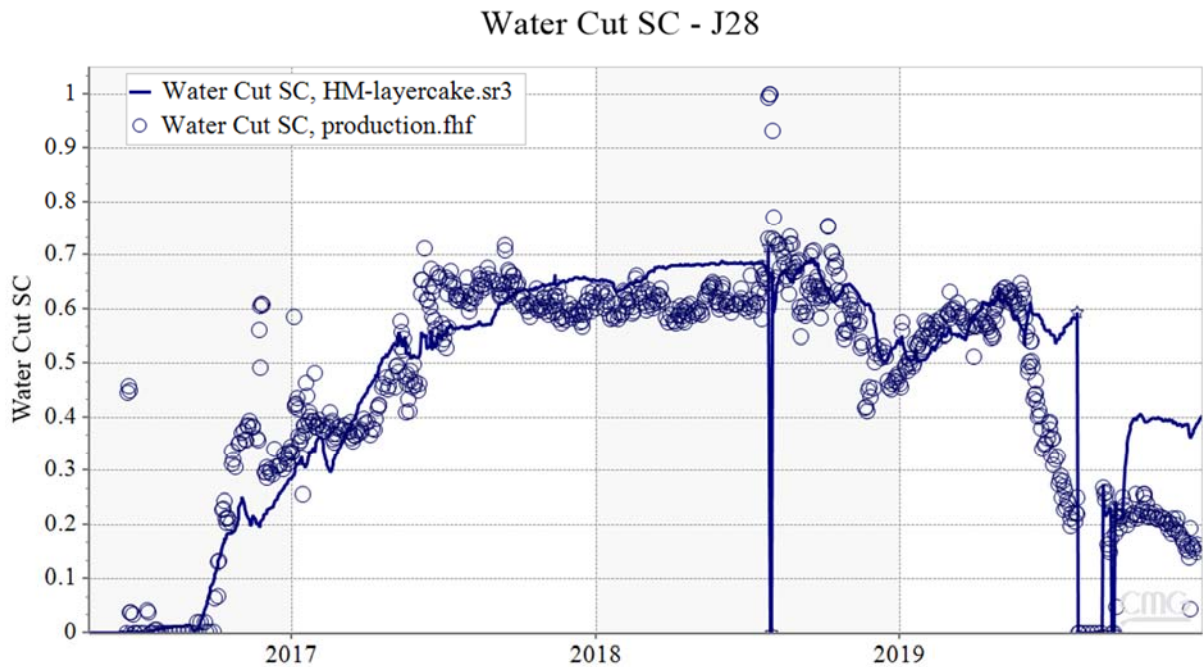
(b) Water cut of producer J28

Figure 4.13: History matching results of water cut for two producers.

Water saturation distribution. The water saturation distributions of all layers after waterflooding are shown in **Figure 4.14**. As can be seen, the water saturation is not evenly distributed in each layer. More of the injected water flows from the injection wells to the production wells in the layer #6, layer #7 and layer #8. In these three layers, the water saturations are higher in the stripes with larger transmissibility multiplier.

(a) Layer #1	(b) Layer #2	(c) Layer #3
(d) Layer #4	(e) Layer #5	(f) Layer #6
(g) Layer #7	(h) Layer #8	
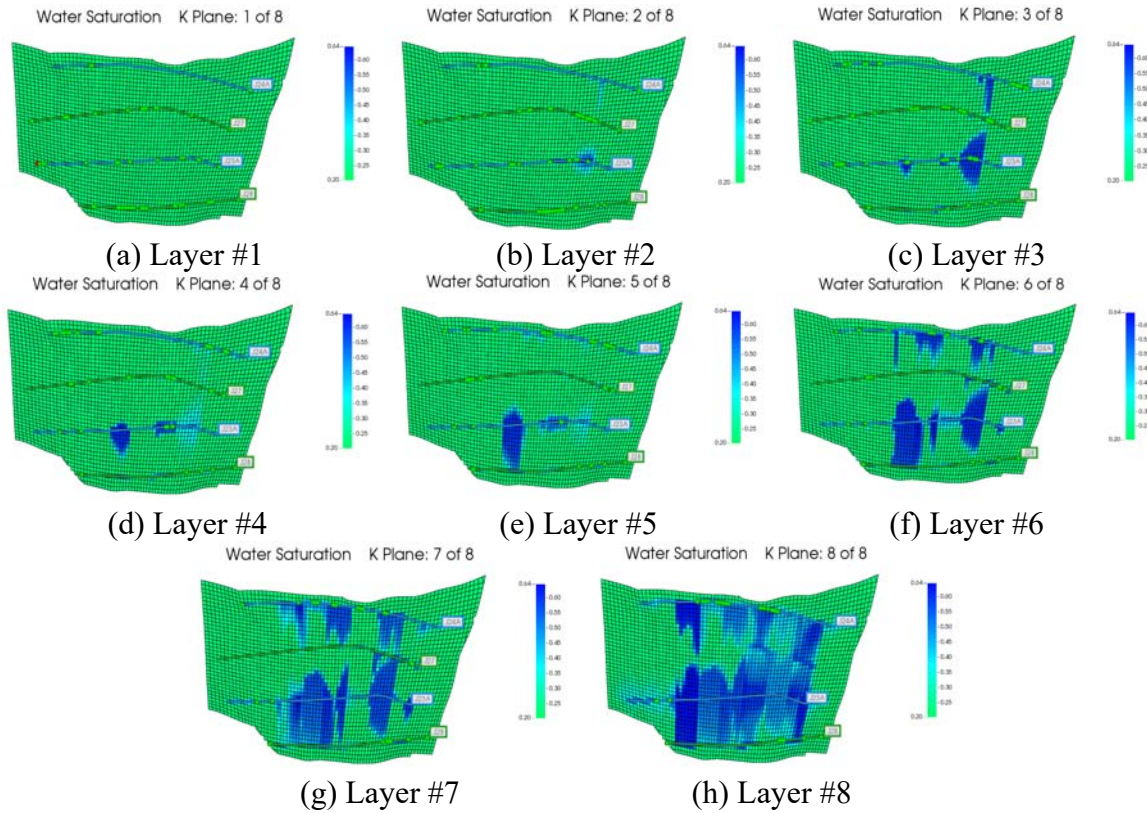
Figure 4.14: Water saturation distributions after waterflooding.

UAF's future work will focus on improving the history matching results of water cut during the polymer flooding period. The effects of capillary pressure and KvKh ratio on the water production profiles and water saturation distributions will be investigated through reservoir simulation. A new reservoir model including capillary pressure will be employed to conduct the history matching process.

Both UND and UAF activities are ongoing.

● Task 5.0 - Implementation of Polymer Flood Field Pilot in Milne Point

Since the start of polymer injection in August 2018, there have been a few shutdown events that lasted longer than 2 weeks. The first major shut down happened in September 2018, about a month after startup, when more than expected amount of hydrocarbon gas was detected from the source water used to make polymer solution. The polymer slicing unit (PSU) was shut down for 3 weeks to modify the pressure letdown module for operation safety. The second major shutdown was in November 2018 for pump and

auger repairs. The third major shutdown happened in June 2019 due to polymer solution quality issues as discussed in previous reports. Detailed pilot activities are summarized below:

Polymer Injection Status Timeline
- 8/23 polymer skid (PSU) online with water
- 8/28 polymer injection starts
- 9/25 PSU shutdown
  - More HC gas found in SW
  - Need to modify and reclassify PSU to Class I Div II
- 10/15 Resume polymer injection
  - Ran downhole gauge
  - Performed post polymer step rate test
- 11/9 J-23A shut in for PFO while waiting for pump repair
- 11/16 J-24A shut in for PFO while repairing augur
- 12/3 Resume polymer injection
- 1/17/19 Attempted IPROF for J-23A, but tool covered by black goo
- 3/28/19 Pumped 8 kg Tracer T-801 into J-24A
- 3/29/19 Pumped 8 kg Tracer T-803 into J-23A
- 3/29/19 Coil tubing clean out J-23A, repeat IPROF.
  - Tool did not go all the way down, got partial results
  - ICD#1=5.6%, ICD#2=27.8%, ICD#3=40.7%
  - 74% polymer injecting into first segment (heel-2766')
- 6/7/19-6/14/19 J-28 false polymer positive by flocculation test
- 6/19/19 shut down PSU due to polymer hydration issues
- 6/22/19 PSU back online, J-23A rate decreased by 400 bpd, J-24A by 200 bpd
- 7/6/19 J-23A PFO test, no damage identified
- 7/8/19 Treat injectors with hot KCL water to remove damage – not effective
- 7/15/19 J-23A and J-24A step rate test
- 7/18-8/28/19 straight water or low concentration polymer while diagnosing
- 8/29/19 polymer hydration problems resolved, resume polymer injection
- 9/2/19 J-23A and J-24A step rate test
- 12/2/19 shut down PSU to repair augur and replace plungers
- 12/6/19 back on line with new plungers
- 1/9/20 install automated filter ratio test
- 5/20/20 Shutdown due to pad maintenance
- 5/21/20 water flush
- 5/26/20 resume polymer injection

Polymer Injection Performance
Polymer injection progressed smoothly in this quarter except a 1-day shutdown on May 20th due to a power maintenance on the drilling pad. Then from May 21st to May 25th both injectors were put on water flush to resolve polymer hydration issues prior to resuming polymer injection on May 26th. As of end of May 2020, total cumulative polymer injected was 708,000 lbs into the two injectors and the total amount

of polymer solution injected was 1.4 million barrels which was approximately 8.8% of the total pore volume in the 2 flood patterns. During the reporting period, injected polymer concentration was between 1500 and 1700 ppm to achieve a target viscosity of 40 cP as shown in **Figure 5.1**.
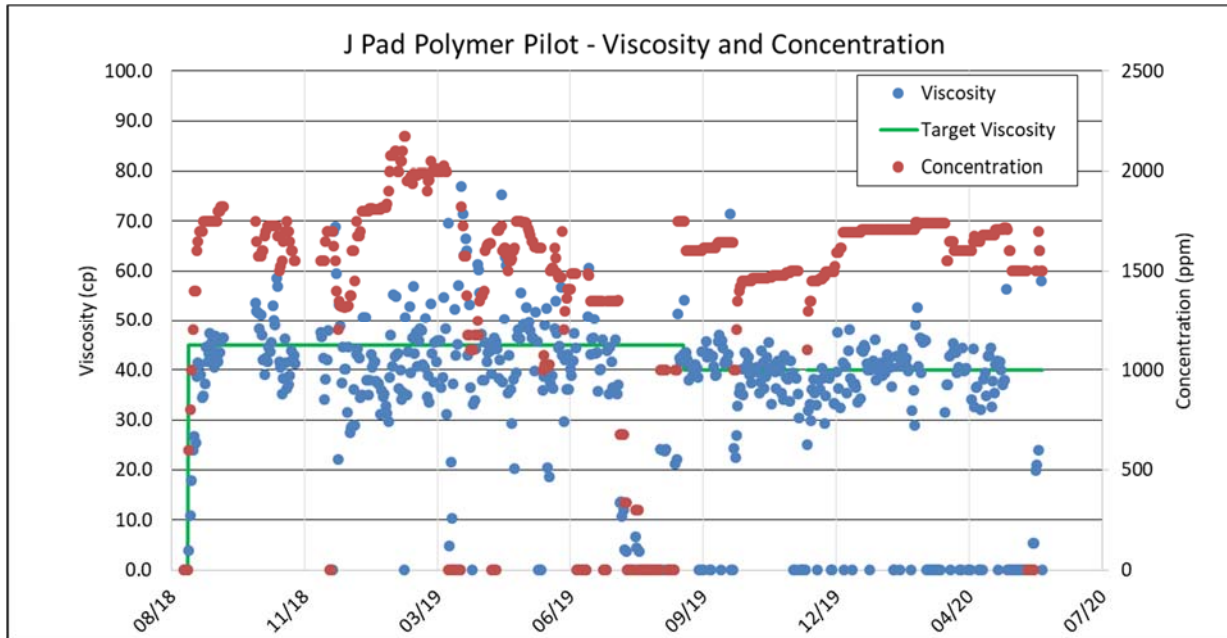
Figure 5.1: Polymer concentration and viscosity vs. time.

Polymer solution quality control

Proper Quality Control (QC) is the key for a successful polymer flood. If there is an unexpected early rise in injection pressure, it can be caused by the reservoir itself, or by poorly hydrated polymer. It is therefore important to eliminate poorly hydrated polymer as a cause. Poorly hydrated polymer can be caused by issues such as: composition change in water (salinity), freeze protection fluids (diesel/methanol) in source water, polymer dosing/wetting process not running consistently, poor polymer quality from supplier, insufficient hydration time, or insufficient mixing in the hydration tank. As part of the normal operation of the J-pad unit the filter ratio is therefore measured on a daily basis.

Polymer solution filter ratio is defined as the ratio of the time needed to filtrate from 180 cc to 200 cc to the time needed to filtrate from 60 cc to 80 cc using a specified filtration device. If this ratio is less than 1.2, the polymer solution is considered good enough to flow through the reservoir rocks without blocking. Filter ratio testing was developed as a laboratory analysis and implementing this method in the oilfield required some extra care.

Initially, the operators had to measure and calculate this parameter manually every day which was time consuming and prone to human errors. The resulting swings in filter ratio number were significant, and as the test were considered inaccurate, no action was taken on bad readings. The first improvement was to standardize the measurement and to automate the calculation in a spreadsheet. While this showed some

improvements, the measurements could still not be relied on. At the same time the equipment was ordered to automate the filter ratio testing.

The second iteration used a scale with 0.02 g accuracy, linked to a computer to measure and calculate the filter ratio. In the office this set-up led to repeatable and accurate results. However, in the field the results were not repeatable. Separate tests of identical samples would lead to different filter ratio results. The difference would be several standard deviations. These tests were done in the middle of winter (outside -35°F), and the temperature in the testing area would swing by as much as 30°F due to the electrical heater switching on or off. In the third iteration, an enclosure was built for the test, and the heater was swapped for a smaller model. Finally, the tests resulted in repeatable and accurate filter ratio results.

However, when comparing the tests carried out, samples taken from the same sample point showed a significant difference in filter ratio and viscosity depending on the operator taking the sample. By manipulating the pressure drop over the small bore sample valves, a small or large shear force can be created. While the sample procedure was specific on the order of the valves to use, it was not specific on valve shear. This would lead to either sheared or unsheared polymer depending on the valve settings. The same operator would use the same valve settings, and therefore get consistent results. However, different operators would not use the same valve settings between them. The filter ratio test needs to be carried out on an unsheared sample in order to give meaningful results. Therefore, the sampling procedure was updated to ensure consistent and unsheared polymer samples. For some bottle tests, the sheared polymer sampling method is used in order to predict separation and emulsions. Because the filter ratio results are now considered as accurate, action is taken when poor filter ratios are measured.

Figure 5.2 shows the automated measurement and the intervals used for the filter ratio calculation. In the specific example below the ratio is 1.10, which is considered a passing number. The derivative and the linear fit are also shown in the figure, as any deviation from the linear trend indicates a bad filter ratio.
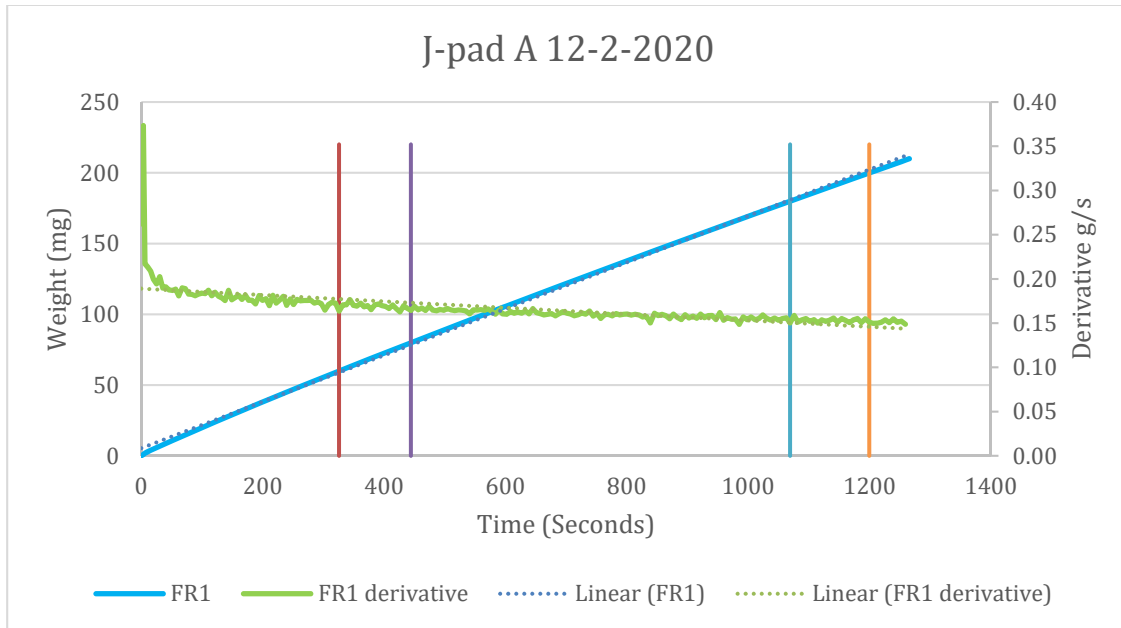
Figure 5.2: Automated measurement for polymer solution quality control.

Figure 5.3 presents daily injection rate and pressure for J-23A which shows that the injection rate stabilized at 1350 barrels per day (bpd) while the wellhead pressure stabilized around 1000 psi for the reporting period. To date 485,000 pounds of polymer have been injected into J-23A and the cumulative volume of polymer solution injected is 955,000 barrels representing approximately 10% of the total pore volume of the flood pattern.
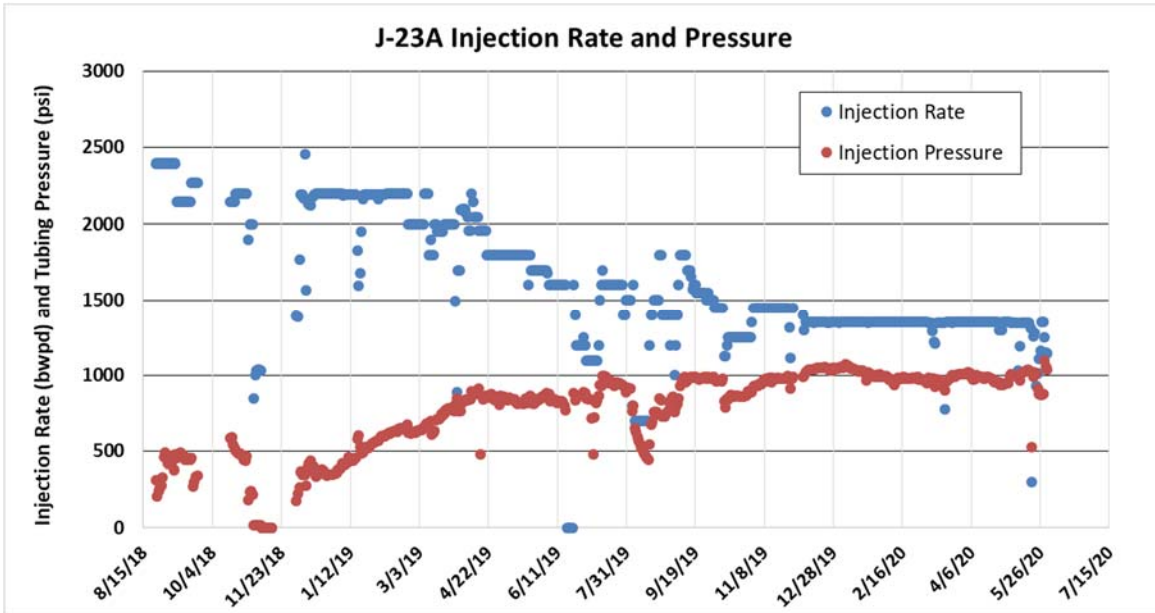
Figure 5.3: J-23A injection rate and pressure.

Figure 5.4 presents daily injection rate and pressure for J-24A. The injection rate stabilized at 700 bpd at a wellhead pressure of approximately 1000 psi, although higher injection rate was achieved at higher pressure for a short period of time prior to stabilization. To date 223,000 pounds of polymer have been injected into J-24A and the cumulative volume of polymer solution injected is 443,000 barrels representing 7% of the total pore volume of the flood pattern.
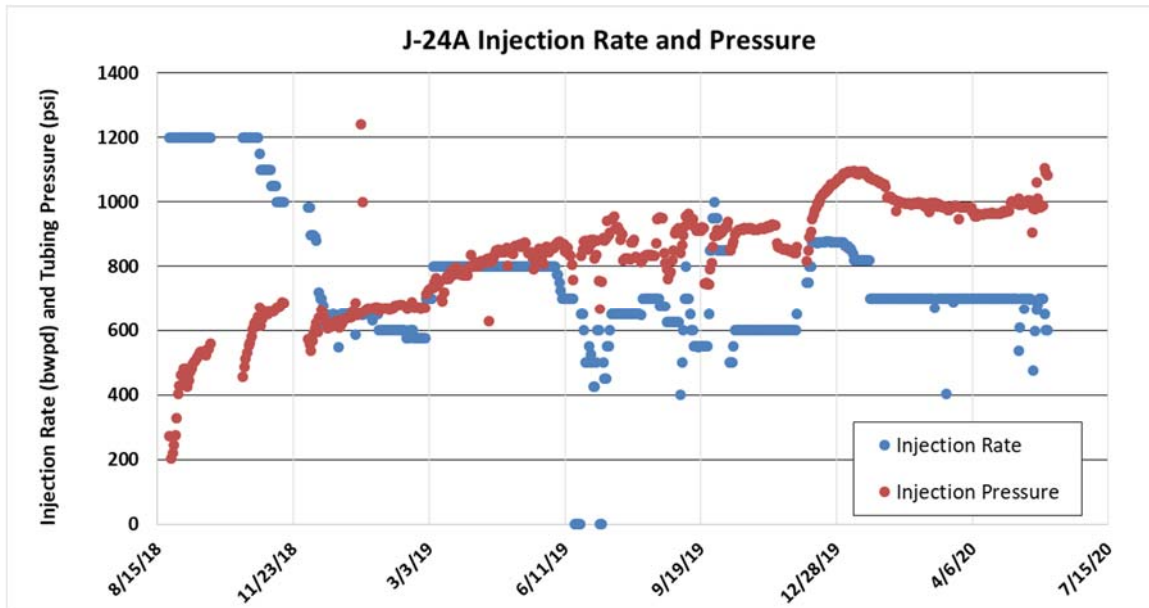
Figure 5.4: J-24A injection rate and pressure.

Figure 5.5 is a Hall (Hall, 1963) Plot for both J-23A and J-24A, which plots the integration of the differential pressure between the injector and the reservoir versus cumulative water injection. The data would form a straight line if the injectivity stays constant over time, curve up if the injectivity decreases and vice versa. After a decrease in the injectivity earlier, current Hall plot diagnostic indicates that the injectivity of both J-23A and J-24A have stabilized.
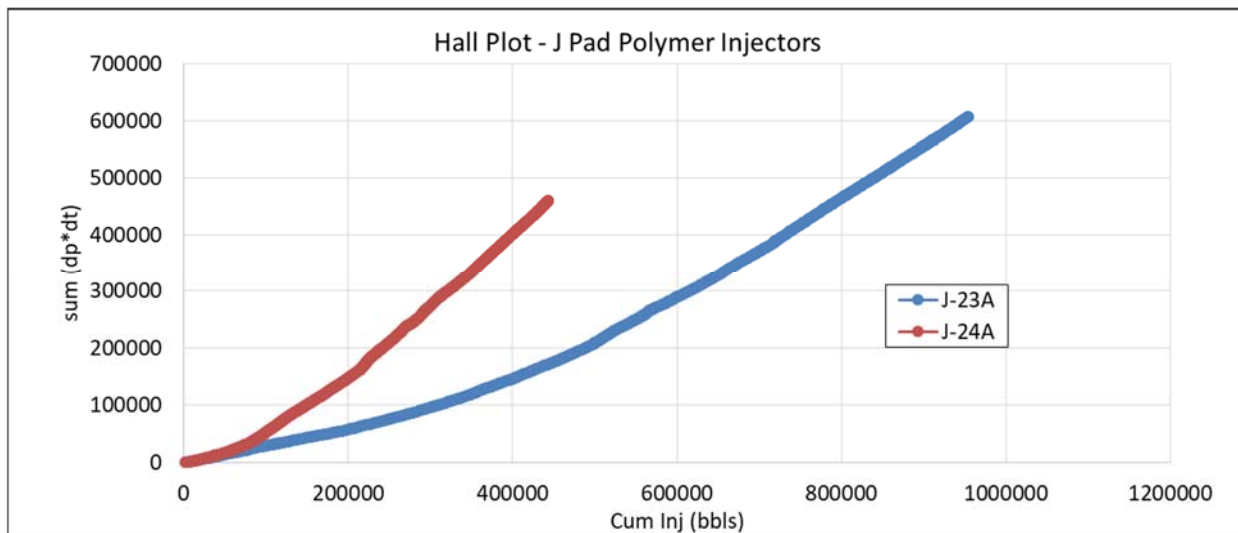
Figure 5.5: Hall plot for J-23A and J-24A.

Production Performance
Figure 5.6 depicts the production performance of producer J-27 which is supported by both injectors, J-23A from the south side and J-24A from the North. Since the start of polymer injection, water-cut has decreased from 67% to less than 15% indicating that the injected polymer is indeed helping improve sweep efficiency. The total fluid rate has stabilized and the oil rate has been increasing as the water cut decreases.
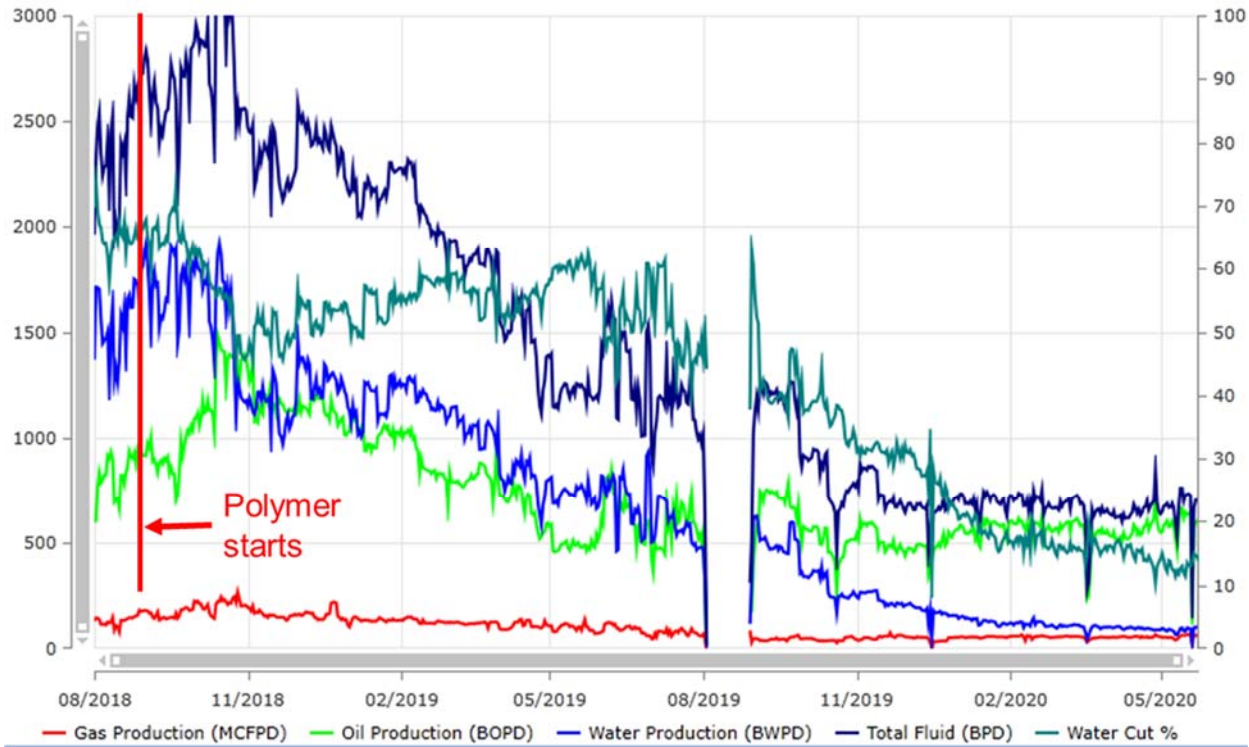
Figure 5.6: J-27 production performance.

Figure 5.7 depicts the production performance of producer J-28 which is supported only by J-23A from the north since the south side is adjacent to a sealing fault. Water-cut has also decreased from about 70% to less than 15% since the start of polymer injection. The fast response in water-cut is most likely caused by polymer blocking off the water fingers developed during the prior waterflood process. Oil rate increased to approximately 700 bpd in late 2019 then declined to circa 500 bpd caused by slowing down the ESP in mid-December which is still much higher than the expected oil rate had polymer injection never started.
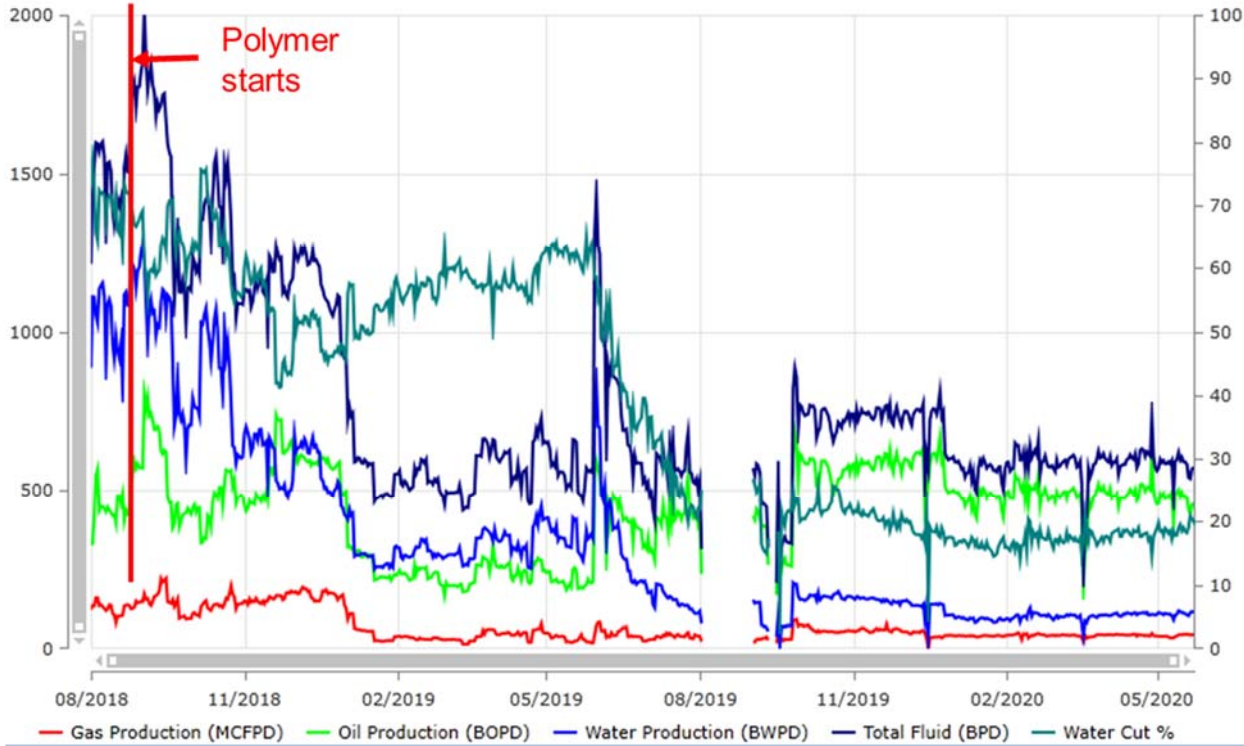
Figure 5.7: J-28 production performance.

EOR benefit

Figure 5.8 plots the actual oil production rate with polymer flood compared with predicted oil rate had waterflood continued without polymer. The difference between the two curves is deemed as EOR benefit. The actual oil rate in May 2020 is approximately 1100 bopd from the two producers and the predicted oil rate without polymer injection is about 400 bopd, giving an estimated EOR benefit of approximately 700 bopd. Up to end of May 2020, estimated cumulative Incremental Oil Recovery (IOR) is approximately 300,000 bbls from polymer injection and cumulative polymer injected is 708,000 lbs. If we define polymer utilization as the ratio of cumulative amount of polymer injected to cumulative IOR, polymer utilization would be approximately 2.4 pounds of polymer injected per barrel of incremental oil (lbs/bbl).
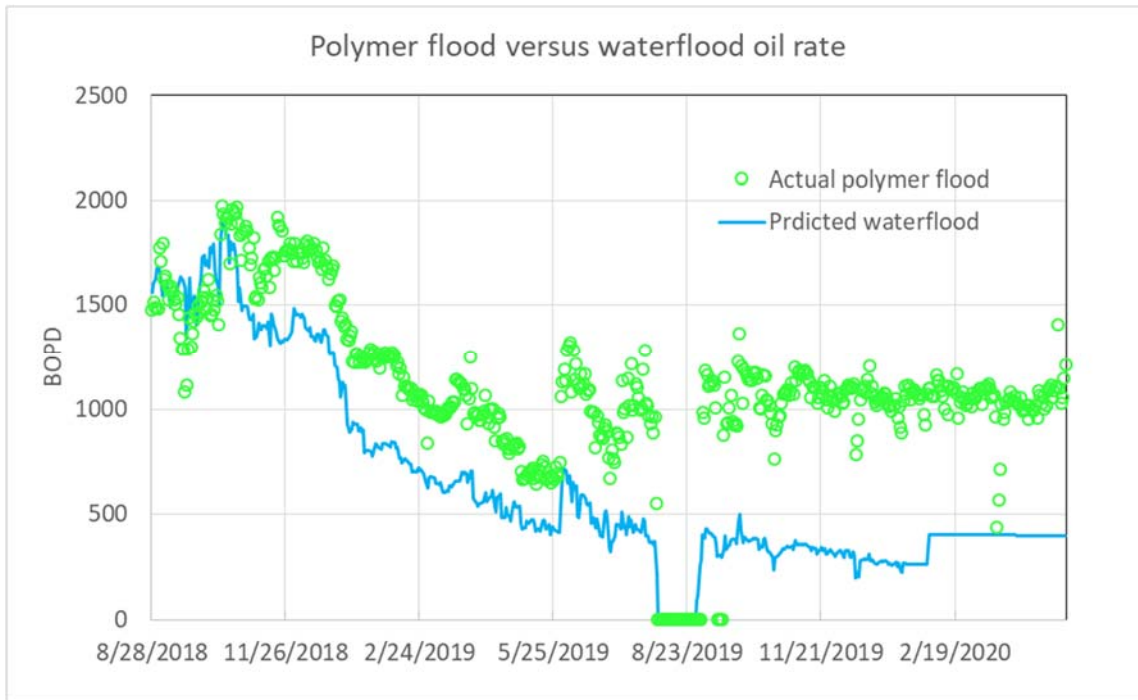
Figure 5.8: Actual oil rate versus predicted waterflood oil rate.

Based on the estimated IOR to date and the actual project expenses, a preliminary economic analysis has been performed. **Figure 5.9** presents instantaneous and cumulative cost per barrel of IOR. Instantaneous cost is defined as quarterly project expenses divided by the IOR realized in the same quarter. Similarly, cumulative cost is defined as cumulative project expenses up to a certain date divided by the cumulative IOR realized from the start of polymer injection to the date of interest. **Figure 5.9** shows that the instantaneous cost started high but leveled off at approximately $5 per barrel of IOR after 20 months of polymer injection. The cumulative cost also started high initially then declined to approximately $16 per barrel of IOR by end of March 2020. As more and more polymer is injected, we expect the cumulative cost will decrease to less than $10/bbl in the next year.
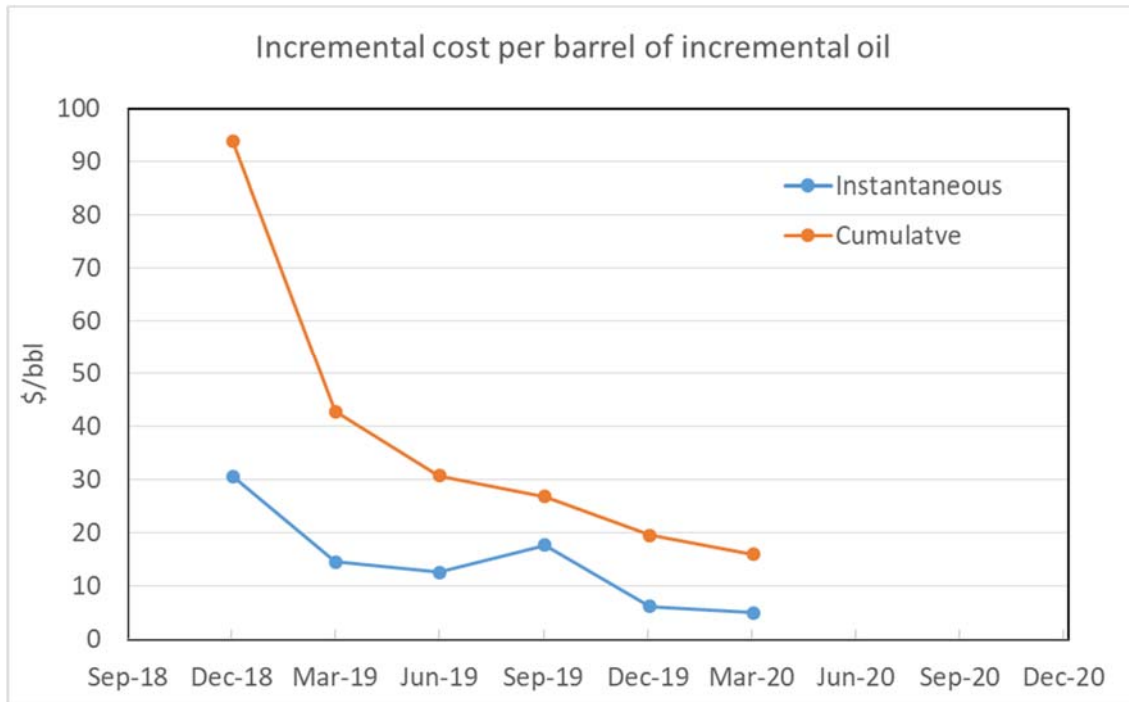
Figure 5.9: Incremental cost per barrel of incremental oil.

Excluded in this preliminary economic analysis is the benefit of the reduced water production. Prior to the start of polymer injection, the 2 producers were producing approximately 3000 bpd of water which declined to about 200 bpd in May 2020. Since the associated cost of handling produced water is beyond the scope of this project, we did not include this factor in estimating the incremental benefit.

Monitoring Polymer Breakthrough
Since the start of polymer injection, produced water samples have been collected weekly when possible and analyzed onsite using the clay flocculation test, as well as in the laboratory via nitrogen-fluorescence water composition analyses to detect the presence of produced polymer in the production stream. As of the end of May 2020, 21 months after the start of polymer injection, no polymer has been confirmed in the production stream.

Main Observations from Field Pilot to Date
1. Adequate polymer injectivity can be achieved with horizontal wells in the Schrader Bluff N-sand reservoir. However, polymer solution quality control is critical to ensure polymer propagation through the reservoir.
2. Water-cut has decreased from approximately 70% to less than 15% in the project wells since the start of polymer injection. Estimated EOR benefit is approximately 700 bopd at the present time. Estimated polymer utilization to date is approximately 2.4 pounds per barrel of incremental oil.
3. Twenty one months after the start of polymer injection, no polymer production has been confirmed from the producers yet, compared with waterflood breakthrough timing of 3 months.

Furthermore, no post polymer tracer production has been detected 16 months after tracer injection indicating that the sweep efficiency has been significantly improved. However, continued polymer injection is needed to accurately define the EOR benefit and calibrate the reservoir simulation models.

4. Encouraged by the promising results of this pilot, Hilcorp Alaska is planning to apply polymer flood technology in the Schrader Bluff reservoir throughout the Milne Point Field.

Activity is ongoing.

● Task 6.0 -Analysis of Effective Ways to Treat Produced Water that Contains Polymer

Experimental Details
In the reporting quarter, emulsion type has been determined, and drop size distribution (DSD) analysis has been performed for synthetic emulsions to better understand the microscopic mechanisms of oil/water separation. To illustrate the effect of polymer, emulsions with a water cut of 20% and 75% were prepared by mixing crude oil and polymer solution at the speed of 5,000 rpm for 3 minutes. To further probe the effect of KCl concentration on emulsion at 75% water cut, the emulsion was prepared by mixing crude oil and polymer solution with a concentration of 800 ppm at the speed of 15,000 rpm for 3 minutes. Followed by the emulsion preparation, the designed volume of KCl was added to the emulsion and mixed at a speed of 3,000 rpm for 3 minutes. The detailed procedures for emulsion preparation have been described in the previous report; thus, they are not repeated here. The dilution method, in which a small volume of fresh emulsion sample was observed whether to be dispersed after added to the white oil or polymer solution, was employed to determine the emulsion type. The rest emulsion sample was poured into a 50 mL bottle and placed into the water bath. At the time period of 30 min, 60 min, and 120 min, an aliquot of the emulsion was sampled from different positions and diluted by 50 times to take the high-quality microscope images at the magnification of 200 times. A minimum of two samples was observed under the microscope, and several images were taken from each slide for statistical analysis. The drop size distribution was analyzed through Image J software by incorporating at least 1,000 droplets from each emulsion sample.

Results and Discussion
The effect of polymer on emulsion type. In the process of dilution, the emulsion prepared with polymer solution at the concentration of 150 ppm could be completely dispersed into the white oil, implying the formation of w/o emulsion. After the addition of emulsion containing 400 and 800 ppm polymer to the aqueous phase, most of the sample could be dispersed into the white oil and a small part of the emulsion could be dispersed into the aqueous phase, which indicated that both w/o and o/w emulsion were present in the system. With the increasing polymer concentration, more oil would be emulsified into the aqueous phase, as indicated by the fact that a larger portion of emulsion could be dispersed into the aqueous phase.

The effect of polymer on DSD of emulsion at 20% WC. The drop size distribution is one of the crucial indicators of emulsion stability. As a rule of thumb, smaller drop size results in higher emulsion stability (Moradi et al. 2010). In the experiment, a small volume of the emulsion was sampled from the position which is 1 cm below the air/emulsion interface. **Figure 6.1** shows the drop size distribution of the

emulsion sample right after the homogenization for three different polymer concentrations. At the polymer concentration of 150 ppm, the presence of a large number of smaller droplets indicated the emulsion was more stable at low polymer concentration. As polymer concentration increased to 400 ppm or above, the increase in the frequency of larger droplets and the decrease in the number of smaller droplets demonstrated that more rapid coalescence between droplets occurred at high polymer concentration, resulting in a less stable emulsion.

The drop size distribution as a function of time was measured at three polymer concentrations, as shown in **Figure 6.2**. As can be seen from **Figure 6.2(a)**, a decrease in the droplet size and an increasing number of smaller droplets was observed as time prolonged for emulsion with 150 ppm polymer. At the first glimpse, the increasing frequency for the presence of smaller droplets with time seemed contradictory to the decreasing stability of emulsion during bottle test, in which more water separated over time. This uncommon phenomenon, as illustrated in **Figure 6.3**, could be attributed to the rapid coalescence of small droplets and the sedimentation of the resulting larger droplets to give a separated water phase; thus, the drop size distribution in the remaining emulsion on the top shifted to a smaller size (Binks et al. 1996). A similar trend of the drop size distribution as a function of time was observed at the polymer concentration of 400 ppm. The more significant change of drop size distribution at 400 ppm polymer concentration also confirmed the reduced emulsion stability resulting from increasing polymer concentration. As polymer concentration increased to 800 ppm, an increase of droplets in both size and frequency was detected at the measured time intervals, resulting from the coalescence of the dispersed water droplets.
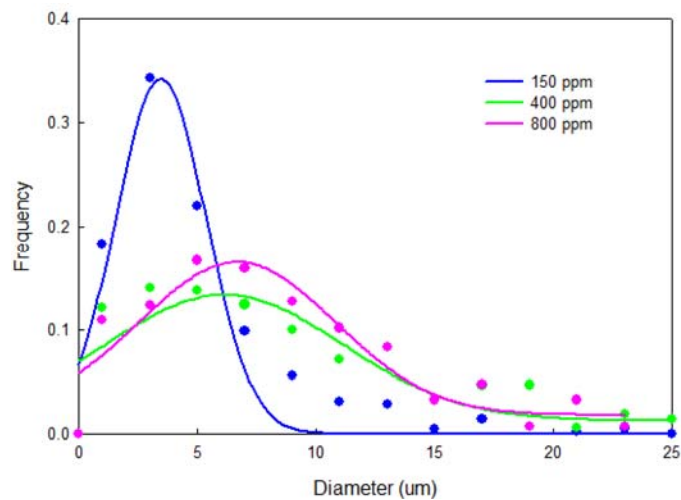

Figure 6.1: The effect of polymer on DSD of emulsion at 20% WC.

Figure 6.2: The evolution of DSD for emulsion at 20% WC with a polymer concentration of (a) 150 ppm, (b) 400 ppm, and (c) 800 ppm.

(a)   (b)   (c)

Figure 6.3: Evolution of w/o emulsion. (a) After homogenization, a polydisperse system is created. (b) After a period of settling, the small droplets coalesce into larger ones, and the resulting larger droplets migrate to the bottom of the vial. (c) As a result of further coalescence, a layer of water is separated at the bottom.

*Note that the gray color represents the oil phase, and the blue color represents the water phase.

The effect of polymer on DSD of emulsion at 75% WC. Similar experiments were performed to determine the type of the emulsion prepared at 75% WC at the presence of polymer. The emulsion samples at each polymer concentration right after homogenization could be completely dispersed in the respective polymer solution. It indicated that o/w emulsion was initially generated at all tested polymer concentrations. After a period of time, the emulsion tended to separate into three layers: the top layer (w/o emulsion), the intermediate layer (concentrated o/w emulsion), and the bottom layer (o/w emulsion). Since the intermediate layer was too thin to obtain the sample precisely, the study mainly focused on the sample from the top layer and the bottom layer. **Figure 6.4** shows the microscope images of emulsions obtained from the top layer at three different polymer concentrations. As can be seen, a portion of water was trapped in the top layer in the form of small water droplets for all three polymer concentrations. The water droplets at the polymer concentration of 150 ppm were smaller and more densely packed than that at higher polymer concentrations. It revealed that the emulsion that remained at the top layer became less stable with increasing polymer concentration.
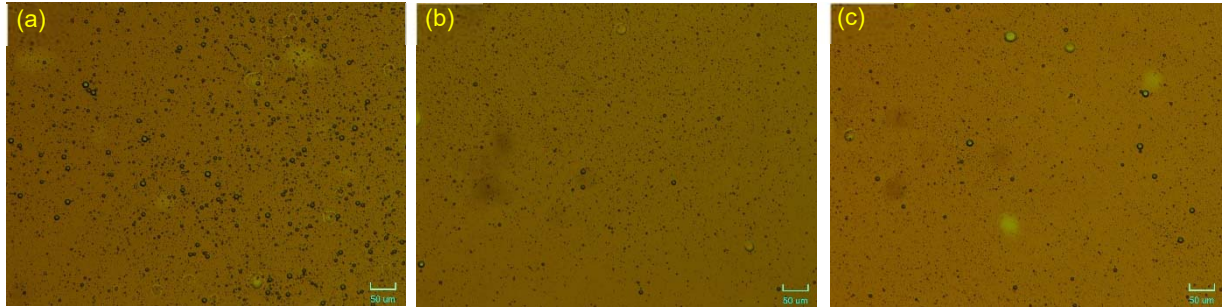
Figure 6.4: Microscope images of top-layer emulsions at a polymer concentration of (a) 150 ppm, (b) 400 ppm and (c) 800 ppm.

To illustrate the effect of polymer concentration on the drop size distribution of emulsions at 75% WC, the emulsion samples prepared at each polymer concentration were immediately diluted by the polymer solutions at the same concentration. **Figure 6.5** shows that the increasing polymer concentration resulted in a decrease of the droplet size, denoting that the emulsion stability was enhanced as the polymer concentration increased. The drop size distribution as a function of time was also measured at all three tested polymer concentrations, as depicted in **Figure 6.6**. To ensure the conformity of the emulsion type (o/w emulsion) throughout the experiment, the emulsion sample was obtained from the position which is 1 cm below the theoretical oil/water interface. Generally, the decrease of smaller droplets and the increased frequency of larger droplets indicated the growth of small droplets to large droplets due to the creaming and coalescence in the destabilization process of the o/w emulsion, as illustrated in **Figure 6.7**. On the other hand, minor changes of DSD as a function of time at high polymer concentration compared to significant changes of DSD at low polymer concentration proved that the emulsion at low polymer concentration was less stable.

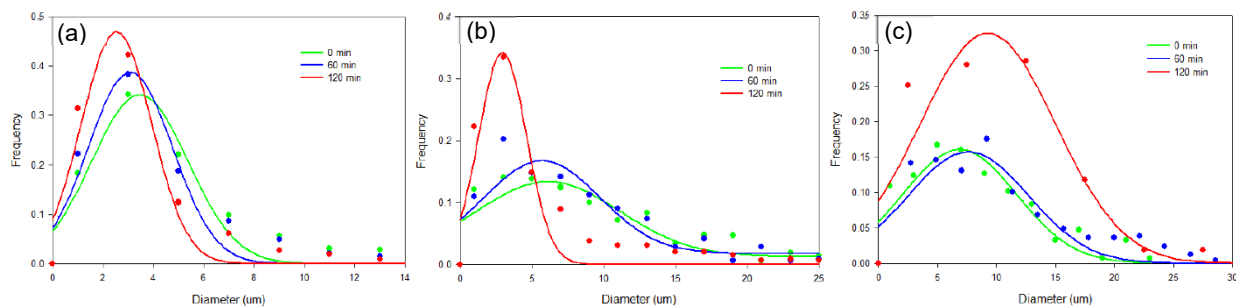**Figure 6.5: The effect of polymer on DSD of emulsion at 75% WC.**
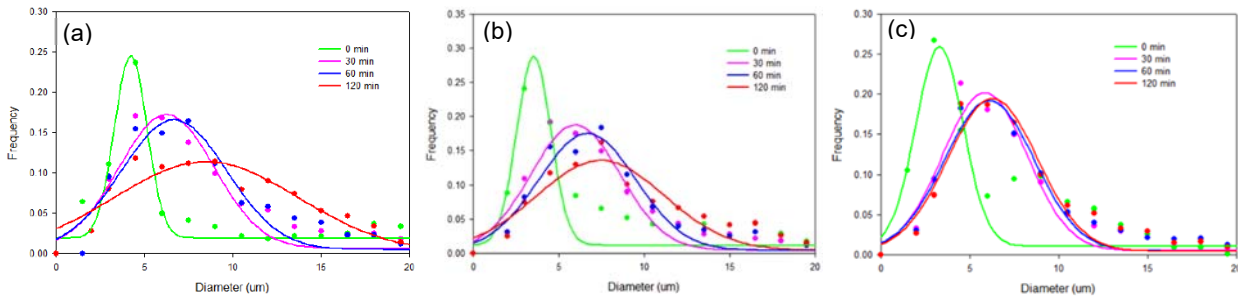
Figure 6.6: The evolution of DSD for emulsion at 75% WC with a polymer concentration of (a) 150 ppm, (b) 400 ppm, and (c) 800 ppm.
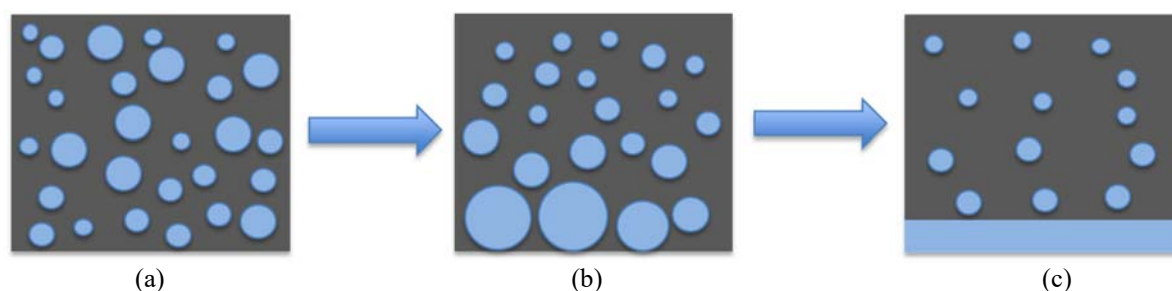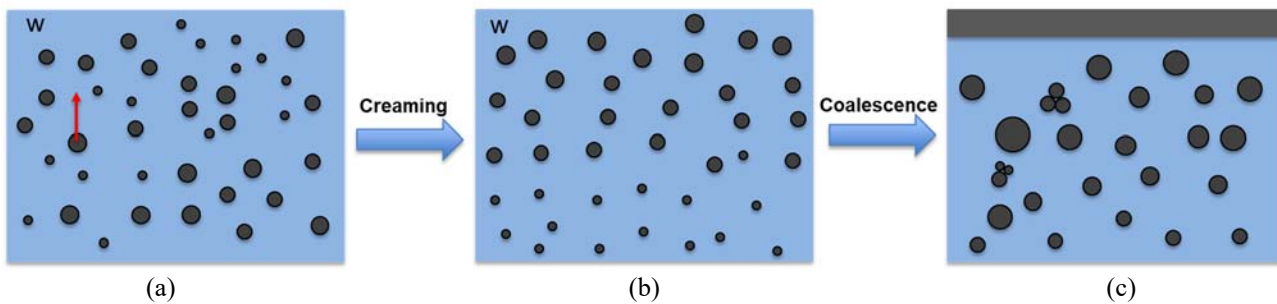

Figure 6.7: Evolution of o/w emulsion. (a) After homogenization, a polydisperse system is created. (b) After a period of creaming, the larger droplets migrate to the top of the vial, and the small droplets are left behind at the bottom. (c) As a result of coalescence, the oil droplets become larger and a layer of oil sits at the top.

*Note that the gray color represents the oil phase, and the blue color represents the water phase.

The effect of KCl on DSD of emulsion at 75% WC. As mentioned in the previous quarterly report, the o/w emulsion prepared at harsh conditions (such as high shear intensity and high polymer concentration) is more stable. On the other hand, the addition of KCl could mitigate the difficulty in separating oil and water by reducing the oil content in the water (OIW) and the basic sediment and water (BS&W). In this experiment, the effect of KCl on emulsion stability was explored by analyzing the DSD from the microscopic perspective. Similar experiments were performed to determine the type of the emulsion prepared at 75% WC in the presence of KCl. It was observed that o/w emulsion was initially generated at all tested KCl concentrations and separated into three layers after a period of time as aforementioned. **Figure 6.8** shows that the size of water droplets in the top layer increased with increasing KCl concentration. More irregular droplets were observed as the concentration of KCl increased due to the large-scale coalescence of water droplets, indicating that the increasing KCl concentration had a negative effect on the stability of the top-layer emulsion.
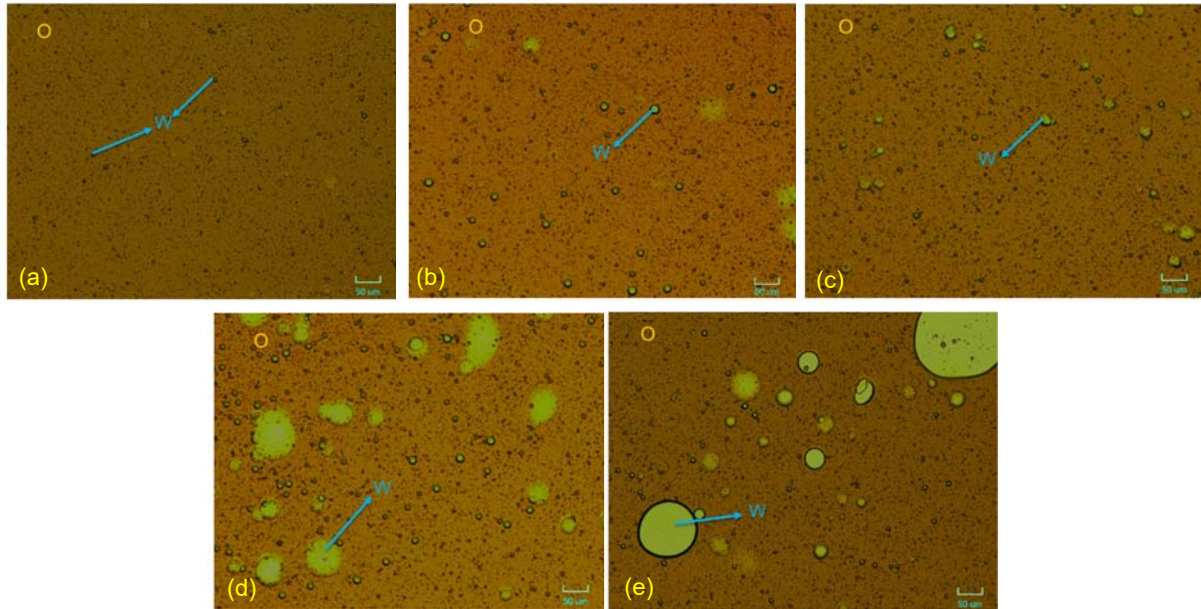
Figure 6.8: Microscope image of top-layer emulsions at KCl concentration of (a) 0 ppm, (b) 8000 ppm, (c) 12000 ppm, (d) 16000 ppm and (e) 20000 ppm.

To investigate the impact of KCl concentration on the drop size distribution of emulsions, polymer solution with different concentrations of KCl was prepared and used to dilute the emulsion samples with the same KCl concentration to eliminate the effect of other factors on the drop size. As shown in **Figure 6.9**, the center of the peak in the curve was almost the same, while the width of the curve slightly increased with the increasing KCl concentration. It indicates that the water droplets became more polydispersed, although there was little variation in the average drop size, which caused the emulsion to be less stable but to a small degree. The drop size distribution as a function of time for all tested KCl concentration is plotted in **Figure 6.10**. To ensure the conformity of the emulsion type (o/w emulsion) throughout the experiment, the emulsion sample was obtained from the position which is 1 cm below the theoretical oil/water interface. Compared to the results in **Figure 6.6(c)**, minor changes of drop size distribution as a function of time in **Figure 6.10(a)** testified the better emulsion stability caused by the intense shearing. Meanwhile, the insignificant difference between curves at different time intervals at all tested KCl concentrations elaborated on the poor performance of KCl to break the emulsion stabilized by the polymer.
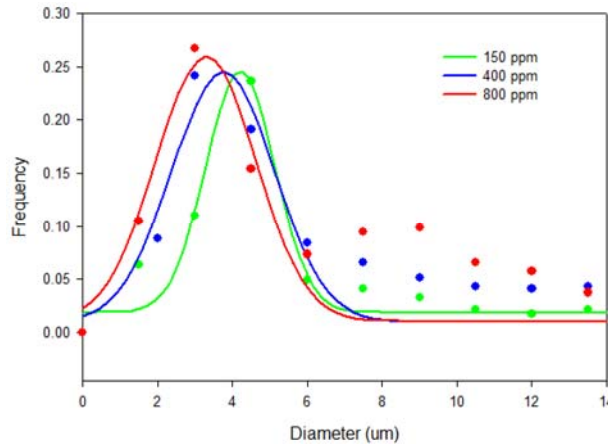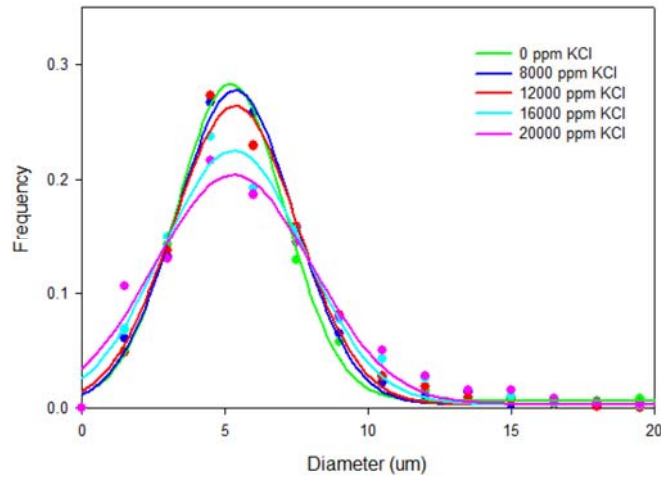
Figure 6.9: The effect of KCl on DSD of emulsion at 75% WC.
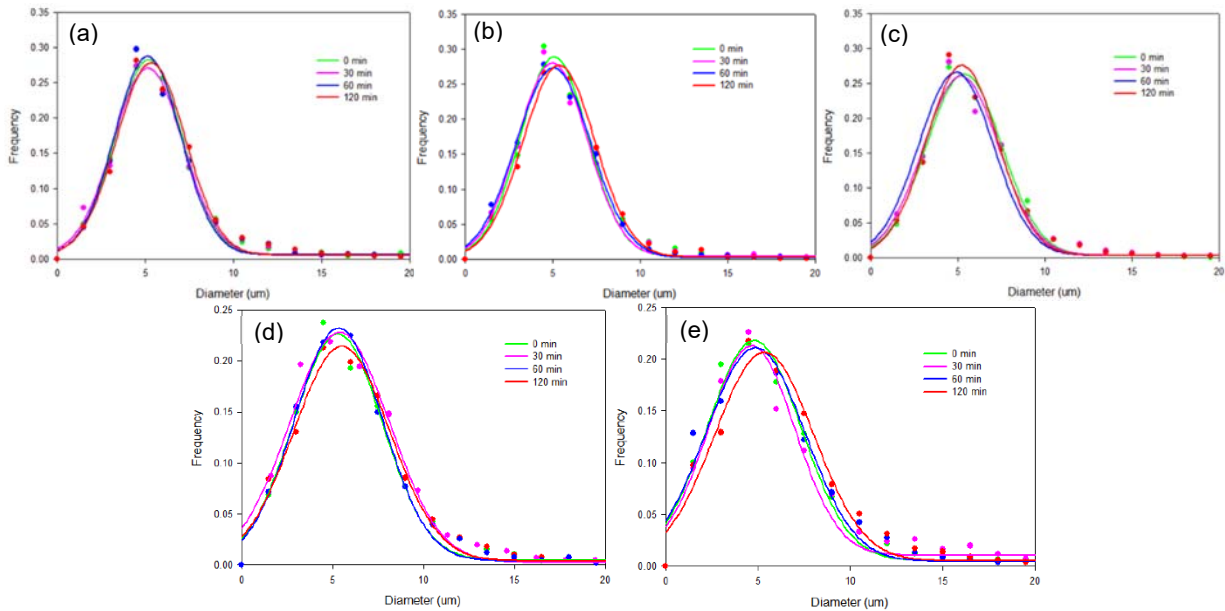
**Figure 6.10: The evolution of DSD for emulsion at KCl concentration of (a) 0 ppm, (b) 8000 ppm, (c) 12000 ppm, (d) 16000 ppm, and (e) 20000 ppm.**

Future Work

This will focus on studying the effect of clay particles on the separation behavior of emulsions and the performance of emulsion breakers.

● Task 6.0a –Polymer Fouling of Heater Tubes

Experimental Details

In the reporting quarter, fouling experiments were continued using Dynamic Scale Loop. Cloud point testing was done again with new bottles which prevents evaporation to predict the stability of polymer solutions at different temperatures. The detailed procedure is given below.

1. Polymer solutions of different concentrations were prepared in Milne Point formation brine composition – 0ppm, 160ppm, 400ppm, 800ppm.
2. The solutions were placed in the special glass bottles, sealed using Teflon tape and then these bottles were placed in a preheated oven at 165°F and heated for 24 hours.
3. After 24 hours these containers were taken out and pictures were taken to see if any precipitation of polymer has occurred. The precipitation of polymer implies that the solution has reached its cloud point.
4. Then the temperature of oven was increased to 180°F and the containers were placed back inside the oven and heated again for 24 hours. This process was done in the temperature incremental steps shown in **Table 6.1** below.

Table 6.1: Experimental approach for cloud point experiment.

Temperature (°F)	Heating Period	Duration of Heating (hours)
165	0-24	24
180	24-48	24
200	48-72	24
220	72-96	24
240	96-120	24
250	120-144	24

A sample representation is shown below in **Figure 6.11**.

Sample Representation

OVEN ⟶

Bottles heated at a fixed temperature and observed visually after periodic intervals
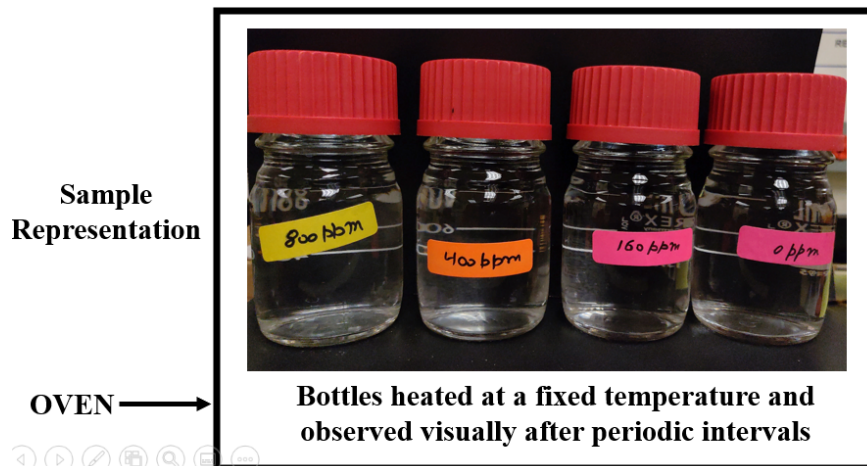
Figure 6.11: Sample representation of the Cloud Point experiment with special sealed bottles.

The updated experimental plan for the Dynamic Scale Loop is given in the **Table 6.2** below. The update is that instead of testing for 60mL/min that flow rate is replaced by a flow rate which makes sure that the fluids enter and exit the tubing at the same temperatures as Milne Point heaters fluid inlet and outlet temperatures respectively. This was thought of to try and mimic the process happening at Milne Point more closely. The bold conditions have been tested in this quarter.

Table 6.2: Experimental plan for Dynamic Scale Loop (DSL).

Test #	Temp (ºF)	Temp (ºC)	Polymer conc. (ppm)	Flow Rate (mL/min)		Velocity (m/s)	Residence Time (min)	% Residence Time of field	%Velocity of Field
1				3.94		0.043	1.194	100.00	1.57
2	165	73.88	800	20		0.217	0.235	19.72	7.95
3				251.53		2.735	0.019	1.57	100.00
4				3.94		0.043	1.194	100.00	1.57
5	165	73.88	400	20		0.217	0.235	19.72	7.95
6				252		2.740	0.019	1.57	100.19
7				**3.94**		**0.043**	**1.194**	**100.00**	**1.57**
8	165	73.88	0	**20**		**0.217**	**0.235**	**19.72**	**7.95**
9				252		2.740	0.019	1.57	100.19
10				3.94		0.043	1.194	100.00	1.57
11	200	93.33	800	23		0.250	0.205	17.15	9.14
12				252		2.740	0.019	1.57	100.19
13				3.94		0.043	1.194	100.00	1.57
14	200	93.33	400	23		0.250	0.205	17.15	9.14
15				252		2.740	0.019	1.57	100.19

16				**3.94**		**0.043**	**1.194**	**100.00**	**1.57**
17	200	93.33	0	**23**		**0.250**	**0.205**	**17.15**	**9.14**
18				252		2.740	0.019	1.57	100.19
19				3.94		0.043	1.194	100.00	1.57
20	350	176.66	800	TBD					
21				252		2.740	0.019	1.57	100.19
22				3.94		0.043	1.194	100.00	1.57
23	350	176.66	400	TBD					
24				252		2.740	0.019	1.57	100.19
25				**3.94**		**0.043**	**1.194**	**100.00**	**1.57**
26	350	176.66	0	TBD					
27				252		2.740	0.019	1.57	100.19

Results and Discussion

Cloud Point Results – The results of the cloud point experiment are shown in **Figures 6.12** – **Figure 6.18**.
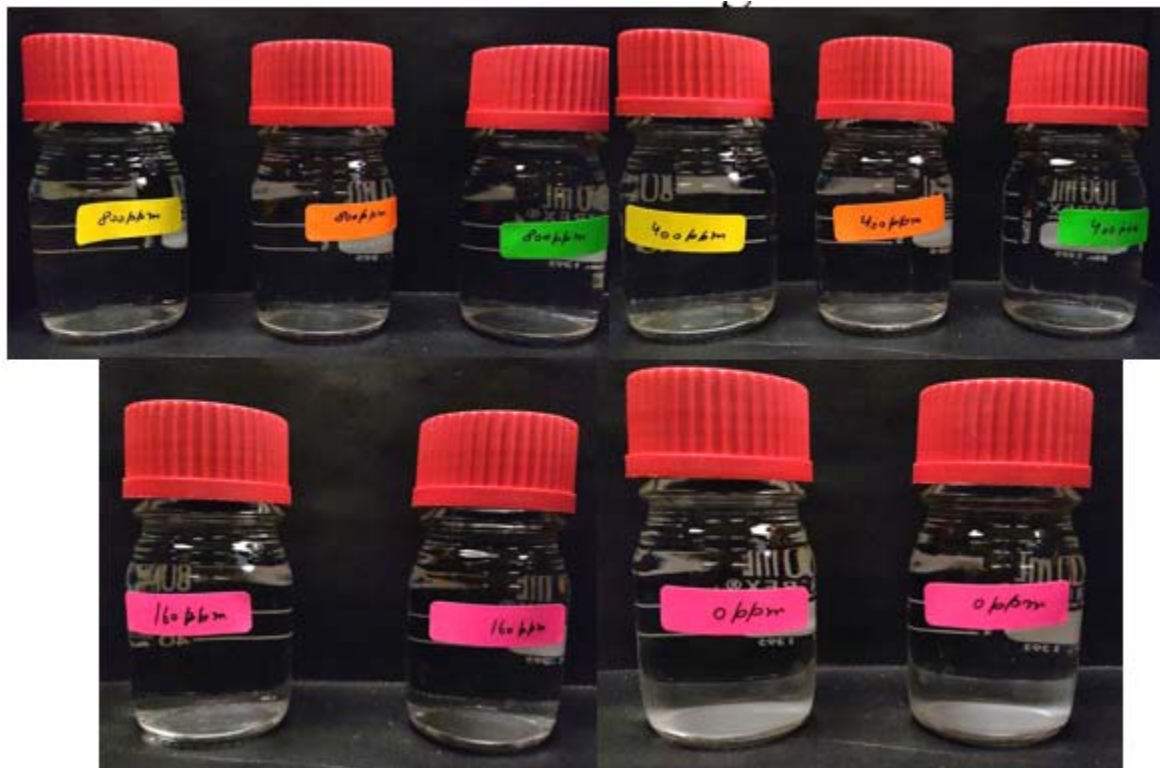
Figure 6.12: Cloud point test solutions after 24 hours at 165ºF.

No change in solutions was observed after 24 hours at 165ºF.

Figure 6.13: Cloud point test solutions after 5 hours at 240ºF.

Up to this point pictures were taken at 180ºF, 200ºF, 220ºF but no cloudy appearance was seen at any of those temperatures. First cloudy appearance was observed at 240ºF. All polymer solutions showed cloudy appearance but the solution without polymer (0ppm) did not show any cloudiness.
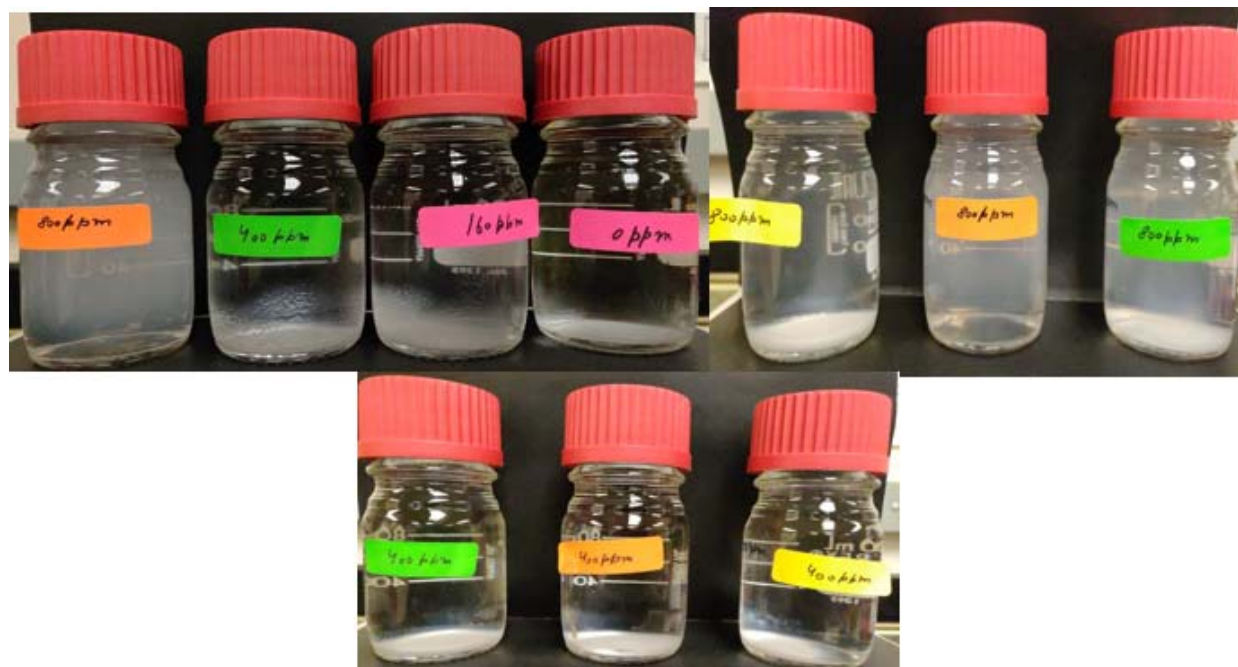
Figure 6.14: Cloud point test solutions after 24 hours at 240ºF.

More prominent cloudy appearance in 800ppm and polymer starts to settle at bottom in 400ppm and 160ppm.

Figure 6.15: Cloud point test solutions after 24 hours at 250ºF.

Polymer settles at bottom in 160ppm, 400ppm & 800ppm. Nothing seen in 0ppm bottle.

- The experiment was restarted with fresh solutions with the objective of narrowing down temperature range for polymer instability
- 230ºF chosen as starting point as previous experiment showed cloudy appearance at 240ºF
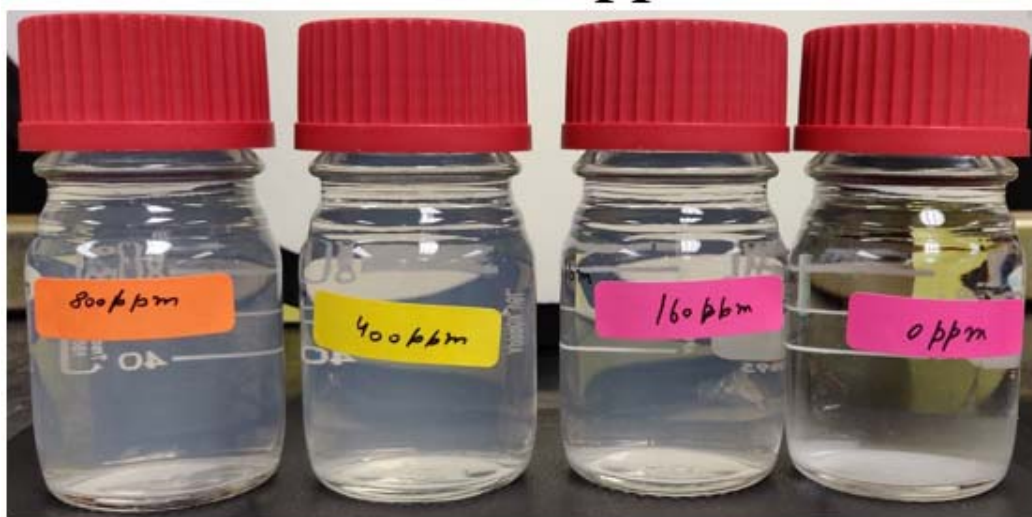

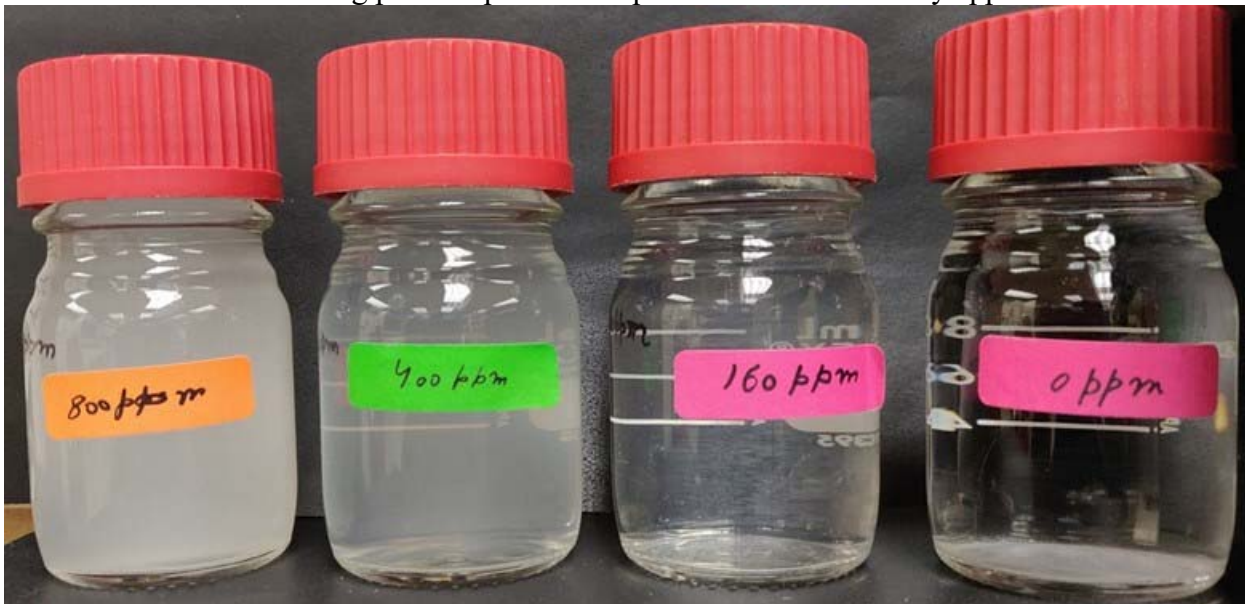**Figure 6.16: Cloud point test solution after 24 hours at 230ºF.**

Cloudy appearance was clearly seen in all polymer solutions whereas the solution without polymer remained clear. It was inferred that the cloud point of the polymer in this brine lies somewhere between

66

220ºF and 230ºF as cloudy appearance was observed at 230ºF.

Dynamic Scale Loop Results – The results of the first experiments of the Dynamic Scale Loop are shown in **Figure 6.17** – **Figure 6.23.** The test conditions of the experiment and their comparison with field parameters at Milne Point are also given below each figure.

The **Figure 6.17** shows that when polymer is absent and the fluids spend a reasonable time inside the heated tubing (same as the amount of time fluids spend in heaters at Milne Point) the differential pressure across the ends of the tubing does not vary much at 165ºF skin temperature. In **Figure 6.18** which is for skin temperature of 200ºF (rest of the conditions same) a similar situation is seen which implies no blocking of the tube.

Figure 6.19 is for the flow rate at which fluids enter and exit the tubing at the temperatures at which they enter and exit respectively at Milne Point field heaters. In this scenario also we did not observe any tube blocking. **Figure 6.20** is for experiment with 200ºF skin temperature where again the flow rate was adjusted to mimic the inlet and outlet Milne Point fluid temperatures in heaters. This scenario also showed a safe situation without any tube blocking.

Figure 6.21 is for higher skin temperature of 350ºF at 3.94mL/min – in this situation although the differential pressure did show some variations but there was no consistent blocking of the tube and the researchers felt these variations could be due to cavitation and evaporation of the fluids. Therefore, it was decided to carry out further experiments with a back pressure of 50-100 psi.

Figure 6.22 and **Figure 6.23** show experiments which are a repeat of **Figure 6.19** and **Figure 6.21** but this time carried out with a backpressure applied constantly to prevent the pressure variations due to the cavitation and it can be seen that the backpressure clearly helped eliminate those differential pressure variations which means that the differential pressure was not fluctuating due to tube blocking and thus when there is no polymer present the tube is not getting blocked.
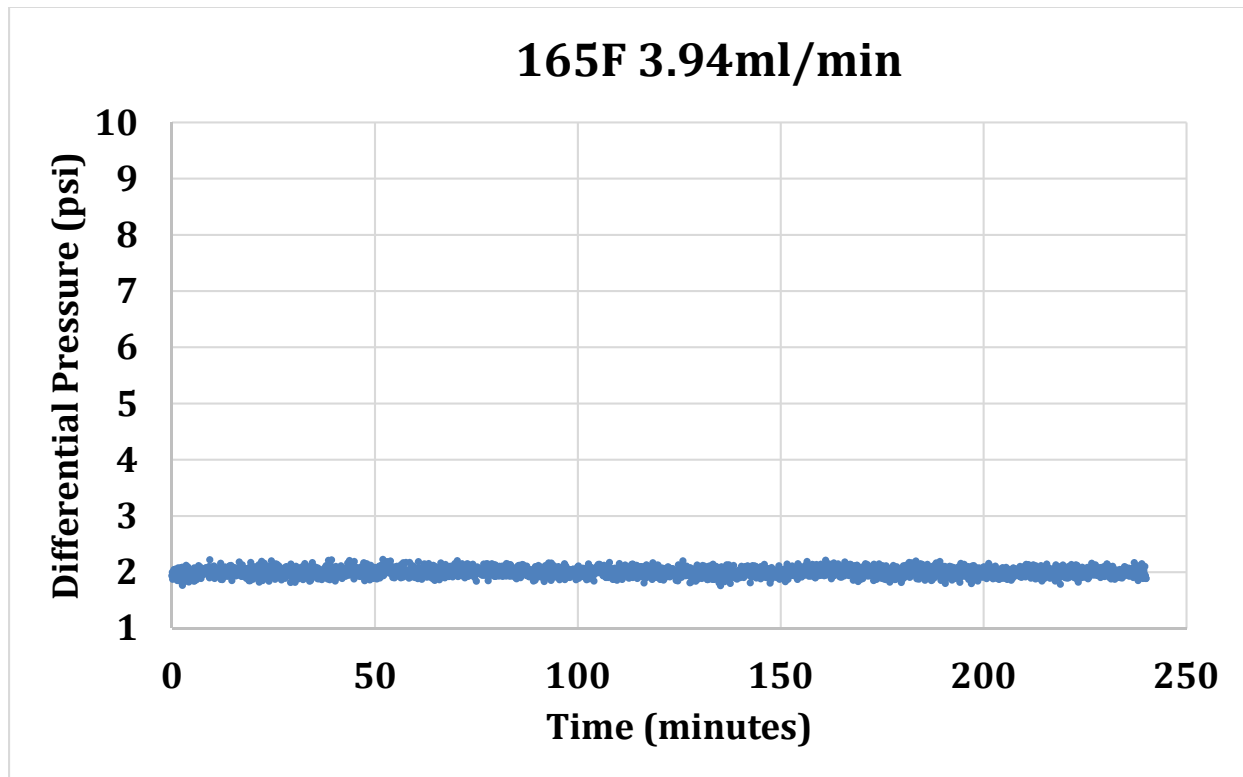
165F 3.94ml/min

PARAMETER	LAB VALUE	FIELD VALUE
Velocity (m/s)	0.043	2.735
Residence time in Tubing (minutes)	1.194	1.194

Figure 6.17: DSL test result at 165°F at 3.94mL/min with 0ppm polymer.
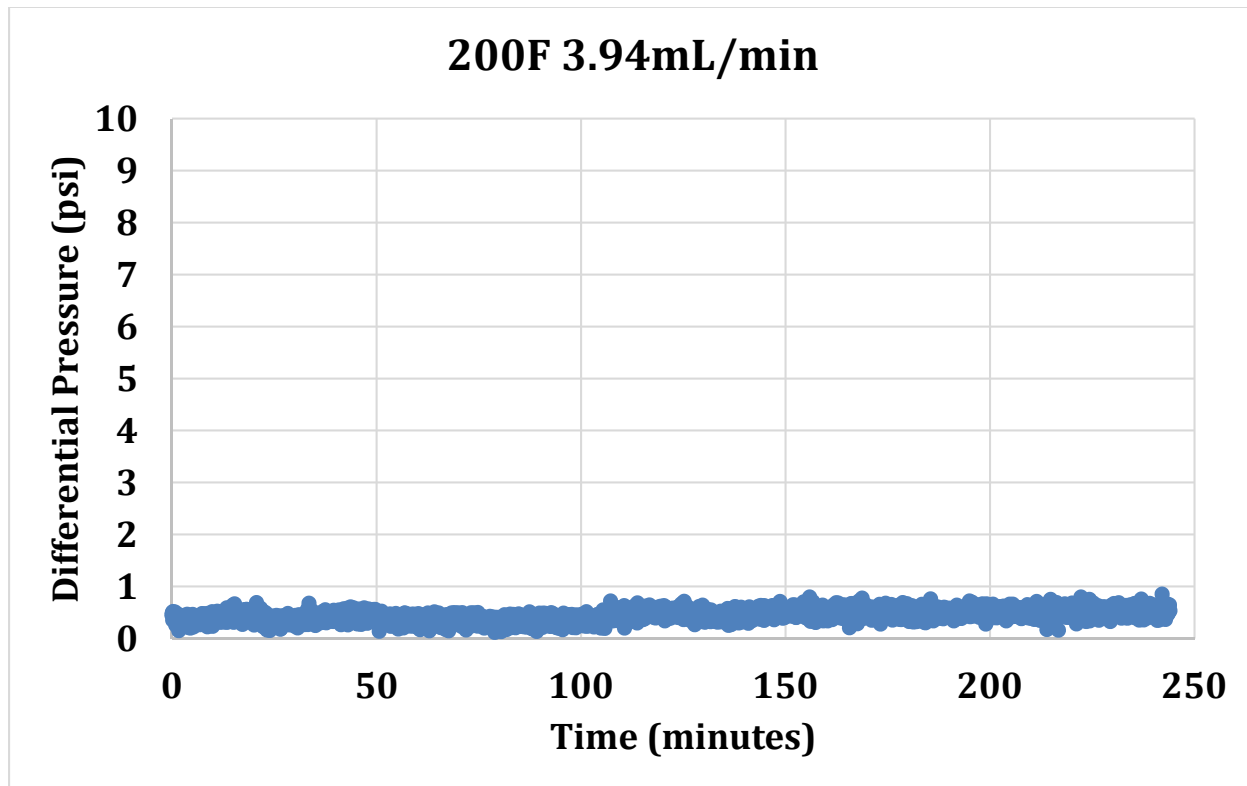
200F 3.94mL/min

PARAMETER	LAB VALUE	FIELD VALUE
Velocity (m/s)	0.043	2.735
Residence time in Tubing (minutes)	1.194	1.194

Figure 6.18: DSL test result at 200ºF at 3.94mL/min with 0ppm polymer.
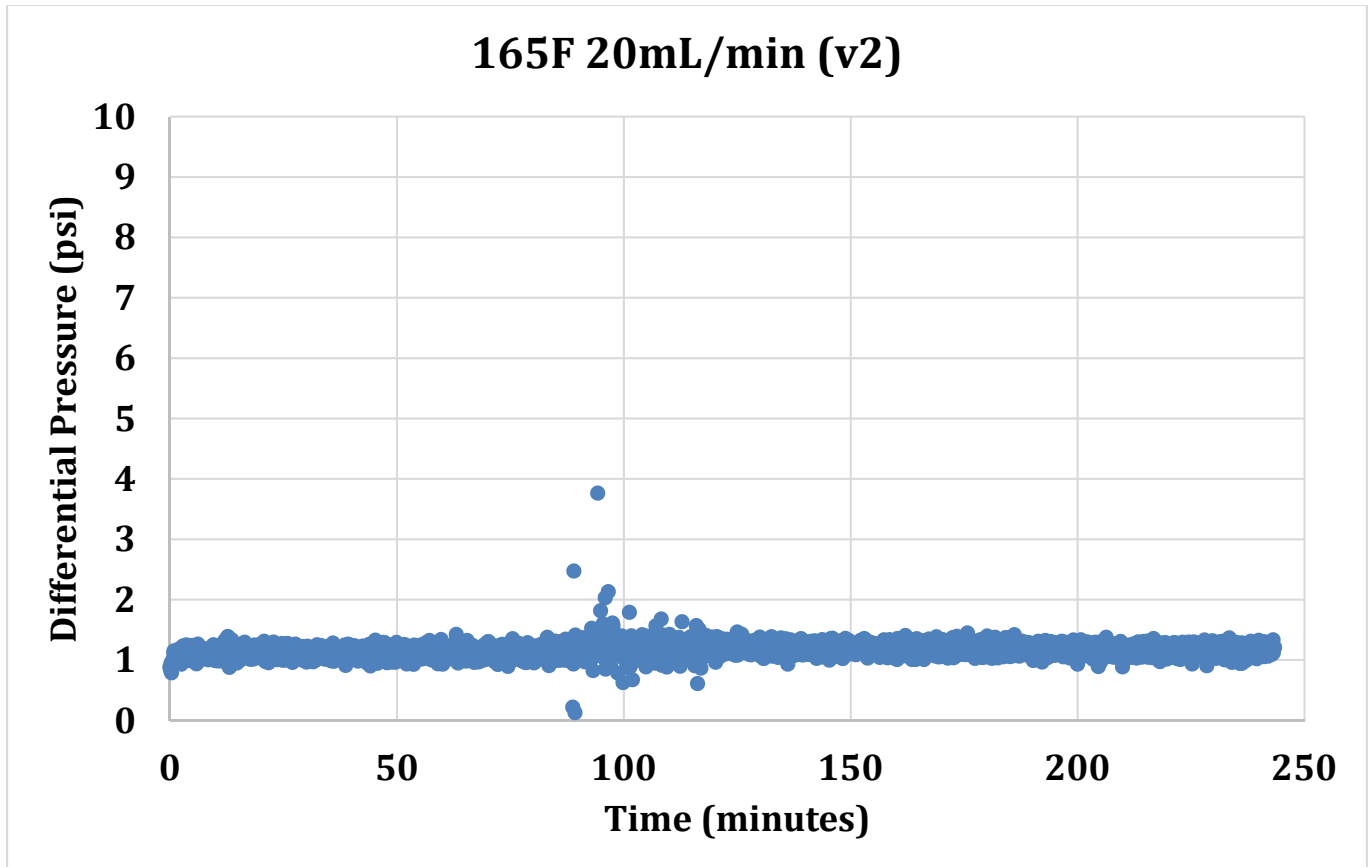
165F 20mL/min (v2)

PARAMETER	LAB VALUE	FIELD VALUE
Velocity (m/s)	0.217	2.735
Residence time in Tubing (minutes)	0.235	1.194

Figure 6.19: DSL test result at 165°F at 20mL/min with 0ppm polymer.

200F 23 mL/min

PARAMETER	LAB VALUE	FIELD VALUE
Velocity (m/s)	0.25	2.735
Residence time in Tubing (minutes)	0.205	1.194

Figure 6.20: DSL test result at 200ºF at 23mL/min with 0ppm polymer with backpressure.

350F 3.94mL/min

PARAMETER	LAB VALUE	FIELD VALUE
Velocity (m/s)	0.043	2.735
Residence time in Tubing (minutes)	1.194	1.194
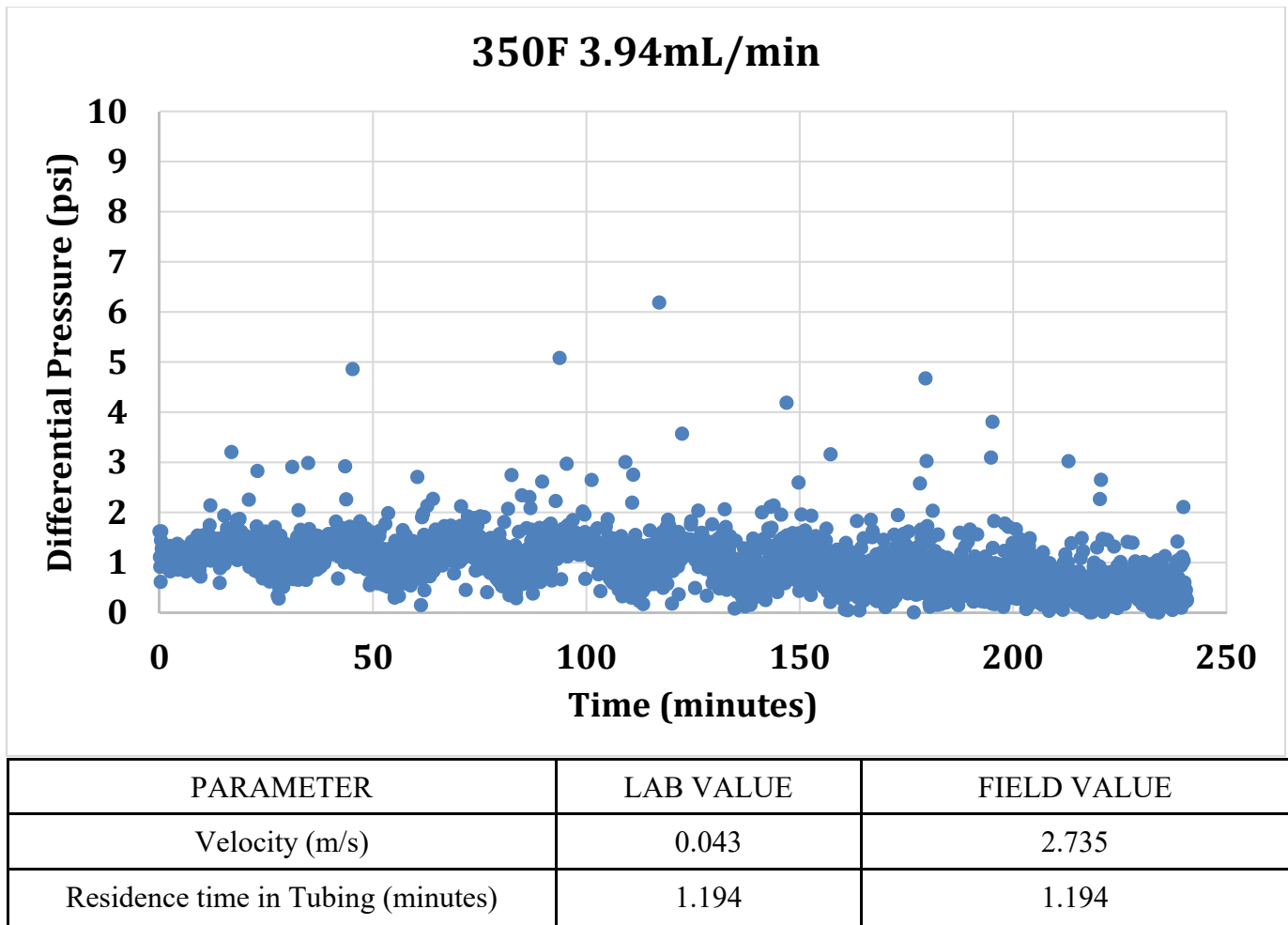
Figure 6.21: DSL test result at 350°F at 3.94mL/min with 0ppm polymer.
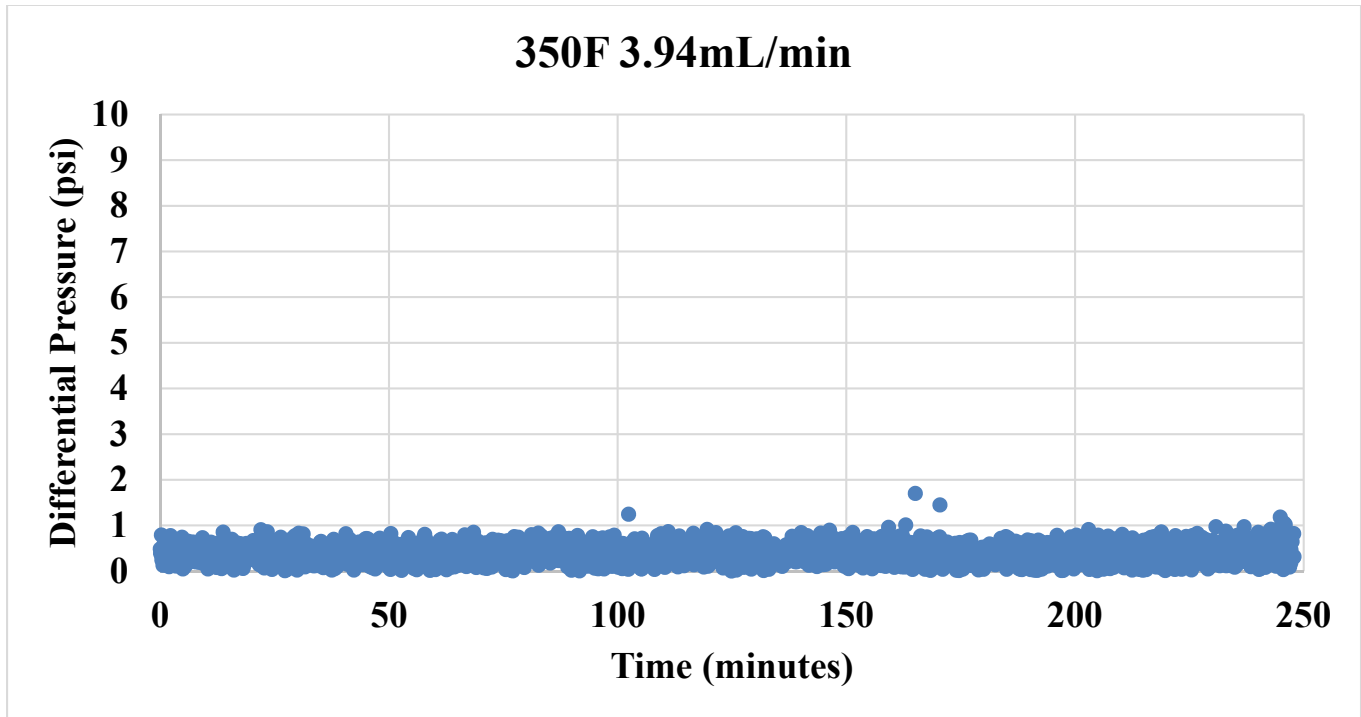
350F 3.94mL/min

PARAMETER	LAB VALUE	FIELD VALUE
Velocity (m/s)	0.043	2.735
Residence time in Tubing (minutes)	1.194	1.194

Figure 6.22: DSL test result at 350°F at 3.94mL/min with 0ppm polymer with backpressure applied.

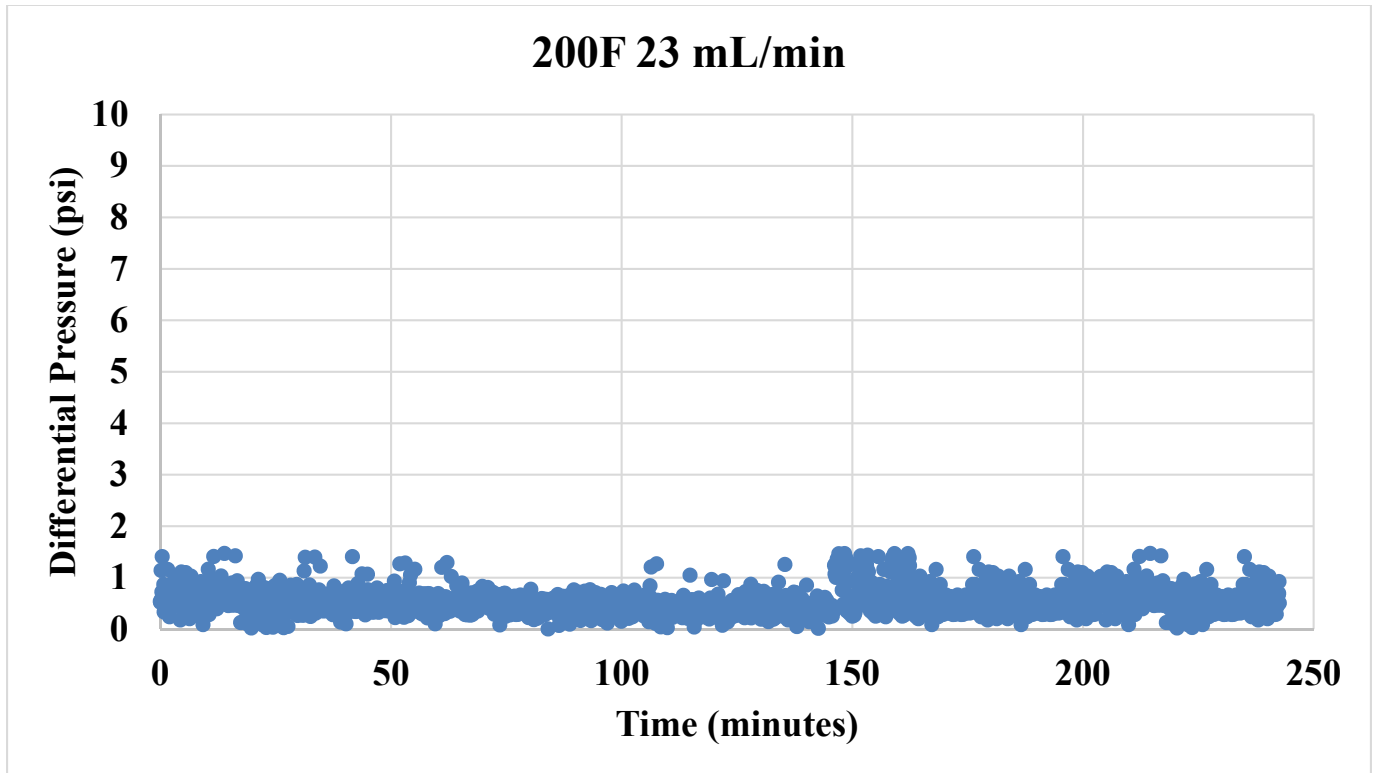| PARAMETER	LAB VALUE	FIELD VALUE
Velocity (m/s)	0.217	2.735
Residence time in Tubing (minutes)	0.235	1.194
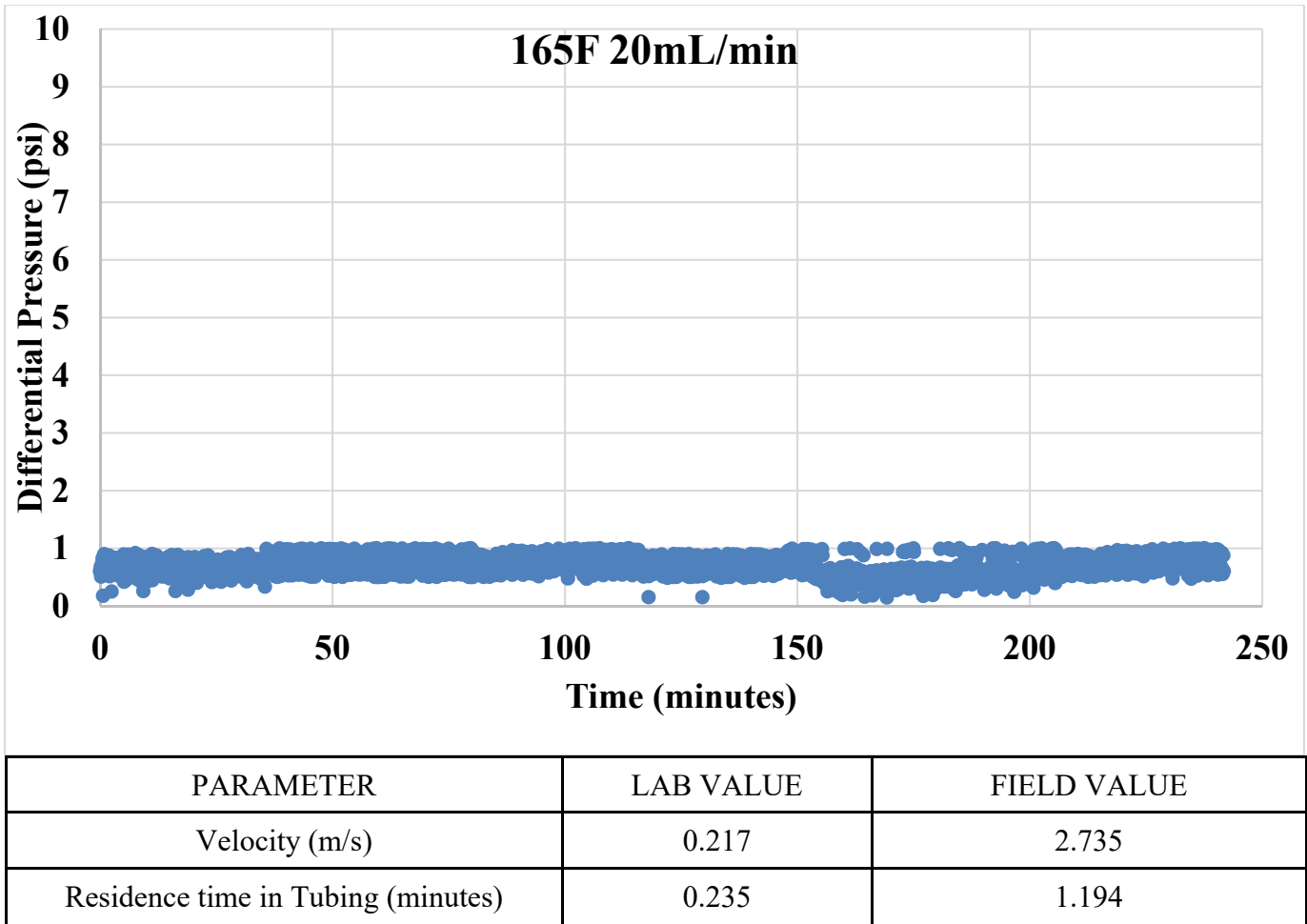
Figure 6.23: DSL test result at 165°F at 20mL/min with 0ppm polymer with backpressure applied.

Future Work
Additional Dynamic Scale Loop (DSL) experiments will be conducted in the next quarter with polymer solution at both low and higher flow rates mimicking the different parameters of Milne Point fluids. Also, a backpressure will be applied going forward in all experiments.

Both activities are ongoing.

● Task 7.0 - Feasibility of Commercial Application of the Proposed Advanced Polymer Flooding in ANS Heavy Oil Reservoirs

Activity has not yet started, since it is scheduled for BP4.

74

c.   Opportunities for Training and Professional Development

All the graduate students working on the project are obvious recipients of training and professional development in petroleum engineering. For the most part, first authors of publications resulting from this project are graduate students supported by the project. Depending on the status of the various conferences due to Covid-19, graduate students will be provided the opportunity to present the papers, which again is excellent professional development.

d.   Dissemination of Results to Communities of Interest

Engineers from ConocoPhillips and Hilcorp continue to communicate about the project on a regular basis. Additionally, most of the project related information is publically available or disseminated through the NETL website, which is accessible to any communities that have interest in the project. Similarly, publications resulting from the project work also serve the same purpose.

e.   Plan for Next Quarter

Building on the current progress achieved by the research team, work planned for the next quarter will include steadily progressing toward the planned completion dates outlined in **Table A** below.

Table A: Summary of milestone status.

Milestones	Task No.	Planned Completion Date	Actual Completion Date	Verification Method	Comments
Project Management Plan	1a	o 9/30/2022	o Ongoing (latest revision 4/30/2019)	Report/Bi-weekly meetings	None
Data Management Plan	1b	o 8/31/2018	o 7/20/2018 (latest revision 4/30/2019)	Report/Bi-weekly meetings	None
● Quantify polymer retention	2	o 3/31/2019	o Several tests completed but continues to be a topic of investigation	Report/Bi-weekly meetings, publication	None
● Effect of water salinity on S_{or}	3	o 4/30/2019	o Several tests completed per the planned date; however, August 16th marks the true completion.	Report/Bi-weekly meetings, publication	None
● Screening of gel products for conformance control		o 6/30/2019	o Some tests completed, and		

			continues to be a topic of investigation		
● Pilot area model waterflooding history match	4	o 12/312018	o Several iterations, however, an improved history match in the waterflooding period achieved in January 2020. Continues to be a topics of investigation.	Report/Bi-weekly meetings	None
● Coreflooding model history match		o 4/30/2019	o Some completed per plan, but the effort continues.		
● Updated area model for polymer flood prediction		o 5/31/2019	o Polymer flooding period WC history match is a challenge, but several prediction runs have been completed and are ongoing.		
● Reservoir modeling report		o 5/31/2019	o Extensively reported in Quarterlies, but a formal report was submitted on July 11, 2019 as special status report		

• Injection profile with polymer inj. • PFO (post-polymer) • Tracer tests (post-polymer)	5	o 12/31/2018 o 12/31/2018 o 12/31/2018	o Ongoing o Ongoing o Ongoing *Note – all have been completed from the reporting standpoint, but given the dynamic nature of the pilot these are also ongoing*	Report/Bi-weekly meetings, publications	None
• Initial treatment plan recommendation based upon literature survey	6	o 12/31/2018	o Ongoing refinement and additional tests. However, recent tests have been used to identify/screen an effective emulsion breaker.	Report/Bi-weekly meetings, publications on both topics	None
• Static polymer deposition quantification and analyses		o 09/30/2019	o Tests on copper, carbon steel and stainless steel already completed and the deposit imaged; mostly complete in last quarter		
• Finalization of the fouling flow loop design		o 06/30/2019	o Completed in 6th quarter, some tests have been carried out, and ongoing, results documented in this quarter		

2. PRODUCTS
Samson Ning, John Barnes, Reid Edwards, Walbert Schulpen, Abhijit Dandekar, Yin Zhang, Dave Cercone, Jared Ciferno: First Ever Polymer Flood Field Pilot to Enhance the Recovery of Heavy Oils on Alaska North Slope – Producer Responses and Operational Lessons Learned. Accepted for 2020 SPE ATCE, location and dates TBD at the time of writing this report.

Zhao, Y., Yin, S., Seright, S.R., Ning, S., Zhang, Y., Bai, B. 2020. Performance of Low Salinity Polymer Flood in Enhancing Heavy Oil Recovery on the Alaska North Slope. Paper URTeC1082 to be presented (virtually) at the Unconventional Resources Technology Conference held in Austin, TX, USA, 20-22 July 2020.

3. PARTICIPANTS & OTHER COLLABORATING ORGANIZATIONS
Hilcorp hired two operators dedicated to the project operations. Two reservoir engineers are in charge of the test design and analysis; one facilities engineer is in charge of polymer skid design and installation; and one operations engineer is in charge of downhole well work.

All the listed project personnel identified on the second page, and graduate students working on different tasks formally contribute 3 hours every other Friday in a project working meeting. Additionally, sub-group working meetings, typically lasting for 2-4 hours in a month are also held to discuss specific tasks such as reservoir simulation. For graduate students, the typical formal working hours per week are 20. Besides these, additional hours are typical in preparing reports, presentations for meetings, and potential publications. Given the telework of the PI and Co-PI, separate hourly meetings with UAFs graduate students are organized every Monday morning to discuss the results, path forward etc.

4. IMPACT
The project continues to be an outreach tool since it is actually showcased (relevant parts of it) in the petroleum engineering curriculum, and is a topic of frequent technical discussions, at many places.

5. CHANGES/PROBLEMS
- Based on earlier team discussions, current polymer concentration has been lowered to less than the initial 1750 ppm.

6. SPECIAL REPORTING REQUIREMENTS
Nothing to Report.

7. BUDGETARY INFORMATION
A summary of the budgetary information for the first budget period of the project is provided in **Table B**. This table shows the planned costs, reported costs, and the variance between the two. Reported costs is the sum of UAF's incurred expenses and the sum of the invoices received from our project partners.

University of Alaska Fairbanks

Table B: Budgetary information for Budget Period 2, Q4.

Baseline Reporting Quarter	Budget Period 2	
	March 1 2020-May 31 2020	
	Q4	Cumulative Total
Baseline Cost Plan		
Federal Share	302,301	4,428,131
Non-Federal Share	119,994	1,308,489
Total Planned	**422,295**	**5,736,619**
Actual Incurred Cost		
Federal Share	633,149	3,557,193
Non-Federal Share	119,920	1,719,685
Total Incurred Cost	**753,069**	**5,276,878**
Variance		
Federal Share	-465,647	870,937
Non-Federal Share	-5,120	-411,196
Total Variance	470,767	459,741

Please note that the PMP also has a spending plan that is based on calendar quarters.

8. PROJECT OUTCOMES
Nothing to Report.

9. REFERENCES

Binks, B. P., et al. "Stability of oil-in-water emulsions in a low interfacial tension system." *Langmuir* 16.3 (2000): 1025-1034.

Dr Juan-E Juri, Ana Ruiz, Viviana Serrano, Paula Guillen, Mercedes Thill, Lucas Kichick, Pablo Alonso, Ariel Lucero, Victor De Miranda, Walter Mac Donald, Emilio Figueroa, Nestor Robina, Maximiliano Vera, Emilio Figueroa, Fernando Di Pauly, Walter Rojas, and Natalia Ojeda. 2020. A Successful 18%STOOIP 4-Injector Polymer Pilot Expands To 80 New Injectors In 6 Years Adopting A Modular Concept In Grimbeek Fluvial Reservoirs, IPTC-20285-MS.

Hall, H.N., "How to Analyze Waterflood Injection Well Performance," World Oil, 1963 (October): p. 128-130.

Luo Haishan, Mohanty, Kishore, and Delshad Mojdeh. 2017. Modeling and Upscaling Unstable water and Polymer Floods: Dynamic Characterization of the Effective Viscous Fingering. ***SPE RE & E,*** November, pp: 779-794.

Moradi, M., Alvarado, V., & Huzurbazar, S. (2011). Effect of salinity on water-in-crude oil emulsion: evaluation through drop-size distribution proxy. *Energy & fuels*, *25*(1), 260-268.

Seright, R. S., Fan, T., Wavrik, K., & Balaban, R. de C. (2011, March 1). New Insights Into Polymer Rheology in Porous Media. Society of Petroleum Engineers. doi:10.2118/129200-PA